농학박사학위논문

Molecular Mechanisms of MicroRNA Maturation and Destabilization in Human Argonautes

Argonaute 단백질에서의 마이크로RNA 성숙 및
불안정화 조절 메커니즘에 대한 연구

2017년 2월

서울대학교 대학원
농생명공학부 응용생명화학전공
박 준 현

A Dissertation for the Degree of Doctor of Philosophy

Molecular Mechanisms of MicroRNA Maturation and Destabilization in Human Argonautes

February 2017

June Hyun Park

Applied Life Chemistry Major

Department of Agricultural Biotechnology

Seoul National University

Molecular Mechanisms of MicroRNA Maturation and Destabilization in Human Argonautes

Argonaute 단백질에서의 마이크로RNA 성숙 및 불안정화 조절 메커니즘에 대한 연구

지도교수 신 찬 석

이 논문을 농학박사학위논문으로 제출함
2017년 1월

서울대학교 대학원
농생명공학부 응용생명화학전공

박 준 현

박준현의 박사학위논문을 인준함
2017년 1월

위 원 장 _____ (인)
부 위 원 장 _____ (인)
위 원 _____ (인)
위 원 _____ (인)
위 원 _____ (인)

Molecular Mechanisms of MicroRNA Maturation and Destabilization in Human Argonautes

Advisor: Chanseok Shin

A Dissertation Submitted in Partial Fulfillment of the Requirement for the Degree of

DOCTOR OF PHILOSOPHY

to the Faculty of
Applied Life Chemistry Major,
Department of Agricultural Biotechnology

at

SEOUL NATIONAL UNIVERSITY

by

June Hyun Park

Date Approved

_____ _____

_____

_____

_____

_____

ABSTRACT

Small RNA silencing is mediated by the effector RNA-induced silencing complex (RISC) that consists of an Argonaute protein (Ago 1–4 in humans). A fundamental step during RISC assembly involves the separation of two strands of a small RNA duplex, whereby only the guide strand is retained to form the mature RISC, a process not well understood. Despite the widely accepted view that 'slicer-dependent unwinding' via passenger-strand cleavage is a prerequisite for the assembly of a highly complementary siRNA into the Ago2-RISC, here I show by careful re-examination that 'slicer-independent unwinding' plays a more significant role in human RISC maturation than previously appreciated, not only for a miRNA duplex, but, unexpectedly, for a highly complementary siRNA as well. I showed that in human cells, the elevated physiological temperature and the functional L1-PAZ domain of the Ago proteins, drive small RNA strand separation, even when slicer-assisted pathway is absent. In contrast to the previous models, I found that slicer-deficient Ago proteins can also be programmed with highly complementary siRNAs at the physiological temperature of humans, which now clearly explains why both miRNA and siRNA are found in all four human Ago proteins.

Little is known about the regulation of miRNA stability. Mature miRNAs are stabilized by binding to Ago proteins, the core components of the RISC. Recent studies suggest that interactions between miRNAs and their highly complementary target RNAs promote release of miRNAs from Ago proteins, and this in turn can lead to destabilization of miRNAs. However, the physiological triggers of miRNA destabilization with molecular mechanisms remain largely unknown. Here, using an *in vitro* system that consists of a minimal human Ago2-RISC in HEK293T cell

lysates, I sought to understand how miRNAs are destabilized by their targets. Strikingly, I showed that miRNA destabilization is dramatically enhanced by an interaction with seedless, non-canonical targets. I then showed that this process entails not only unloading of miRNAs from Ago, but also 3′ end destabilization of miRNAs occurred within Ago. Furthermore, mutation analysis suggests that conformational changes in the hinge region of the Ago PAZ domain are likely to be the main driving force of the miRNA destabilization. These collective results suggest that non-canonical targets may provide a stability control mechanism in the regulation of miRNAs in humans and also highlight the remarkable flexibility of human Ago proteins that experience dynamic conformational changes during their catalytic cycle. In sum, my findings reflect another layer onto the mutual regulatory circuits between Ago proteins, miRNAs and their targets, which may provide a means to fine-tune, refine and diversify miRNAs in cells.

Keywords: small RNA, microRNA, siRNA, passenger-strand cleavage, slicer-independent strand separation, Argonaute, target-directed miRNA destabilization

***Student Number*: 2012-30322**

CONTENTS

LIST OF FIGURES AND TABLES

General introduction

Chapter 1

Chapter 2

Conclusion and prospect

LIST OF ABBREVIATIONS

Ago: Argonaute
Anti-miR: Antisense-microRNA
bp, base pair
ATP: Adenosine triphosphate, single letter abbreviation A
C. elegans: *Caenorhabditis elegans*
D. melanogaster: *Drosophila melanogaster* (fruit fly)
DNA: Deoxyribonucleic acid
DTT: Dithiothreitol
dsRNA, double stranded RNA
E. coli: *Escherichia coli*
endo-siRNA: endogenous siRNA
mRNA: Messenger RNA
miRNA: microRNA
nt, nucleotide
Oligo: Oligonucleotide
PAZ: PIWI/Argonaute/Zwille
PCR: Polymerase chain reaction
PIWI: P-element induced wimpy testes
Pri-miRNA: Primary miRNA
Pre-miRNA: Precursor miRNA
Pol II: RNA polymerase II
RISC: RNA-induced silencing complex
RNA: Ribonucleic acid
RNAi: RNA interference
SDS: Sodium dodecyl sulfate
siRNA: Small-interfering RNA
ssRNA, single-stranded RNA
T7: Lytic bacteriophage T7 that infects *E. coli*
qRT-PCR: quantitative real-time PCR

GENERAL INTRODUCTION

MicroRNA biogenesis and mechanism of action in mammals

MicroRNAs (miRNAs), discovered in *C. elegans* (Lee et al., 1993), are a class of non-coding small RNAs with significant roles in the regulation of many cellular processes. (Bartel, 2004). miRNA biogenesis begins with the transcription of hairpin-structured precursors known as primary miRNAs (pri-miRNAs) by RNA polymerase II (Lee et al., 2004) (Fig. 1). The transcript is recognized by the RNase III-type enzyme, Drosha in the nucleus (Lee et al., 2003) and Dicer in the cytoplasm (Bernstein et al., 2001; Knight and Bass, 2001) for two sequential cleavages. These tandem actions convert pri-miRNAs into precursor miRNAs (pre-miRNAs) and finally results in the production of the 21–23 nucleotide (nt) miRNAs (Fig. 1). In a miRNA duplex, one strand (the miRNA passenger-strand or star strand) is discarded (Park and Shin, 2015), and the other strand (the miRNA guide strand) is retained in the RNA-induced silencing complex (RISC) for target recognition (Fig. 1), which is governed by nucleotide complementarity between the miRNA and the target mRNA. Most miRNAs characterized in mammals imperfectly base-pair with sequences in the 3′ untranslated region (3′ UTR), with most of the pairing specificity provided by the miRNA 5′ proximal "seed" region (positions 2–8). In some cases, a 3′ compensatory site (Friedman et al., 2009) compensates for insufficient 5′ seed pairing by substantially pairing outside the seed region. This partial complementarity often facilitates translational repression and/or target destabilization via deadenylation of the message (Bazzini et al., 2012; Huntzinger and Izaurralde, 2011; Subtelny et al., 2014) (Fig. 1). Argonaute proteins form the core of the RISC complex. In humans, there are four Argonaute paralogs

(hAgo1–4), of which only Ago2 possesses slicer activity (often termed as slicer) (Fig. 1). Direct cleavages by Ago2 are only operative when there are perfect or near-perfect complementarity between the miRNAs and target mRNAs, which occur predominantly in plants (German et al., 2008). Such a mechanism resembles the action of small-interfering RNAs (siRNAs), which are produced by Dicer cleavage of double-stranded RNAs (dsRNAs) of an endogenous or exogenous origin.

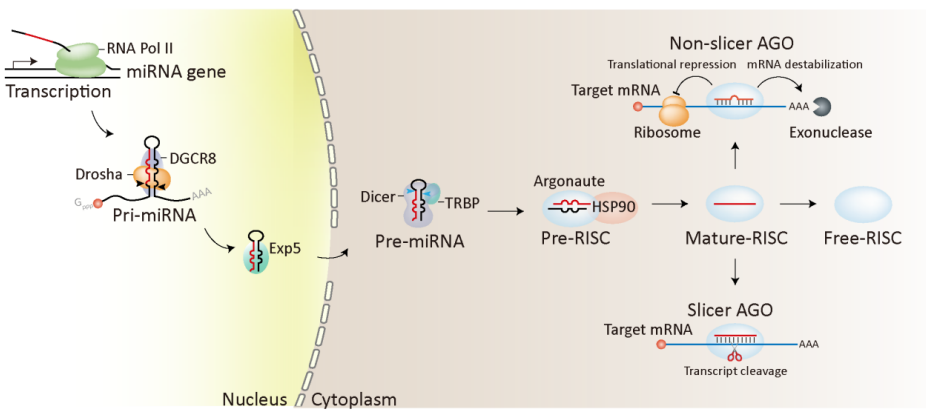

Figure 1. MicroRNA biogenesis and mechanism of action in mammals

Structural features of Argonaute proteins

A hallmark of RNA interference (RNAi) pathway is their dependence on Argonaute proteins that have specialized small RNA binding modules and are highly conserved among species. The Argonaute protein was first discovered by screening for ethyl methanesulfonate (EMS) mutations that pleiotropically affected general plant architecture in *Arabidopsis* (Bohmert et al., 1998). These mutants exhibited a filamentous structure which resembled the tentacles of the sea creature *argonaute*, a type of a small squid. Many organisms encode a set of Argonaute proteins, ranging from one in *S. pombe*, 10 in *Arabidopsis*, and up to 27 in *C. elegans* (Ender and Meister, 2010). The Argonaute protein is defined by the presence of two characteristic domains, PAZ (Piwi-Argonaute-Zwile) and PIWI (P element induced wimpy testes) (Cerutti et al., 2000). The family can be subdivided into two classes, based on their sequence homology: those that resemble *Arabidopsis* Ago1 (related to siRNAs and miRNAs) and those that resemble *Drosophila* PIWI (mainly associates with piRNAs).

Although substantial progress had been made in studying the biochemical functions of Argonaute proteins in early stages, many questions regarding the details of the mechanism remained elusive due to lack of structural information. A breakthrough was first achieved by the crystal and NMR structures of the PAZ domain of *Drosophila* Ago1 (Yan et al., 2003) and Ago2 (Lingel et al., 2003; Song et al., 2003). These studies revealed that the PAZ domain contains an OB (oligonucleotide / oligosaccharide binding) fold, a typical single-stranded nucleic acid binding motif, which provides a pocket to accommodate 2-nt 3′ terminal overhang (Ma et al., 2004). Further studies have shown that the initial interaction between the 2-nt 3′ overhang of the miRNA strands and the PAZ domain, which

occurs between the final phosphate and sugar, is essential for efficient target silencing (Wang et al., 2009).

A complete crystal structure of a prokaryotic Argonaute protein from the archaeal species *Pyrococcus furiosus*, shed light on the overall structural insight for the remaining domains and possible molecular mechanisms (Song et al., 2004). The study found that the N-terminal, MID (middle), and PIWI domains formed a crescent-shaped base, with the PAZ domain held above the base by a “stalk”-like region (Song et al., 2004). A further structural study of *Thermus thermophiles* Argonaute (*Tt*Ago), with a 5′ phosphorylated DNA guide strand, identified a nucleotide binding channel and a pivot-like conformational change during complex formation (Wang et al., 2008b). The organization indicates a bilobal architecture, with the PAZ lobe [N-terminal, Loop1 (L1) and PAZ domains] connected by Loop2 (L2) to the PIWI lobe (MID and PIWI domains) (Jinek and Doudna, 2009) (Fig. 2).

The MID domain mediates the interaction with the phosphorylated 5′ end of the guide strand, with 5′ nucleotide preference being conferred by key residues of a specificity loop that prefers U or A (Boland et al., 2011; Frank et al., 2010). The MID domain recognizes the 5′ end of the miRNAs for asymmetric guide loading prior to the duplex separation, which partly explains why the asymmetric selection is directly driven by Argonautes (Suzuki et al., 2015). A follow-up study examined the ternary complex of *Tt*Ago bound to a guide strand with an added target RNA, which revealed that the pivot-like conformational changes are associated with nucleation, propagation and cleavage steps during the catalytic cycle (Wang et al., 2009). Most recently, the structure of full-length human Ago2 was determined (Fig. 2). These studies showed that, although the individual domains of hAgo2 are similar to their prokaryotic counterparts, the core domains

of hAgo2 have extended loops and additional secondary structures that may interact with PAZ domain.

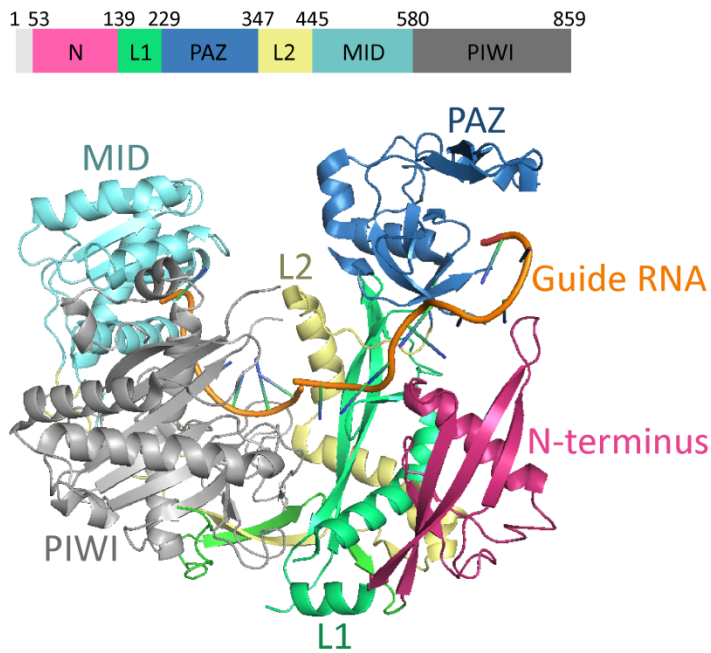

Figure 2. Structure of human Ago2

Top: Schematic of the Ago2 primary sequence. Bottom: Front view of Ago2 with the N (pink), PAZ (navy), MID (cyan), and PIWI (gray) domains, linkers L1 (green) and L2 (yellow) and the guide RNA (orange). Snapshot of the structure 4W5N taken in pymol.

Argonaute as a slicer

The PIWI domain, located across the primary groove from the PAZ domain, has a tertiary structure belonging to the RNase H family of enzymes, originally described as being responsible for catalyzing the RNA cleavage of the RNA/DNA hybrids, using a conserved Asp-Glu-Asp-Asp (DEDD) motif for divalent metal ion binding (Katayanagi et al., 1990; Nowotny et al., 2005). Early biochemical work identified the catalytic triad DD(D/H) of *Pyrococcus furiosus* Argonaute (PfAgo) (Rivas et al., 2005), which appears to differ from the catalytic tetrad (DEDD) of bacterial RNase H enzymes. A solution to this conundrum came from comparative analyses of the structures of *Kluyveromyces polysporus* Argonaute (KpAgo) and the NcQDE-2 MID-PIWI lobe (Boland et al., 2011), which found a significant difference in loop L2 (Nakanishi et al., 2012). This led Nakanishi et al. to examine whether a conserved glutamate at the tip of this loop was likely to be the fourth catalytic residue of Argonaute.

The release of the 3′ end of the guide strand from the PAZ domain allows passenger-strand separation and facilitates the formation of a catalytically competent Argonaute (Wang et al., 2009). During this process, the loops L1 and L2 undergo a post-rearrangement that refold to form a ‘plugged-in’ conformation, which inserts the invariant glutamate finger into the catalytic pocket that helps to coordinate an active-site metal ion (Nakanishi et al., 2012). Further mutational analyses suggest that this glutamate indeed constitutes the second residue of the universally conserved RNase H-like DEDD catalytic tetrad that completes the active site of Argonaute (Nakanishi et al., 2012).

Despite the high sequence conservation of the four human Argonaute proteins (Agos1-4), a slicing mechanism is only inherent to Ago2 even though

Ago3 also has a complete DED(D/H) motif. This raises the question as to whether additional determinants other than the presence of the catalytic triad are required for slicer activity. Recent studies provided a vital clue in this regard. They exploited DNA shuffling technology to generate chimeric Ago protein libraries and discovered that two N-terminal motifs are key for the slicing activity in concert with the PIWI domain (Schurmann et al., 2013). Interestingly, by swapping the N-terminal motifs and PIWI domains of Ago2 into Ago1, the chimera became an active slicer with activity comparable to wild-type Ago2 (Faehnle et al., 2013). Another study found that mutations in the PIWI-domain of Ago1 might misarrange the catalytic triad (Hauptmann et al., 2013). Recent improvements in these findings help in understanding the additional structural elements that make Argonaute protein an active endonucleolytic enzyme, and solidified the fact that slicing not only requires the catalytic residues but also involves an exquisite interplay between the catalytic residues and more distant regions of the protein.

Experimental validation of miRNA targets

Understanding the biological function of miRNAs first required identification and characterization of their target mRNAs by a bioinformatics approach, incorporating as many factors as possible that could influence the miRNA and target interaction. In contrast to animal miRNAs, the extensive complementarity between plant miRNAs and their targets allows capturing predicted targets with relatively high confidence, without too many false positives (Jones-Rhoades et al., 2006). This approach has been in use since the first prediction algorithms, developed in the Bartel laboratory (Rhoades et al., 2002), became available and several refinements have been made to improve overall

confidence of predictions, such as position-dependent penalty scores that add strong penalties for base mismatches near the 5′-end or the central region of miRNAs; these areas are critical for functional interactions (Schwab et al., 2005). Once miRNA targets are predicted, experimental validation of miRNA-target interaction usually follows. I will discuss several experimental techniques for miRNA-directed cleavage target identification.

The Carrington laboratory pioneered this field through an experimental approach for the validation of putative cleavage targets (Llave et al., 2002). A modified RNA-ligase-mediated Rapid Amplification of cDNA Ends (5′-RLM-RACE) experiment, the most widely used method to date, has enabled researchers to map the 5′-ends of target mRNAs within the expected cleavage site by taking advantage of the characteristic of Argonaute-mediated cleavage, which leaves ligation-competent 3′-cleavage fragments ending with 5′-monophosphates (Fig. 3A). The plant miRNAs are generally known to induce a site-specific cleavage within the target RNA strand between 10^{th} and 11^{th} nucleotides, relative to the 5′-end of the miRNAs, which is a diagnostic indication for the cleavage. Well-established techniques such as Northern blot analysis (Fig. 3B) and qRT-PCR (Fig. 3C), can be used and are especially useful when miRNA-defective mutants are available. Of these techniques, Northern blot analysis most closely reflects a steady state level of mRNA following miRNA action – as two populations, of cleaved and uncleaved transcripts, so the extent of miRNA-directed cleavage can be estimated (Fig. 3B). The accumulation of fast-migrating 3′-cleavage fragments indicates a high degree of cleavage. On some occasions, a substantial level of full-length target mRNAs is detectable, suggesting that only a minor fraction of targets are under the control of miRNA-directed cleavage. miRNA-mediated inhibition at the protein

level is generally evaluated by a reporter assay (or western blot analysis) with miRNA target sequence inserted into the 3′-UTR after the luciferase ORF, but this type of method can also be used to validate miRNA-directed cleavage because the downregulation of mRNA levels is often accompanied by a reduction in protein levels (Fig. 3D).

Biochemical approaches using cell lysates or purified Argonaute proteins have been used widely for the faithful and effective validation of miRNA-directed cleavage *in vitro* (Fig. 3E). This cell-free system was first developed by Tuschl and colleagues (Tuschl et al., 1999). The lysates prepared from *Drosophila melanogaster* embryos effectively recapitulate *in vitro* RNA interference triggered by miRNAs and allow the identification of 5′-cleavage products because a cap-radiolabeled target RNA without a poly(A) tail is stable in this lysates for several hours. Other cell lysates, including HeLa cell cytosol extract, wheat germ extract, and HEK 293T cells, stably or transiently overexpressing hAgo2, have been used successfully for *in vitro* cleavage assays. However, these methods are specific for a single miRNA at a time and are labor-intensive. Furthermore, a certain experiment, such as 5′-RLM-RACE, is a qualitative but not a quantitative method, which does not reflect the extent of miRNA-directed cleavage in target gene regulation. Inspired by these appreciations, the recent advent of high-throughput sequencing of RNA cleaved fragments (Addo-Quaye et al., 2008; German et al., 2008; Gregory et al., 2008), since named “degradome sequencing” (also referred to as “parallel analysis of RNA ends,” PARE) enables a large-scale experimental validation (Fig. 3F).

Figure 3. Experimental approaches for miRNA target identification

(A) 5′-RLM-RACE. In this modified protocol, particular steps (dephosphorylation and cap-removal reactions) from the original 5′-RACE protocol are omitted. A 5′-RNA adaptor is directly ligated to the 3′-end of miRNA-directed cleavage products that contain ligation-competent 5′-monophosphate. The ligated RNAs are reverse-transcribed, PCR-amplified, cloned, and sequenced, allowing determination of their mRNA cleavage sites. (B) Northern blot analysis. Shown are typical molecular phenotypes of transient or stable overexpression of miRNAs in plants, which often lead to reduced accumulation of the full-length target RNA and increased accumulation of cleavage product [miRNA (+); left lane on the blot]. miRNA-deficient mutant, such as *dcl-1* (right lane on the blot), served as a negative control. (C) qRT-PCR. Shown is a typical qRT-PCR output of relative target mRNA expression in wild-type and miRNA mutants [miRNA (-): knockout / miRNA (+): overexpression]. (D) Reporter assay. Reporter constructs containing WT or a mutant 3′-UTR were co-transfected with a miRNA of interest [miRNA (+)] or a non-cognate miRNA [miRNA (-)]. To support the direct interaction, mutation of the miRNA-binding site is often introduced in the reporter construct, which should eliminate miRNA-target interaction. The level of repression for cleavage targets is usually expected to be higher than that are observed for seed-matched targets. (E) *in vitro* cleavage assay. The DNA fragment encoding a target RNA is *in vitro* transcribed under the control of a T7 promoter. This target RNA is cap-radiolabeled and incubated with lysates containing an endogenous miRNA or an exogenously assembled miRNA of interest. When such a target RNA substrate is cleaved, its 5′-end cleavage product remains detectable by autoradiography. A time-course *in vitro* RNAi reaction is performed and analyzed in a denaturing gel, with the wild-type and target site-mutated substrates as a negative control. (F) Degradome sequencing. Shown is the schematic description of degradome library construction and data analysis. (1) Poly(A)-tailed RNAs are purified from total RNA with oligo-dT magnetic beads. (2) A 5′-adaptor is ligated to the 5′-end of the cleaved molecules with 5′-monophosphate. (3) Reverse transcription and subsequent alkaline hydrolysis of the RNA templates are performed to construct the first-strand cDNA templates. Primer extension is carried out to generate the second-strand cDNAs. (4) Restriction enzyme MmeI cleaves ~20-nt within the double-stranded cDNAs, which are ligated with a dsDNA 3′-adaptor. (5) The resulting products are PCR-amplified and submitted for high-throughput sequencing. (6) The pre-processed 20-nt sequences are matched to the transcriptome. The miRNAs, extracted from small RNA sequencing data from the same tissue or samples for degradome library construction, are aligned to find miRNA-target transcript base pairing.

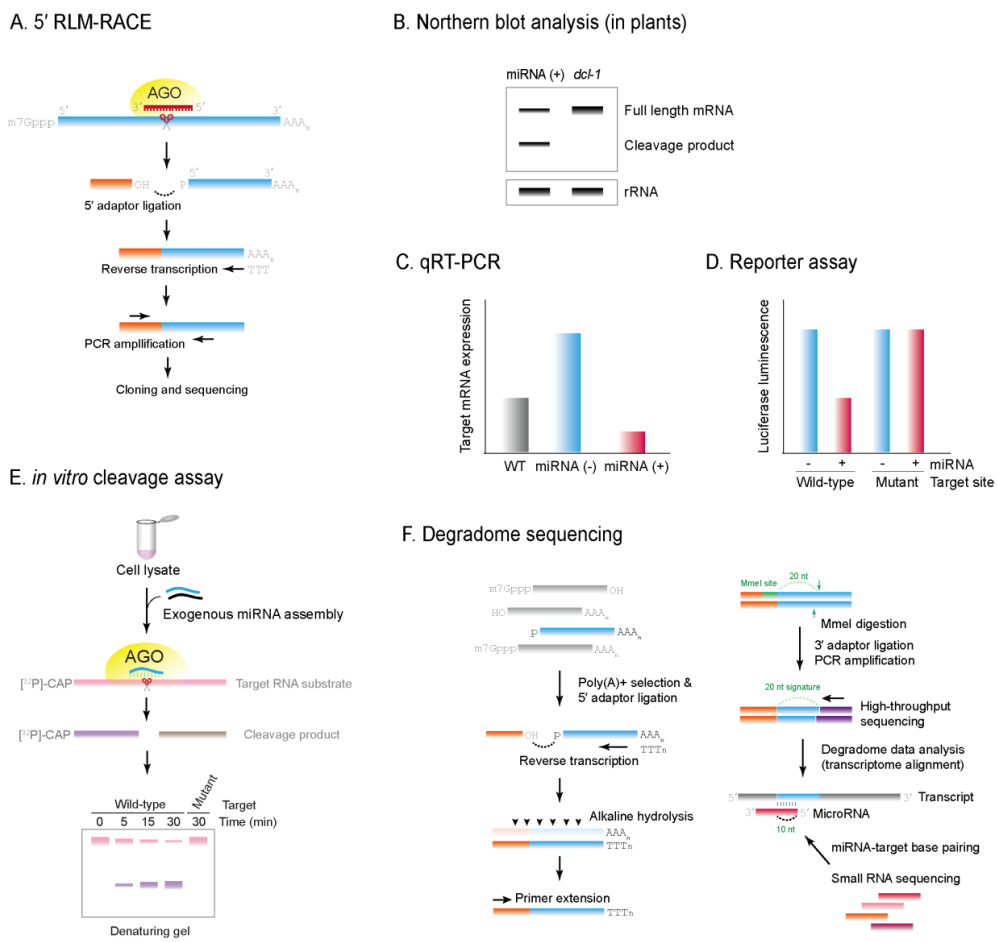

Figure 3. Experimental approaches for miRNA target identification (Park and Shin, 2014)

The aims and scope of this dissertation

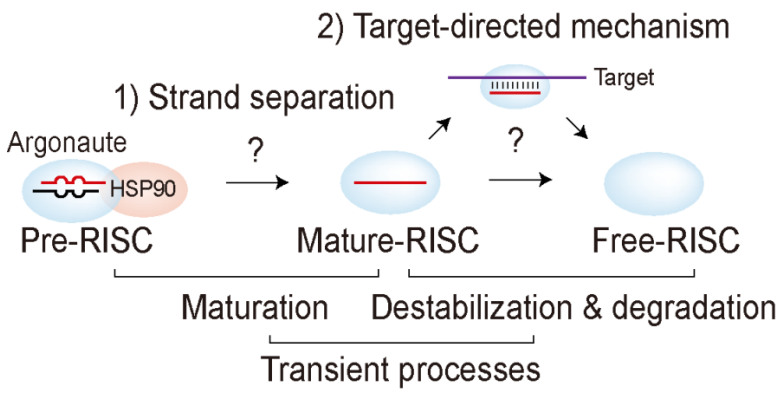

Figure 4. The aims and scope of this dissertation

In the past few years, we have seen rapid progress in our understanding of small RNA biogenesis and the mechanism by which small RNAs regulate their targets. As yet, very little is known about the small RNA maturation and destabilization processes occurring within Argonaute protein, the effector complex in small RNA regulation. This has been largely due to lack of biochemical framework for studying these transient processes and their kinetic behaviors at the early stages. Motivated by these, using an *in vitro* experimental system prepared from mammalian cells, I sought to understand 1) how human Ago proteins mediate the strand separation of the small RNA duplex to form the mature-RISC, and 2) how small RNAs in human Ago proteins are destabilized by their targets. Especially, for the second part of my dissertation, I developed an *in vitro* assay that recapitulates target RNA-directed miRNA destabilization in human Ago proteins. Overall, my dissertation highlights the remarkable flexibility of Argonaute proteins that enables to facilitate both small RNA strand separation and target-directed small RNA destabilization. This work also illustrates how efficient nucleic acid enzymes (*i.e.*, Argonaute proteins) favor substrates over products and how the intrinsic properties of Argonaute proteins can be associated with significant changes upon binding to ribonucleic acids (*i.e.*, small RNAs).

CHAPTER 1

Slicer-independent Mechanism Drives Small-RNA Strand Separation during Human RISC Assembly

This chapter was previously published as;

Park, J.H., and Shin, C. (2015). Slicer-independent mechanism drives small-RNA strand separation during human RISC assembly. *Nucleic Acids Res.* 43, 9418-9433

Introduction

Small RNA-mediated silencing pathways are essential mechanisms that regulate gene expression in many eukaryotic organisms. Small RNAs function through a cytoplasmic ribonucleoprotein complex, known as the RNA-induced silencing complex (RISC), whose core component is a member of the Argonaute (Ago) subfamily of proteins, of which there are four in humans (Ago proteins 1–4) (Hutvagner and Simard, 2008). The assembly of a small RNA duplex into the RISC mainly comprises two steps: RISC loading and strand separation (duplex unwinding) (Kawamata and Tomari, 2010). Small RNA duplexes are actively incorporated into Ago proteins to form pre-RISCs, which requires the Hsc70-Hsp90 chaperone machinery (Iki et al., 2010; Iwasaki et al., 2010; Iwasaki et al., 2015; Miyoshi et al., 2010). This machinery, which is fueled by ATP hydrolysis, drives a dynamic conformational change in the Ago proteins, thereby allowing them to accommodate the duplex (Iki et al., 2010; Iwasaki et al., 2010; Iwasaki et al., 2015; Miyoshi et al., 2010). The two strands of the duplex are subsequently unwound within the Ago proteins, in which one of the strands (the guide strand) is retained, while the other strand (the passenger-strand) is discarded to form the mature RISC. The specific selection bias of the guide strand is governed by the relative thermodynamic asymmetry of the first few bases at each end of the duplex, as the strand with less stably paired 5′ end preferentially serves as the guide (Khvorova et al., 2003; Schwarz et al., 2003). Given that small RNAs are loaded into Ago proteins as double strands, the strand selection is already determined by the polarity of small RNA duplexes upon RISC loading prior to the duplex unwinding (Betancur and Tomari, 2012; Kawamata and Tomari, 2010).

There are two types of duplex unwinding — slicer-dependent and –independent (Kawamata and Tomari, 2010). Slicer-dependent unwinding relies on an Ago2-mediated slicer activity that cleaves the passenger-strand to facilitate its rapid removal (Leuschner et al., 2006; Matranga et al., 2005; Miyoshi et al., 2005; Rand et al., 2005). Therefore, the siRNA duplexes that are incorporated into slicer-deficient Ago proteins (1, 3, and 4) cannot be unwound by the slicer-assisted pathway. In contrast, most miRNA duplexes undergo slicer-independent unwinding because they often contain seed and/or central mismatches. Beyond the slicer-assisted pathway for highly complementary siRNAs, how slicer-independent unwinding occurs, under what conditions, and whether additional factors are needed, remains largely unknown (Meister, 2013).

The initial motivation for this study was provided by the fact that the thermodynamic properties of the guide-target duplex greatly affect the efficacy of target recognition and silencing (Carmel et al., 2012; Garcia et al., 2011; Hibio et al., 2012). As previously proposed, slicer-independent unwinding can be viewed as the reverse process of target RNA recognition, with the passenger-strand being regarded as a target of the guide strand (Gu et al., 2012; Kawamata et al., 2009; Kawamata and Tomari, 2010). Therefore, I hypothesized that the thermodynamic properties of the guide-passenger duplex may also play a role. Indirect support for this idea was provided by the observation that the thermostability of the stem structures of small hairpin RNAs greatly affects the loading of Ago proteins (Gu et al., 2011).

These accumulating observations led me to carefully examine slicer-independent unwinding in human RISCs using various biochemical approaches. Of these, a native gel system provides a powerful tool for detecting RISC complexes

assembled with small RNA duplexes (Kwak and Tomari, 2012; Yoda et al., 2010) or precursor miRNAs (Liu et al., 2012) from mammalian cell lysates. Here I carefully revisited the role of Ago2 slicing activity in RISC assembly, now showing that in human cells, the elevated physiological temperature dramatically contribute to strand separation, even when slicer-assisted pathway is absent. In contrast to the previous models, in-depth biochemical analyses showed that cleavage-deficient Ago proteins can also be programmed with highly complementary siRNAs at the physiological temperature of humans. In addition, the functional analysis with several mutant Ago proteins supports the previous hypothesis that slicer-independent unwinding is mediated by the functional domains of the Ago protein (Gu et al., 2012; Kawamata et al., 2009; Kwak and Tomari, 2012; Yoda et al., 2010) that experience dynamic conformational changes during its catalytic cycle (Nakanishi et al., 2012; Wang et al., 2008a; Wang et al., 2009; Wang et al., 2008b). Altogether, these data reveal that the RISC maturation process has many more nuances, and that these events can be fine-tuned in various organisms according to their body temperature.

Materials and methods

Cell culture and siRNA transfection

HEK293T and HeLa S3 cells were cultured in Dulbecco's modified Eagle's medium supplemented with 10% (v/v) fetal bovine serum in 5% CO_2. Lipofectamine 2000 was used for siRNA transfections according to the manufacturer's protocol (Invitrogen). *Drosophila* S2 cells were cultured at 25°C in Schneider’s medium supplemented with 10% FBS.

Cell lysate preparation

HEK293T cells at 50% confluence were transfected with FLAG-tagged Ago expression plasmids (10 μg per 100-mm dish) using the calcium phosphate method and harvested after 48 h. Naïve HeLa S3 and *Drosophila* S2 cells were used for lysate preparation. Cells were washed three times with cold PBS, pH 7.4, and collected by centrifugation at 3,000 rpm at 4°C for 5 min. Cell pellets were resuspended in two packed-cell volumes of hypotonic lysis buffer (20 mM HEPES-KOH, pH 7.4, 10 mM KOAc, 1.5 mM $Mg(OAc)_2$, 5 mM DTT, 0.1% Tween-20 and 1× EDTA-free Protease Inhibitor cocktail [Roche]) and incubated for 10 min on ice. Subsequently, the cytoplasmic fraction was clarified by centrifugation at 15,000 rpm at 4°C for 20 min. The supernatant was flash frozen in liquid nitrogen and immediately stored at –80°C in single-use aliquots. To obtain the expression plasmids encoding the FLAG-tagged human Ago proteins, the coding region of each cDNA fragment was inserted into pcDNA-based vectors (Invitrogen). Non-slicer (D597A), N domain (F181A) and truncation (ΔPAZ and ΔN) mutants of Ago2 were generated by site-directed mutagenesis.

General methods for *in vitro* RNAi

in vitro RNAi reactions were performed under standard assay condition (Haley et al., 2003) that typically contained 5 μl of cell lysate, 3 μl of reaction mix (Haley et al., 2003), 1 μl of small RNA duplex and 1 μl of target substrate in a 10-μl reaction volume. The reaction temperature and final concentration of magnesium are indicated in the figures, and the details of each assay are described below. Phosphorimaging was performed using a BAS-2500 image analyzer (Fujifilm) and signal intensities were quantified using MultiGauge (Fujifilm). The sequences of the oligonucleotides used for the assays are shown in Table 1.

Target RNA cleavage assay

To prepare targets, DNA fragments containing the target site were amplified by PCR, *in vitro* transcribed and radiolabeled at the 5′-cap by guanylyl transferase and [α-^{32}P] GTP (3000 Ci/mmole, PerkinElmer) using the mScript mRNA production system (Epicentre) according to the manufacturer's instructions, followed by denaturing polyacrylamide gel purification. Fifty nanomolar of 5′-phosphorylated small RNA duplex was pre-incubated before the addition of ~5 nM of ^{32}P-cap-radiolabeled target RNA. The reactions were quenched by adding 2× proteinase K buffer (200 mM Tris-HCl, pH 7.5, 25 mM EDTA, 300 mM NaCl and 2% [w/v] SDS), 2 mg/ml proteinase K, and 1 μg glycogen, and incubated for 15 min at 60°C. After ethanol precipitation, the target substrate (78-nt) and 5′ cleavage product (37-nt) were analyzed in a 10% denaturing polyacrylamide gel.

***in vitro* RISC assembly assay**

in vitro RISC assembly assays were performed essentially as described previously (Kawamata and Tomari, 2011). Ten nanomolar of guide strand radiolabeled

duplexes (i.e., a 5′-^{32}P-radiolabeled guide strand annealed to an unlabeled phosphorylated passenger-strand) were incubated in the standard reaction mixture with 10 nM of 2′-*O*-methyl ASO as a target for native gel analysis. The RISC complexes were resolved by vertical native 1.4% agarose gel electrophoresis at 300V in a 4°C cold room.

Passenger-strand cleavage assay

in vitro RNAi reactions were performed as described above, but used 10 nM of passenger-strand radiolabeled duplexes and 1 μM of 2′-*O*-methyl oligonucleotide complementary to the passenger-strand to protect the cleavage product from degradation. After proteinase K digestion and ethanol precipitation, the samples were analyzed in a 15% denaturing polyacrylamide gel.

Immunopurification of Ago2 complex and unwinding assay

Ten nanomolar of guide strand radiolabeled duplexes were incubated in lysates from HEK293T cells expressing FLAG-hAgo2. Ten percent of the reaction was removed to serve as the input fraction and the rest of the sample was incubated with anti-FLAG M2 Affinity Gel (Sigma) for 2 h with gentle rocking at 4°C, followed by six washes with 10× bead-volumes of wash buffer containing 150 mM NaCl. RNA samples were then phenol extracted, ethanol precipitated, and resolved by 15% native polyacrylamide gel electrophoresis at 4°C as described previously (Nykanen et al., 2001).

***in vitro* deadenylation assay**

For the preparation of poly(A)-tailed target RNA, DNA fragments containing the target site were amplified by PCR, *in vitro* transcribed and purified by UV

shadowing on denaturing polyacrylamide gel. Subsequently, the purified substrate (A_0) was poly-adenylated by poly(A) polymerase (Takara) and radiolabeled at the 5′-cap by guanylyl transferase and [α-^{32}P] GTP (3000 Ci/mmole, PerkinElmer) using the mScript mRNA production system (Epicentre) according to the manufacturer's instruction, followed by denaturing polyacrylamide gel purification. Radiolabeled A_0 (without the poly(A) tail) substrate was used as the migration marker for the completely deadenylated fraction. Deadenylation by Ago1-RISC was performed with lysates from HEK293T cells expressing FLAG-Ago1. Fifty nanomolar of 5′-phosphorylated small RNA duplex was pre-incubated for 30 min before the addition of ~5 nM of ^{32}P-cap-radiolabeled poly(A)-tailed target RNA. After proteinase K digestion and ethanol precipitation, the samples were analyzed in a 6% denaturing polyacrylamide gel.

Native gel mobility-shift assay

Ten nanomolar of radiolabeled ssRNAs or duplex RNAs were incubated with increasing concentrations (0–200 nM) of purified recombinant hAgo2 in a 10-μl reaction containing 10 mM HEPES-KOH, pH 7.4, 50 mM KCl, 1 mM DTT, 3% (w/v) Ficoll-400 and 0.1 mg/ml BSA. RNA-protein complexes were analyzed by 6% native polyacrylamide gel electrophoresis at 120V in a 4°C cold room.

Northern blotting

RNAs were resolved in a 15% denaturing polyacrylamide gel, electrophoretically transferred to Hybond-NX membrane (GE healthcare), and chemically cross-linked via 1-ethyl-3-(3-dimethylaminopropyl) carbodiimide (Sigma). The DNA probe was radiolabeled using T4 polynucleotide kinase (Takara) and [γ-^{32}P] ATP (6000 Ci/mmole, PerkinElmer) and hybridized with the membrane using PerfectHyb Plus

(Sigma).

Western blotting

The primary antibodies included polyclonal rabbit anti-FLAG (1:5,000; Sigma), polyclonal rabbit anti-alpha tubulin (1:15,000; Abcam) and monoclonal mouse anti-GAPDH (1:10,000; Abcam). The secondary antibodies for chemiluminescent detection were horseradish peroxidase-conjugated goat anti-rabbit (or donkey anti-mouse) IgG antibodies (Jackson ImmunoResearch).

Expression and tandem affinity purification of recombinant human Ago2

To obtain N-terminal FLAG-tagged protein, oligonucleotides corresponding to the FLAG peptide were inserted into the pFastBac-His plasmid (Invitrogen). Recombinant hAgo2 proteins were expressed in insect cells using the Bac-to-Bac Baculovirus Expression System (Invitrogen) according to the manufacturer's instructions. Briefly, recombinant baculovirus DNA was transfected using Cellfectin II Reagent (Invitrogen) into Sf9 cells grown at 26°C in Sf-900 III medium (Invitrogen). Sf9 cells were infected with the recombinant virus for 48 h, harvested and washed with PBS. Cells were lysed in lysis buffer (20 mM HEPES-NaOH, pH 7.4, 300 mM NaCl, 0.5% Triton X-100, 5% glycerol, 15 mM imidazole, 2 mM β-mercaptoethanol, and 1× EDTA-free Protease Inhibitor cocktail [Roche]) and sonicated five 6-sec bursts at 35% amplitude. After centrifugation at 18,500 rpm at 4°C for 25 min, the supernatant was loaded onto a Ni-NTA affinity column (GE Healthcare), washed with an imidazole gradient (20–75 mM) and eluted in 250 mM imidazole. The recombinant protein was further purified via affinity binding to anti-FLAG M2 Affinity Gel (Sigma), eluted with a 3× FLAG peptide (Sigma) and stored in aliquots containing 10% (v/v) glycerol at –80°C.

Table 1. The sequences of oligonucleotides used for the assays

Oligonucleotides	Sequences (5′-3′)
miR-1 guide	UGGAAUGUAAAGAAGUAUGUA
miR-1 passenger	CAUACUUCUUUAUAUGCCCAUA
miR-1 siRNA passenger	CAUACUUCUUUACAUUCCCUA
miR-1 siRNA passenger PS	CAUACUUCU$_{(PO/PS)}$UUACAUUCCCUA
miR-1 passenger (2′-OMe)	$C_mA_mU_mA_mC_mU_mU_mC_mU_mU_mU_mA_mU_mA_mU_mG_mC_mC_mC_mA_mU_mA_m$
miR-1 siRNA passenger (2′-OMe)	$C_mA_mU_mA_mC_mU_mU_mC_mU_mU_mU_mA_mC_mA_mU_mU_mC_mC_mC_mU_mA_m$
miR-1 siRNA passenger OMe9	CAUACUUCU$_m$UUACAUUCCCUA
miR-1 guide ASO (2′-OMe)	$U_mC_mU_mU_mC_mU_mA_mC_mA_mU_mA_mC_mU_mU_mC_mU_mU_mU_mA_mC_mA_mU_mU_mC_mC_mA_mA_mC_mC_mU_mU_m$
miR-1 passenger ASO (2′-OMe)	$U_mC_mA_mC_mA_mU_mG_mG_mA_mA_mU_mG_mU_mA_mA_mA_mG_mA_mA_mG_mU_mA_mU_mG_mU_mA_mA_mU_mC_mU_mC_m$
let-7a miRNA guide	UGAGGUAGUAGGUUGUAUAGUU
let-7a siRNA guide	UGAGGUAGUAGGUUGUAUAGU
let-7a-1 passenger	CUAUACAAUCUACUGUCUUUC
let-7a-2 passenger	CUGUACAGCCUCCUAGCUUUCC
let-7a siRNA passenger OMe9	UAUACAACCmUACUACCUCUUC
let-7a guide ASO (2′-OMe)	$U_mC_mU_mU_mC_mA_mC_mU_mA_mU_mA_mC_mA_mA_mA_mC_mC_mU_mA_mC_mU_mA_mC_mC_mU_mC_mA_mA_mC_mC_mU_mU_m$
siGAPDH guide	CAUGGGUGGAAUCAUAUUGGA
siGAPDH passenger	CAAUAUGAUUCCACCCAUCUU
siGAPDH passenger OMe9	CAAUAUGAU$_m$UCCACCCAUCUU
siGAPDH passenger ASO (2′-OMe)	$U_mC_mA_mC_mA_mA_mA_mG_mA_mU_mG_mG_mG_mU_mG_mG_mC_mA_mA_mU_mC_mA_mU_mA_mU_mU_mG_mA_mU_mC_mU_mC_m$
miR-1 antisense DNA probe	TACATACTTCTTTACATTCCA
let-7a antisense DNA probe	AACTATACAACCTACTACCTCA

Results

Small RNA maturation is highly dependent on the ambient temperature both *in vitro* and in cells.

I first established a cell-free system derived from human embryonic kidney (HEK) 293 cells expressing human Ago2 (hAgo2) (Kwak and Tomari, 2012; Wakiyama et al., 2007; Yoda et al., 2010). I and others (Kwak and Tomari, 2012; Yoda et al., 2010) have found that a naïve HEK293T cell lysate on its own is not competent to reconstitute RNA interference (RNAi) *in vitro* (Fig. 5A and B), possibly because endogenous Ago proteins are largely pre-occupied by endogenous miRNAs (Elkayam et al., 2012; Iki et al., 2010; Iwasaki et al., 2015; Schirle and MacRae, 2012). Transient expression of Ago2 generated free RISCs for exogenous RISC programming, which efficiently recapitulate RNAi *in vitro* (Fig. 5A–C). To specifically examine the relative contribution of slicer-dependent and -independent unwinding of Ago2, I initially used three model duplexes (Fig. 6A): endogenous miR-1, miR-1 siRNA (functionally asymmetric) and miR-1 siRNA with a phosphorothioate (PS) modification of the scissile phosphodiester bond that inhibits passenger-strand cleavage (Matranga et al., 2005) (Fig. 6B). To exclude the possibility of endogenous miRNAs participating in RNAi, miR-1, which is specifically expressed in heart and skeletal muscle (Lim et al., 2005), was used, and its absence in HEK293T cells was confirmed by northern blotting (Fig. 5D).

I initially performed a classical *in vitro* target cleavage and unwinding assay at various temperatures to investigate the thermodynamic properties of small RNA maturation. The miRNA exhibited the most efficient target cleavage and unwinding at 25°C, followed by the siRNA and PS duplexes, which is generally

consistent with previous findings in *Drosophila* (Matranga et al., 2005; Miyoshi et al., 2005; Rand et al., 2005) (Fig. 6C and D). Unexpectedly, the defects of the siRNA and PS duplexes were largely rescued by increasing the temperature to 30°C (Fig. 6C and D). At the physiological temperature (37°C) of human cells, all three duplexes exhibited a similar level of target cleavage (Fig. 6C) and produced a comparable amount of Ago2-bound ssRNA in the immunoprecipitation (IP) fraction (Fig. 6D). These results indicated that the 'slicer-dependency' of unwinding is largely influenced by the temperature. To examine whether this mechanism was operating *in vivo*, I co-transfected HEK293T cells with the FLAG-Ago2 plasmid and small RNAs. The cells were cultured at 28°C or 37°C, and the relative amount of small RNAs and their functional activities were measured by northern blotting and a target cleavage assay, respectively (Fig. 6E and F). The results were mostly consistent with the *in vitro* findings that small RNA maturation is highly dependent on the ambient temperature, which also seemed to have a drastic effect on the degree of passenger-strand cleavage.

Figure 5. Mammalian cell-free system from HEK293T cells that faithfully recapitulates RNAi *in vitro*

(A) miRNA duplex was assembled in lysates from naive HEK293T cells (Mock) and from cells expressing FLAG-hAgo2 for 15 min. Fifty nanomolar of recombinant hAgo2 protein was programmed with a single-stranded guide RNA. Cap-radiolabeled target RNA (78-nt) was then added and further incubated for 15 min, which yielded a 5′ cleavage product at the identical position (37-nt), as a diagnostic for hAgo2-mediated catalysis. (B) Western blot analysis using an anti-FLAG antibody confirmed the expression of tagged Ago2 protein. Anti-tubulin served as an internal control. (C) Coomassie-staining of tandem affinity purified recombinant human Ago2 protein derived from the baculovirus system. (D) Thirty micrograms of total RNA from HEK293T cells was subjected to Northern blot analysis with 5 fmole of synthetic miR-1 standard as a positive control. let-7a and 5s rRNA served as a positive (for total RNA sample) and negative (for synthetic RNA sample) control.

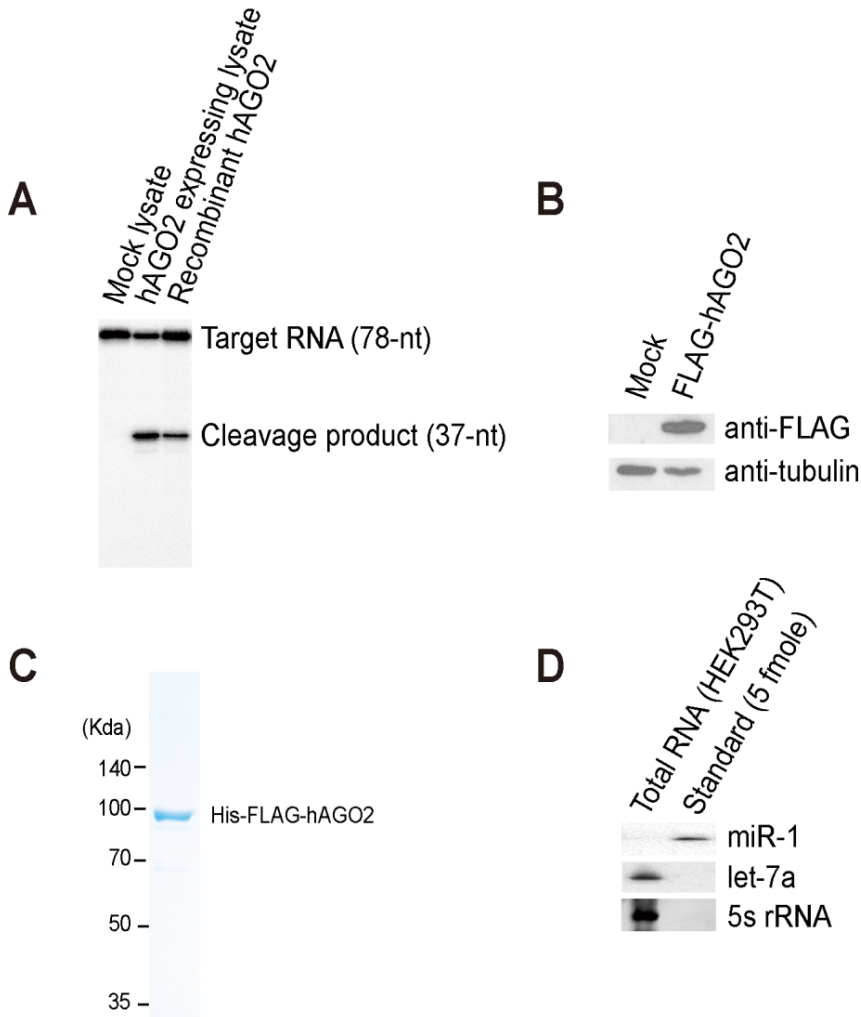
A
Mock lysate
hAGO2 expressing lysate
Recombinant hAGO2
Target RNA (78-nt)
Cleavage product (37-nt)
B
Mock
FLAG-hAGO2
anti-FLAG
anti-tubulin
C
(Kda)
140
100
70
50
35
His-FLAG-hAGO2
D
Total RNA (HEK293T)
Standard (5 fmole)
miR-1
let-7a
5s rRNA

Figure 6. Small RNA maturation is highly sensitive to the ambient temperature both *in vitro* and in cells

(A) Small RNA duplexes used in this study; miR-1 with an endogenous duplex structure, functionally asymmetric miR-1 siRNA (miR-1 was perfectly paired to its antisense, except for the 1st position from the 5′ end) and miR-1 siRNA PS (miR-1 siRNA introduced with phosphorothioate linkage at the scissile phosphate, denoted by a star). The guide and passenger-strands are shown in black and red, respectively. (B) PS modification inhibits the cleavage of the passenger-strand. Small RNA duplexes containing radiolabeled passenger-strands were incubated in lysates expressing tagged Ago2 for the indicated times at 25°C. (C) Distinct efficacy of target cleavage at different temperatures for each different small RNA duplex. Small RNAs duplexes were assembled in lysates expressing tagged Ago2 for 15 min at the indicated temperature (mock refers to the no duplex control). Cap-radiolabeled target RNA was then added and further incubated for 15 min at the indicated temperatures. (D) Distinct efficacy of unwinding at different temperatures for each different small RNA duplex. Small RNA duplexes carrying radiolabeled guide strands were incubated in lysates from expressing tagged Ago2 for 30 min at the indicated temperature. Small RNAs incorporated into the Ago2 complexes were immunopurified and analyzed in native gel, along with the 10% input (IN) relative to the IP. (E) Small RNA maturation is dependent on the ambient temperature in living cells. HEK293T cells were co-transfected with 10 nM of small RNA duplexes and FLAG-Ago2 plasmids. Cells were then cultured either at 28°C or 37°C and harvested at 48 h post-transfection; cell lysates were subjected to FLAG-IP, followed by Northern blotting with the miR-1 probe. The blot was probed for U6 snRNA as a loading control. Ethidium bromide-stained 5S rRNA served as another loading control. The numbers below the blot are the relative expression levels, normalized using the U6 snRNA loading control. (F) Cell lysates prepared as in panel (E) were used for the target cleavage assay. Cap-radiolabeled target RNA was added and incubated for the indicated times.

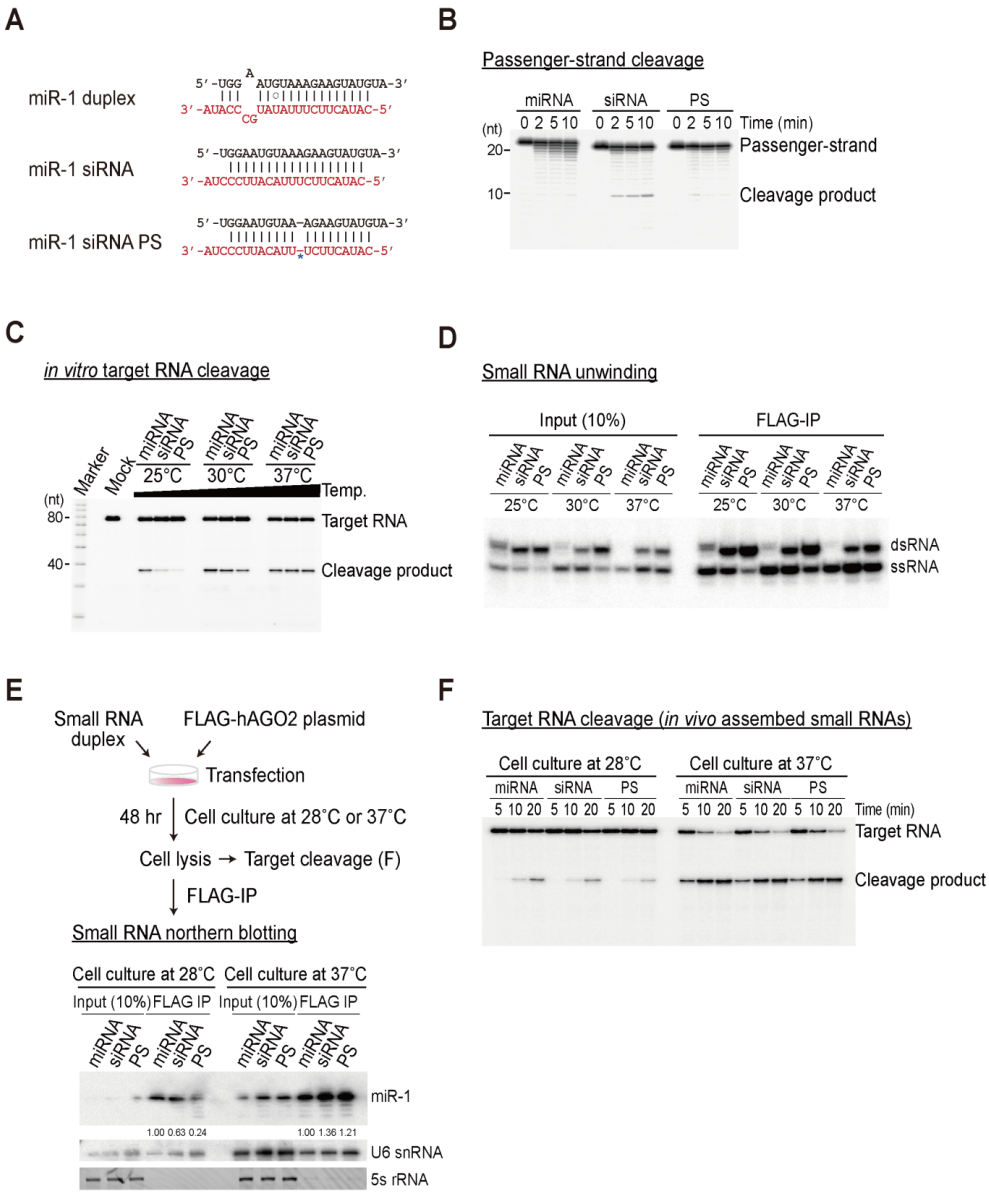
A
miR-1 duplex
5′-UGG A AUGUAAAGAAGUAUGUA-3′
3′-AUACC CG UAUAUUUCUUCAUAC-5′
miR-1 siRNA
5′-UGGAAUGUAAAGAAGUAUGUA-3′
3′-AUCCCUUACAUUUCUUCAUAC-5′
miR-1 siRNA PS
5′-UGGAAUGUAA-AGAAGUAUGUA-3′
3′-AUCCCUUACAUU-UCUUCAUAC-5′
B
Passenger-strand cleavage
miRNA
siRNA
PS
0 2 5 10 0 2 5 10 0 2 5 10 Time (min)
(nt)
20-
10-
Passenger-strand
Cleavage product
C
in vitro target RNA cleavage
Marker
Mock
miRNA siRNA PS
25°C
30°C
37°C
Temp.
(nt)
80-
40-
Target RNA
Cleavage product
D
Small RNA unwinding
Input (10%)
FLAG-IP
miRNA siRNA PS
25°C 30°C 37°C
dsRNA
ssRNA
E
Small RNA duplex
FLAG-hAGO2 plasmid
Transfection
48 hr
Cell culture at 28°C or 37°C
Cell lysis → Target cleavage (F)
FLAG-IP
Small RNA northern blotting
Cell culture at 28°C
Cell culture at 37°C
Input (10%) FLAG IP Input (10%) FLAG IP
miRNA siRNA PS
miR-1
1.00 0.63 0.24
1.00 1.36 1.21
U6 snRNA
5s rRNA
F
Target RNA cleavage (in vivo assembled small RNAs)
Cell culture at 28°C
Cell culture at 37°C
miRNA siRNA PS
5 10 20 5 10 20 5 10 20 5 10 20 5 10 20 5 10 20 Time (min)
Target RNA
Cleavage product

Slicer-dependent unwinding increases with Mg^{2+} concentration and decreases with increasing temperature

Divalent cations, particularly Mg^{2+}, have been shown to have a unique role in nucleic acid duplex stabilization (Nakano et al., 1999; Serra et al., 2002). Given that cleavage-competent Ago proteins are also Mg^{2+}-dependent endonucleases (Schwarz et al., 2004), I hypothesized that the extent of passenger-strand cleavage may be influenced by the Mg^{2+} concentration. To this end, I performed a passenger-strand cleavage assay using the siRNA duplex in which the Mg^{2+} concentration ranged from 0 to 5 mM. Cleavage was abrogated by the addition of EDTA, indicating that Mg^{2+}-dependent Ago2-slicer activity is required (Fig. 7A). Cleavage products increased significantly with Mg^{2+} levels at 25°C (Fig. 7A). These results explained why the cleavage of not only the PS duplex, but also the siRNA, was not very efficient at 25°C in the presence of 1 mM Mg^{2+} (Fig. 7C). In contrast, the cleavage products were barely detectable at 37°C, despite the presence of a 100-fold excess of a 2′-*O*-methylated trap (Matranga et al., 2005; Rand et al., 2005) that protects them from degradation (Fig. 7A). These results suggested that slicer-dependency decreased with increasing temperature, and it raised an intriguing question regarding how Mg^{2+}, together with temperature, influences duplex unwinding during RISC assembly. Because RISC assembly is a transient process, it is fundamentally important to understand its kinetics at the early stage. To do so, I employed an *in vitro* reconstitution system using native agarose gels, which was developed by Tomari and his colleagues (Kawamata et al., 2009; Kawamata and Tomari, 2011; Kwak and Tomari, 2012; Yoda et al., 2010). While RISC complexes cannot be detected using naïve HEK293T cell lysates (Kwak and Tomari, 2012; Yoda et al., 2010), the transient expression of each Ago protein enables the

sensitive detection of the two complexes formed by exogenous RISCs, including pre- and mature RISCs (Yoda et al., 2010) (Fig. 8A–C). Here, I exploited this reconstitution system to further biochemically dissect and functionally characterize duplex unwinding by human Ago proteins (Fig. 7B).

High temperature drives duplex unwinding largely independently of slicer-activity

I set out to explore how temperature and Mg^{2+} affect duplex unwinding during RISC assembly. At 25°C, only the miRNA showed an efficient conversion of pre- to mature-Ago2-RISC, regardless of the Mg^{2+} concentration (Fig. 7C and D). While the RISC maturation of the siRNA was considerably slower than that of the miRNA at 0.75 mM Mg^{2+}, it was significantly promoted by passenger-strand cleavage in the presence of 3.75 mM Mg^{2+}, whereas the PS duplex was minimally affected (Fig. 7C and D), showing that Mg^{2+} is a key determinant of the efficiency of slicer-dependent unwinding. Nevertheless, the PS duplex was comparable to that of siRNA duplex at 37°C in the presence of 0.75 mM Mg^{2+}, indicating that slicer-independent unwinding appeared to exert a dominant influence at this temperature (Fig. 7E). The increased level of Mg^{2+} at 37°C resulted in the earlier saturation of target cleavages, not only for the siRNA duplex, but also for the miRNA and PS duplexes (Fig. 7F), indicating that the enhanced cleavages were mostly due to the tighter binding of targets, rather than their improved unwinding. Based on these results, I concluded that although slicer-dependent unwinding accelerates RISC maturation at low temperatures, its contribution is less important at the physiological temperature of humans.

Figure 7. Slicer-dependency is determined by temperature and the Mg^{2+} level

(A) The effect of temperature and Mg^{2+} on the degree of passenger-strand cleavage. siRNA duplexes containing radiolabeled passenger-strands were incubated in lysates expressing tagged Ago2 for 15 min either at 25°C or 37°C, with Mg^{2+} concentrations ranging from 0 to 5 mM. The incubation with 5 mM EDTA served as a negative control. (B) A schematic of the analysis for (C-F). (C-F) The slicer-dependency of RISC assembly decreases with increasing temperature and decreasing Mg^{2+} levels. Small RNA duplexes containing radiolabeled guide strands were incubated in lysates expressing tagged Ago2 at the indicated temperature and Mg^{2+} concentrations for the indicated times. Under the same condition, target cleavages were analyzed after 30 min of small RNA assembly. Representative data of at least two independent experiments are shown.

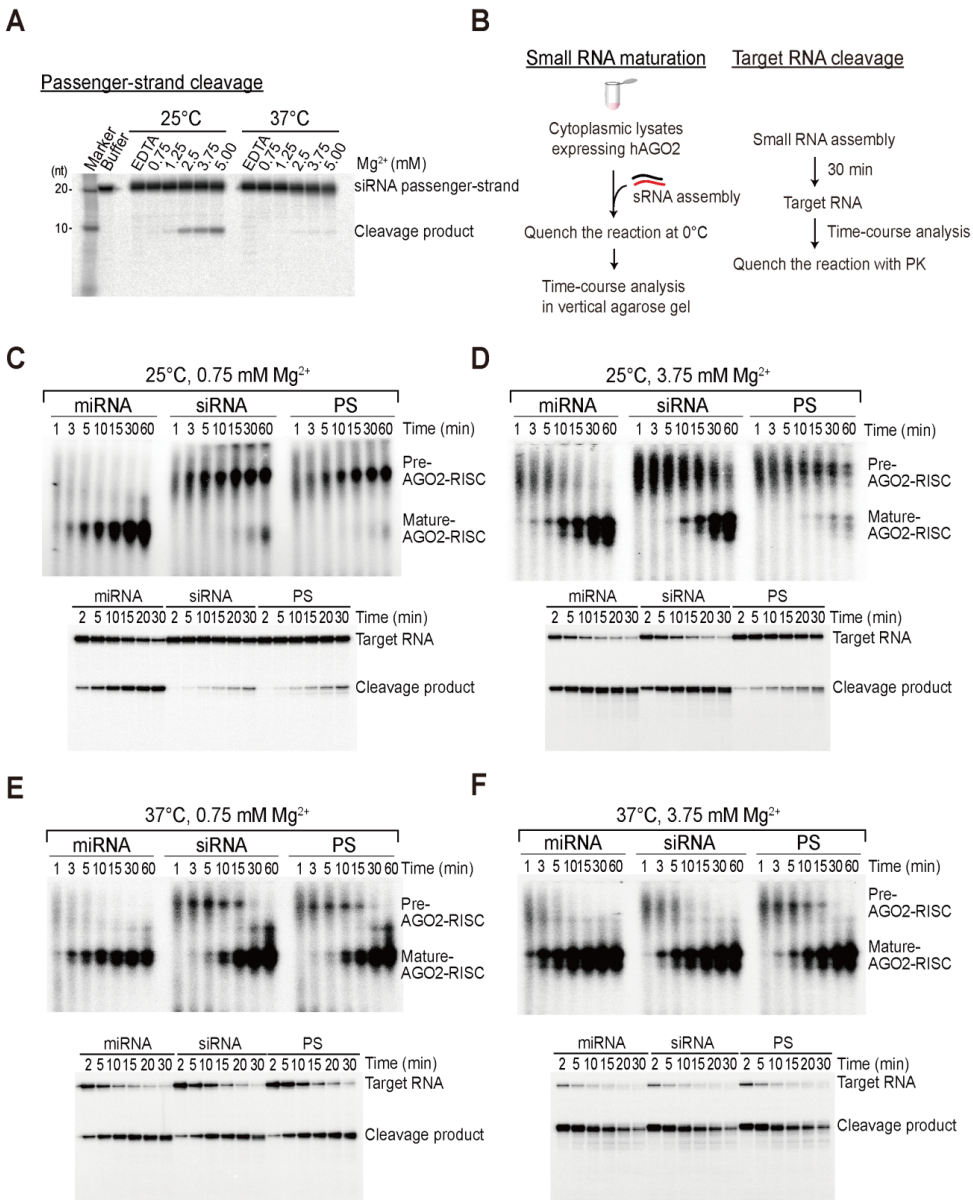
A
Passenger-strand cleavage
25°C
37°C
Marker
Buffer
EDTA
0.75
1.25
2.5
3.75
5.00
(nt)
20-
10-
Mg2+ (mM)
siRNA passenger-strand
Cleavage product
B
Small RNA maturation
Target RNA cleavage
Cytoplasmic lysates expressing hAGO2
sRNA assembly
Quench the reaction at 0°C
Time-course analysis in vertical agarose gel
Small RNA assembly
30 min
Target RNA
Time-course analysis
Quench the reaction with PK
C
25°C, 0.75 mM Mg2+
D
25°C, 3.75 mM Mg2+
E
37°C, 0.75 mM Mg2+
F
37°C, 3.75 mM Mg2+
miRNA
siRNA
PS
Time (min)
Pre-AGO2-RISC
Mature-AGO2-RISC
Target RNA
Cleavage product

Figure 8. Characterization of the RISC complexes detected in lysates from HEK293T cells expressing FLAG-tagged Ago proteins

(A) Western blot analysis using an anti-FLAG antibody confirmed the expression of tagged Ago proteins. Anti-tubulin served as an internal control. (B) Target cleavage assay in lysates from HEK293T cells expressing tagged Ago proteins. miRNA duplex was assembled in lysates from naive HEK293T cells (Mock) and from cells expressing tagged Ago proteins for 15 min. Cap-radiolabeled target RNA was then added and further incubated for 15 min. (C) Small RNA duplexes containing radiolabeled guide strands were incubated in lysates expressing tagged Ago proteins at the indicated temperature and Mg^{2+} for 30 min. The RISC complexes were separated on a vertical agarose native gel at 4°C. The migration of the RISC complexes varied slightly among Ago proteins, possibly due to their different sizes and charges of each Ago protein. M; miRNA, S; siRNA, PS; siRNA with phosphorothioate modification. Please refer to figure 7 to monitor the overall kinetic behavior of the RISC complexes and dependence on temperature and Mg^{2+} level for each different small RNA duplex.

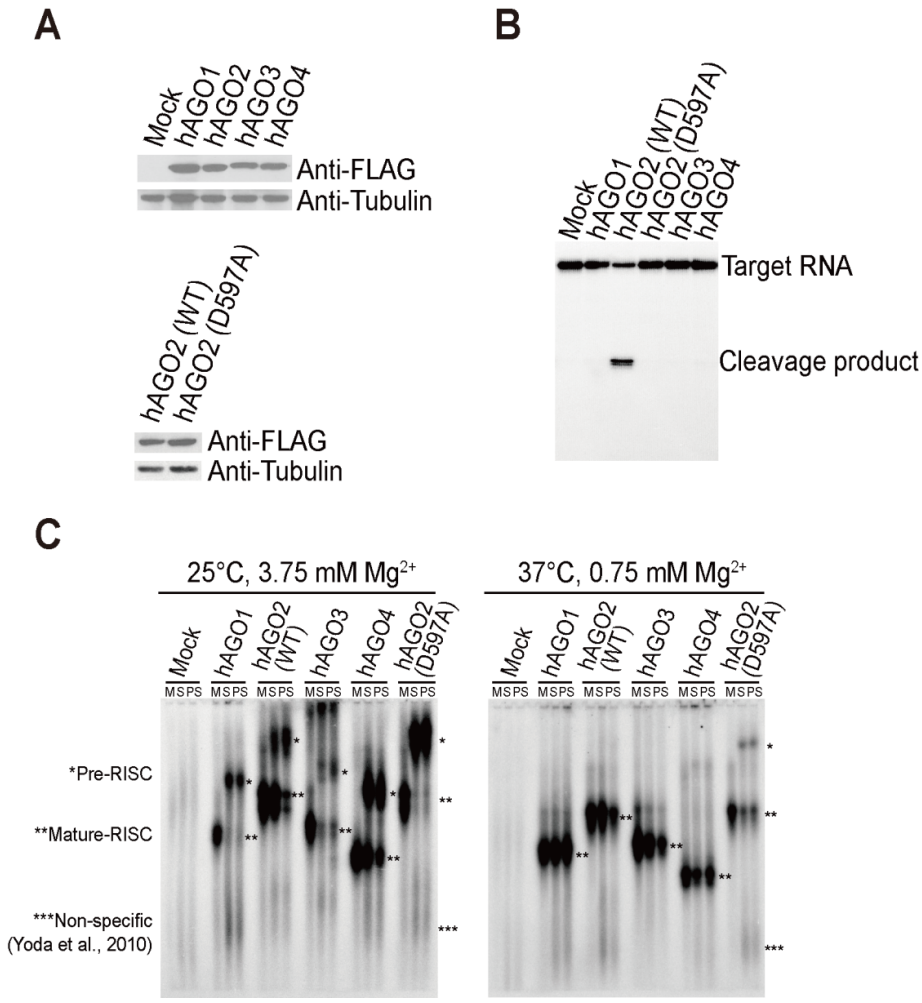
A
Mock
hAGO1
hAGO2
hAGO3
hAGO4
Anti-FLAG
Anti-Tubulin
hAGO2 (WT)
hAGO2 (D597A)
Anti-FLAG
Anti-Tubulin
B
Mock
hAGO1
hAGO2 (WT)
hAGO2 (D597A)
hAGO3
hAGO4
Target RNA
Cleavage product
C
25°C, 3.75 mM Mg2+
37°C, 0.75 mM Mg2+
Mock
hAGO1
hAGO2 (WT)
hAGO3
hAGO4
hAGO2 (D597A)
M S P S
*Pre-RISC
**Mature-RISC
***Non-specific
(Yoda et al., 2010)

Slicer-deficient Ago proteins are capable of unwinding the siRNA duplex in a temperature-dependent manner

Although it has widely been considered that slicer-dependent unwinding via passenger-strand cleavage is required for highly complementary siRNAs, these observations suggest that 'slicer-dependency' significantly decreases with increasing temperature. To more directly validate this hypothesis, I monitored RISC assembly using lysates expressing PIWI catalytic mutant Ago2 (D597A) with impaired slicer activity (Fig. 8B). As expected, only the miRNA achieved full maturation at 25°C, and an increased level of Mg^{2+} did not influence the unwinding of the siRNA, indicating that the slicer-assisted pathway is not available in this mutant (Fig. 9A and B). Nonetheless, both the siRNA and PS duplexes were unwound efficiently at 37°C (Fig. 9C and D), albeit more slowly than by wild-type Ago2 (Fig. 7E and F). Time-course and temperature gradient experiments demonstrated that the higher temperature drives the unwinding of the highly complementary siRNA when slicer-dependent unwinding is not available (Fig. 9E).

If the catalytically defective Ago2 mutant is capable of unwinding the siRNAs, is that also the case for other human Ago proteins (1, 3, and 4) that do not possess slicer-activity? To answer this question, I tested the RISC assembly of other Ago proteins as well. Similar to the Ago2 catalytic mutant, only miRNA was unwound efficiently at 25°C by Ago1 (Fig. 9F), and a higher Mg^{2+} concentration did not accelerate unwinding (Fig. 9G). However, RISC maturation was again feasible at 37°C for both the siRNA and PS duplexes (Fig. 9H and 10A). This conclusion was further supported by an Ago1-mediated deadenylation assay showing that the siRNA is only functionally active at 37°C (Fig. 9I). As expected, human Ago3 and 4 exhibited a similar pattern (Fig. 10B and C), indicating that all

four human Ago proteins have an intrinsic ability to unwind the highly complementary siRNA independently of slicer-activity at their physiological temperature.

Figure 9. Slicer-deficient Ago proteins can unwind the siRNA duplex in a temperature-dependent manner

(A-D) PIWI catalytic mutant Ago2 is capable of unwinding the siRNA duplex. Small RNA duplexes containing radiolabeled guide strands were incubated in lysates expressing tagged Ago2 (D597A) at the indicated temperature and Mg^{2+} concentrations for the indicated times. Representative data of at least two independent experiments are shown. (E) Higher temperature drives the unwinding of the siRNA when slicer-assisted pathway is not available. Left: Small RNA duplexes containing radiolabeled guide strands were incubated in lysates expressing tagged Ago2 (D597A) at the indicated temperature and Mg^{2+} concentrations for the indicated times. Right panel: 30 min of RISC assembly at the indicated temperature using a temperature gradient in a PCR machine. (F-H) Non-slicer Ago protein can unwind the siRNA duplex at the physiological temperature of humans. Small RNA duplexes containing radiolabeled guide strands were incubated in lysates expressing tagged Ago1 at the indicated temperature and Mg^{2+} concentrations for the indicated times. Representative data of at least two independent experiments are shown. (I) The siRNA duplex is only functionally active at 37°C. Deadenylation by Ago1-RISC was monitored in lysates expressing tagged Ago1 at the indicated temperature and 3.75 mM Mg^{2+} at the indicated times.

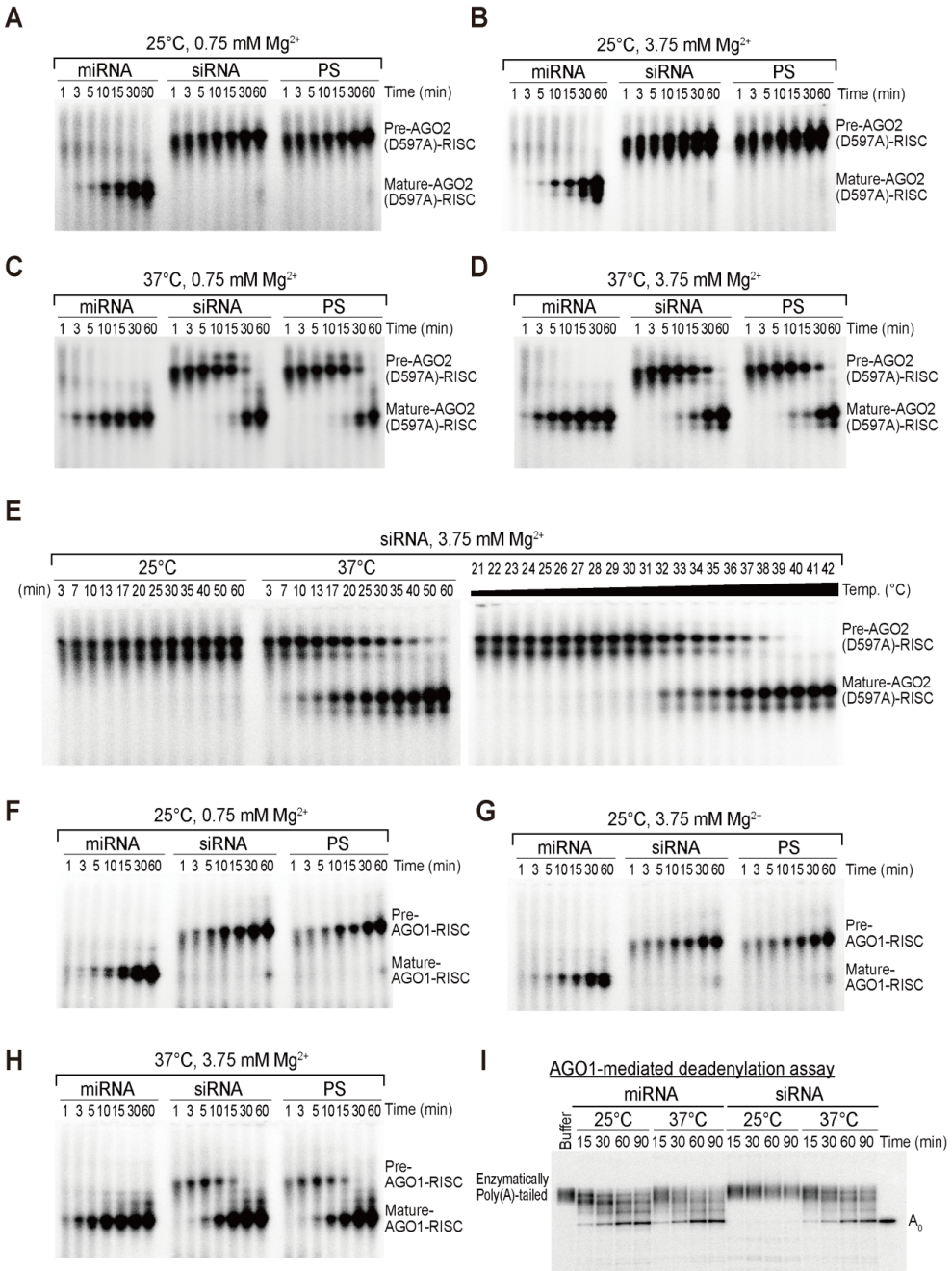
A
25°C, 0.75 mM Mg2+
miRNA
siRNA
PS
1 3 5 10 15 30 60
Time (min)
Pre-AGO2 (D597A)-RISC
Mature-AGO2 (D597A)-RISC
B
25°C, 3.75 mM Mg2+
C
37°C, 0.75 mM Mg2+
D
37°C, 3.75 mM Mg2+
E
siRNA, 3.75 mM Mg2+
25°C
37°C
(min) 3 7 10 13 17 20 25 30 35 40 50 60
21 22 23 24 25 26 27 28 29 30 31 32 33 34 35 36 37 38 39 40 41 42
Temp. (°C)
F
25°C, 0.75 mM Mg2+
Pre-AGO1-RISC
Mature-AGO1-RISC
G
25°C, 3.75 mM Mg2+
H
37°C, 3.75 mM Mg2+
I
AGO1-mediated deadenylation assay
Buffer
25°C
37°C
15 30 60 90 15 30 60 90 15 30 60 90 15 30 60 90 Time (min)
Enzymatically Poly(A)-tailed
A0

Figure 10. Slicer-deficient Ago proteins can unwind siRNA duplex in a temperature-dependent manner – II

(A-C) Non-slicer Ago proteins are capable of unwinding siRNA duplex at the physiological temperature in human. Small RNA duplexes containing radiolabeled guide strands were incubated in lysates expressing tagged Ago1, Ago3 and Ago4 at the indicated temperature and Mg^{2+} for the indicated time points. The RISC complexes were separated on a vertical agarose native gel at 4°C.

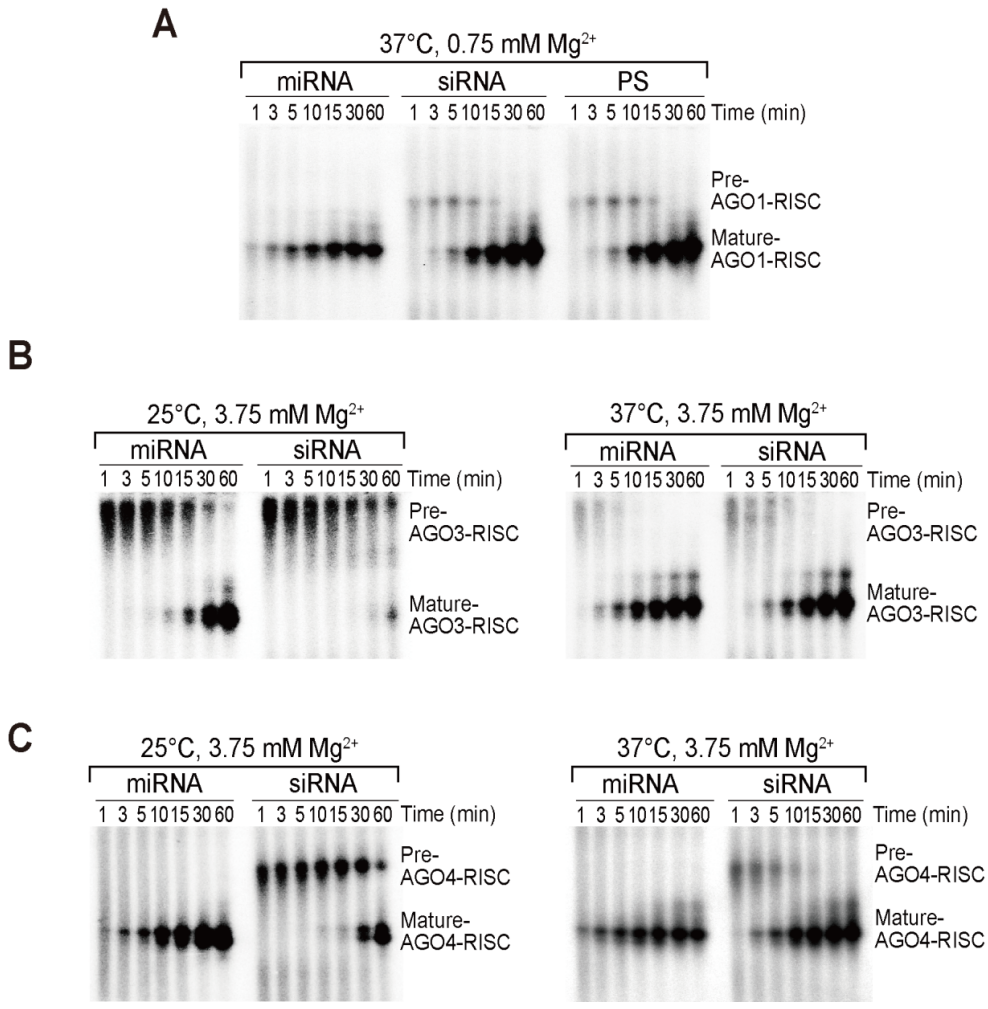
A
37°C, 0.75 mM Mg2+
miRNA
siRNA
PS
1 3 5 10 15 30 60
1 3 5 10 15 30 60
1 3 5 10 15 30 60
Time (min)
Pre-AGO1-RISC
Mature-AGO1-RISC
B
25°C, 3.75 mM Mg2+
miRNA
siRNA
1 3 5 10 15 30 60
1 3 5 10 15 30 60
Time (min)
Pre-AGO3-RISC
Mature-AGO3-RISC
37°C, 3.75 mM Mg2+
miRNA
siRNA
1 3 5 10 15 30 60
1 3 5 10 15 30 60
Time (min)
Pre-AGO3-RISC
Mature-AGO3-RISC
C
25°C, 3.75 mM Mg2+
miRNA
siRNA
1 3 5 10 15 30 60
1 3 5 10 15 30 60
Time (min)
Pre-AGO4-RISC
Mature-AGO4-RISC
37°C, 3.75 mM Mg2+
miRNA
siRNA
1 3 5 10 15 30 60
1 3 5 10 15 30 60
Time (min)
Pre-AGO4-RISC
Mature-AGO4-RISC

Spontaneous unwinding does not occur before duplexes are loaded into the Ago protein

I have shown that temperature is the major determinant for RISC maturation, especially when the slicer-assisted pathway is not functional. Considering that duplex stability is affected by temperature, I examined whether spontaneous unwinding occurs before duplexes are loaded into the Ago protein. To test this, I designed an experiment, which is shown in Fig. 11A. Canonical RISC loading exclusively requires ATP-dependent chaperone proteins (Iki et al., 2010; Iwasaki et al., 2010; Iwasaki et al., 2015; Miyoshi et al., 2010), whereas a purified, recombinant Ago protein can only incorporate single-stranded RNAs (ssRNAs) via 'bypass' loading (Bouasker and Simard, 2012; Miyoshi et al., 2005; Rivas et al., 2005; Yoda et al., 2010) (Fig. 11A). Consistent with the previous observations, the native gel-shift assay demonstrated that purified human Ago2 alone cannot utilize double-stranded RNA (dsRNA) efficiently, and that only ssRNA can be programmed completely (Fig. 12A-C). If temperature changes alone can drive the unwinding of dsRNA spontaneously, the resulting ssRNA can then be successfully incorporated into the purified hAgo2 protein (Fig. 11A). However, none of the small RNA duplexes, even the miRNA with an unstable duplex structure, spontaneously unwound at 37°C and formed a complex with the purified hAgo2 protein (Fig. 11B), indicating that temperature change *per se* is not sufficient for duplex unwinding to occur.

To address whether duplex loading is a prerequisite for unwinding, I first assembled pre-RISCs in lysates expressing FLAG-Ago2 at 15°C, where duplex loading, but not unwinding, is permissible. I then immunopurified pre-RISCs containing radiolabeled duplexes, washed them extensively at 4°C, using a high

salt (1 M NaCl) buffer to remove ATP and most of the associated proteins, and finally shifted the temperature to 37°C. When the duplex was pre-loaded into the Ago protein, dsRNA was unwound efficiently (Fig. 11C), indicating that the association of the duplex with the Ago protein is obligatory for duplex unwinding to occur. Additionally, these results are in agreement with those of previous reports showing that duplex unwinding is a passive process that does not require ATP hydrolysis (Iwasaki et al., 2010; Kawamata et al., 2009; Kawamata and Tomari, 2010; Yoda et al., 2010).

Figure 11. Temperature *per se* is not sufficient to induce duplex unwinding, but requires prior Ago loading

(A) A schematic of the experimental design. ssRNA, but not dsRNA, can be incorporated efficiently into purified human Ago2 protein in the absence of chaperone proteins. If the duplex is spontaneously unwound at 37°C, the resulting ssRNA might then be loaded into the purified Ago2 protein. (B) None of the duplexes spontaneously unwound at 37°C and form a complex with the purified Ago2 protein. Radiolabeled ssRNA or duplexes (with radiolabeled guide strands) were incubated with increasing concentrations of recombinant hAgo2 for 30 min at the indicated temperatures. Recombinant hAgo2 forms active complexes only with ssRNA. Representative data of at least two independent experiments are shown. (C) Prior duplex association with the Ago protein is necessary for duplex unwinding. siRNA duplexes carrying radiolabeled guide strands were incubated with lysates expressing tagged Ago2 for 1 h at 15°C, where duplex loading, but not unwinding, is permissible. Pre-RISCs were subsequently immunopurified at 4°C and washed six times with either low salt (150 mM) or high salt (1 M) before shifting the temperature to 37°C.

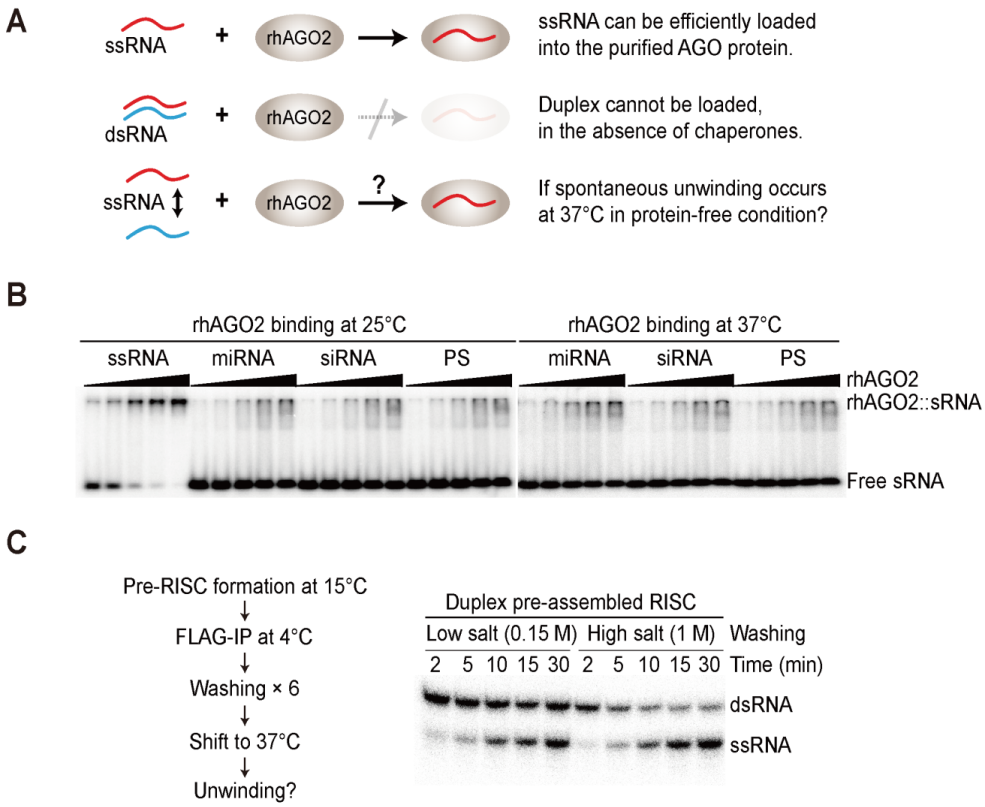
A
ssRNA
+
rhAGO2
ssRNA can be efficiently loaded into the purified AGO protein.
dsRNA
+
rhAGO2
Duplex cannot be loaded, in the absence of chaperones.
ssRNA
+
rhAGO2
?
If spontaneous unwinding occurs at 37°C in protein-free condition?
B
rhAGO2 binding at 25°C
rhAGO2 binding at 37°C
ssRNA
miRNA
siRNA
PS
miRNA
siRNA
PS
rhAGO2
rhAGO2::sRNA
Free sRNA
C
Pre-RISC formation at 15°C
FLAG-IP at 4°C
Washing × 6
Shift to 37°C
Unwinding?
Duplex pre-assembled RISC
Low salt (0.15 M)
High salt (1 M)
Washing
2 5 10 15 30 2 5 10 15 30
Time (min)
dsRNA
ssRNA

Figure 12. Recombinant human Ago2 alone can hardly utilize the siRNA duplex

(A) Radiolabeled ssRNA or siRNA (radiolabeled with guide strand) were incubated with increasing concentration of the recombinant hAgo2 (rhAgo2) for 30 min at 25°C. Complexes were analyzed by 6% native gel electrophoresis at 4°C. Recombinant Ago2 forms active complexes only with ssRNA. (B) The fraction bound to rhAgo2 was plotted against the concentration of the purified proteins. (C) The ssRNA or siRNA were incubated with increasing concentration of the recombinant hAgo2 for 15 min. Cap-radiolabeled target RNA was then added and further incubated for 15 min. The siRNA function much less efficiently than ssRNA in the cleavage assay, consistent with the gel-shift assay in (A).

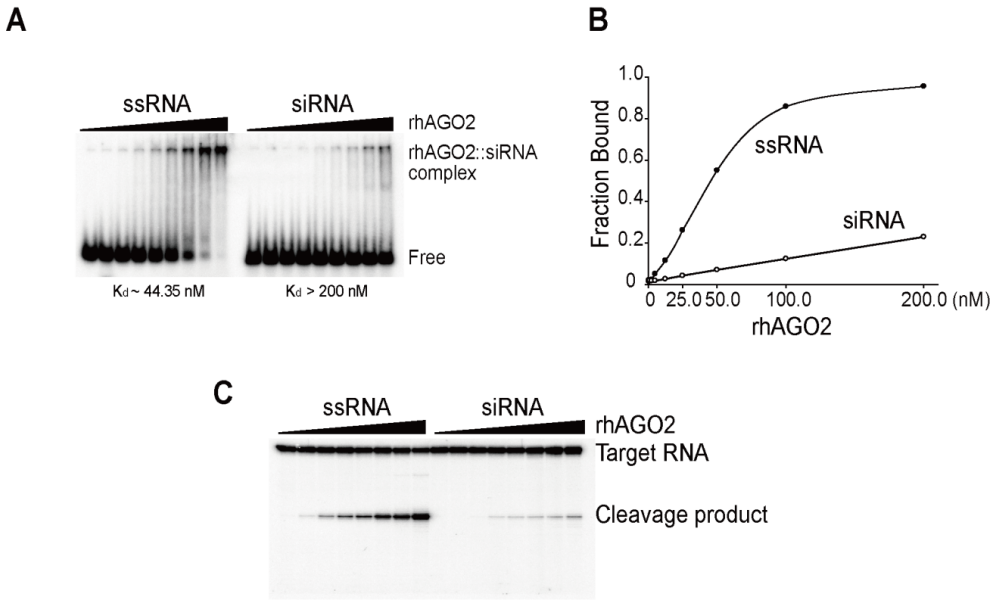
A
ssRNA
siRNA
rhAGO2
rhAGO2::siRNA complex
Free
Kd ~ 44.35 nM
Kd > 200 nM
B
Fraction Bound
1.0
0.8
0.6
0.4
0.2
0
ssRNA
siRNA
0
25.0
50.0
100.0
200.0 (nM)
rhAGO2
C
ssRNA
siRNA
rhAGO2
Target RNA
Cleavage product

Slicer-independent unwinding depends on the thermodynamic stability of the duplex structure

To gain additional mechanistic insights into duplex unwinding, I designed duplexes bearing 2′-*O*-methylated nucleotides (nts) in the passenger-strand. It should be noted that 2′-*O*-methylated nts are not only resistant to nucleases, but also form far more stable duplexes with RNA (Majlessi et al., 1998). The miRNA that retained its structure, but which had a fully 2′-*O*-methylated passenger-strand was abbreviated as miRNA-OMe (likewise, the labeled siRNA was abbreviated as siRNA-OMe) (Fig. 13A). The siRNA-OMe9 was 2′-*O*-methylated only at the 9th nt from the 5′ end of the passenger-strand (Fig. 13A). Unlike the PS modification that includes cleavable chiral isoforms (PO/PS) (Matranga et al., 2005), 2′-*O*-methylation at the 9th nt completely abrogated cleavage, as noted previously (Leuschner et al., 2006; Miyoshi et al., 2005) (Fig. 13B).

Similar to the PS duplex, the siRNA-OMe9 duplex was hardly unwound at 25°C, but efficiently unwound at 37°C, confirming that passenger-strand cleavage *per se* is not required at the physiological temperature of humans (Fig. 13C and D and Fig. 14A). To more directly test whether slicer-independent unwinding is strictly dependent on temperature, I formed pre-RISCs at 15°C for 1 h, added a 20-fold excess of cold siRNA-OMe9 duplexes (at 0 min) to deter further incorporation of radiolabeled duplexes into pre-RISCs, and shifted the temperature from 15°C to 37°C to monitor the ‘pulse-chase’ conversion of RISC maturation. Pre-RISCs were chased efficiently into mature RISCs (Fig. 13E), showing that temperature is the principal controlling factor for slicer-independent unwinding. Surprisingly, the miRNA-OMe was fully matured and functionally active at both 25°C and 37°C (Fig. 13C and D), indicating that nuclease-mediated degradation of

the passenger-strand was not obligatory, at least for an inherently unstable duplex. While duplex unwinding of the siRNA-OMe was significantly reduced (Fig. 13C and D), lowering the Mg^{2+} concentration slightly increased slicer-independent unwinding at 37°C (Fig. 13F), which may have resulted from a decrease in duplex stability. Complete RISC maturation was achieved at 42°C, although the amount of the RISC complexes decreased, possibly due to the reduced stability of the Ago proteins (Fig. 13F). Taken together, I concluded that duplex unwinding and subsequent RISC maturation are highly correlated with certain parameters, such as temperature and Mg^{2+}, which affect the thermodynamic stability of the duplex structure.

Figure 13. Effects of duplex thermodynamic stability on slicer-independent unwinding

(A) 2′-*O*Me modified small RNA duplexes used in this study; miR-1-OMe and miR-1 siRNA-OMe (full 2′-*O*Me-modified passenger-strand) and miR-1 siRNA-OMe9 (with 2′-*O*Me modification only at the 9th of the passenger-strand). Unmodified and 2′*O*Me-modified nts (denoted by N_m) are shown in black and red, respectively. (B) 2′-*O*Me-modification completely blocks the cleavage of the passenger-strand. Small RNA duplexes containing radiolabeled passenger-strands were incubated in lysates expressing tagged Ago2 for the indicated times at 25°C in the presence of 5 mM Mg^{2+} to ensure efficient passenger-strand cleavage. Unmodified siRNA served as a positive control. (C and D) The degree of RISC maturation at different temperatures depends on duplex stability. Small RNA duplexes containing radiolabeled guide strands were incubated in lysates expressing tagged Ago2 at the indicated temperature and Mg^{2+} concentrations for the indicated times. Under the same conditions, target cleavages were analyzed after 30 min of small RNA assembly. Representative data of at least two independent experiments are shown. (E) Slicer-independent unwinding is strictly temperature-dependent. Radiolabeled slicer-resistant duplex (siRNA-OMe9) was first incubated at 15°C for 1 h to assemble the pre-RISCs. Subsequently, a 20-fold excess of non-radiolabeled siRNA-OMe9 duplex (cold-competitor) was added to prevent further incorporation of the radiolabeled duplex (at 0 min) before shifting the temperature to 37°C. (F) RISC maturation is closely correlated with parameters that affect duplex stability. RISC assembly was monitored for the highly stable duplex (siRNA-OMe) in lysates expressing tagged Ago2 at the indicated temperature and Mg^{2+} concentrations at the indicated times.

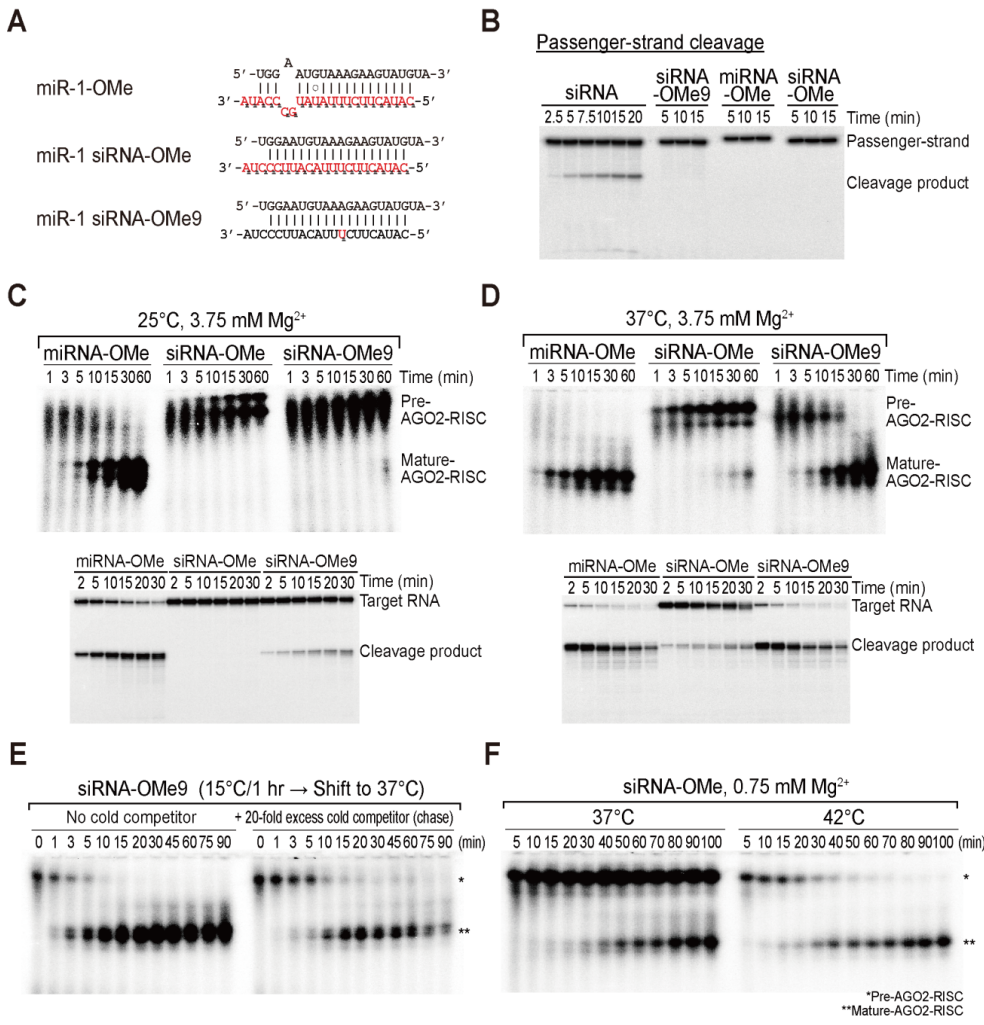
A
miR-1-OMe
miR-1 siRNA-OMe
miR-1 siRNA-OMe9
B
Passenger-strand cleavage
siRNA
siRNA -OMe9
miRNA -OMe
siRNA -OMe
Time (min)
Passenger-strand
Cleavage product
C
25°C, 3.75 mM Mg2+
miRNA-OMe
siRNA-OMe
siRNA-OMe9
Time (min)
Pre-AGO2-RISC
Mature-AGO2-RISC
Target RNA
Cleavage product
D
37°C, 3.75 mM Mg2+
E
siRNA-OMe9 (15°C/1 hr → Shift to 37°C)
No cold competitor
+ 20-fold excess cold competitor (chase)
(min)
F
siRNA-OMe, 0.75 mM Mg2+
37°C
42°C
*Pre-AGO2-RISC
**Mature-AGO2-RISC

Figure 14. Functional domains of the Ago protein are required for slicer-independent unwinding

(A) Effects of duplex stability on slicer-independent unwinding by Ago1 (related to Fig. 13D). Small RNA duplexes containing radiolabeled guide strands were incubated in lysates expressing tagged Ago1 at the indicated temperature and Mg^{2+} concentrations for the indicated times. (B-C) Western blot analysis using an anti-FLAG antibody confirmed the expression of tagged Ago2 mutant proteins. Anti-tubulin served as an internal control. (D) miRNA duplexes containing radiolabeled guide strands were incubated in lysates expressing tagged wild-type and PAZ or N-truncated Ago2 proteins at the indicated temperature and Mg^{2+} for the indicated times.

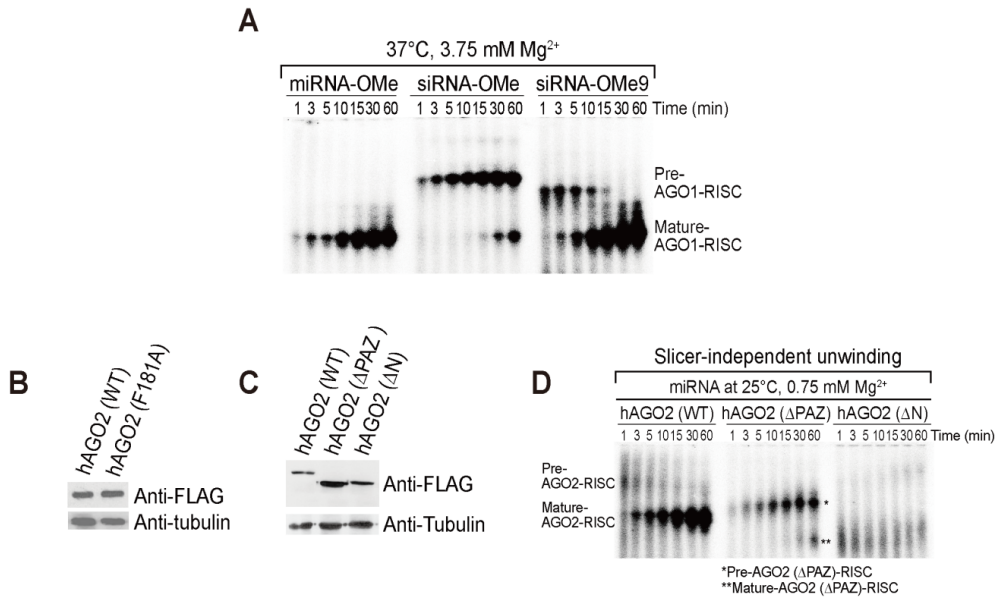
A
37°C, 3.75 mM Mg2+
miRNA-OMe
siRNA-OMe
siRNA-OMe9
1 3 5 10 15 30 60
Time (min)
Pre-AGO1-RISC
Mature-AGO1-RISC
B
hAGO2 (WT)
hAGO2 (F181A)
Anti-FLAG
Anti-tubulin
C
hAGO2 (WT)
hAGO2 (ΔPAZ)
hAGO2 (ΔN)
Anti-FLAG
Anti-Tubulin
D
Slicer-independent unwinding
miRNA at 25°C, 0.75 mM Mg2+
hAGO2 (WT)
hAGO2 (ΔPAZ)
hAGO2 (ΔN)
Pre-AGO2-RISC
Mature-AGO2-RISC
*Pre-AGO2 (ΔPAZ)-RISC
**Mature-AGO2 (ΔPAZ)-RISC

Slicer-independent unwinding requires the functional domains of the Ago protein

As previously proposed, slicer-independent unwinding is the reverse process of target recognition, with the passenger-strand being a target (Gu et al., 2012; Kawamata et al., 2009; Kawamata and Tomari, 2010) (Fig. 15A). Structural studies have shown that during target recognition (nucleation → propagation), the N domain restricts additional base-pairing (beyond 16th) and the PAZ domain dynamically interacts with the 3′ end of the guide strand, with the help of the pivotal movement of the Ago proteins (Wang et al., 2009) (Fig. 15A). Such 'wedging' of the N domain and/or 3′ end anchoring of the PAZ domain are expected to antagonize base-pairing, and thereby pry the duplex apart, as previously reported (Gu et al., 2012; Kwak and Tomari, 2012).

Given that temperature severely influences the efficiency of slicer-independent unwinding, I further examined the effects of temperature, with consideration of these functional domains. I initially tested an N domain mutant (F181A) Ago2 (Fig. 14B) that is defective for unwinding, but not for target cleavage (Kwak and Tomari, 2012). At 25°C, the siRNA duplex was unwound efficiently via passenger-strand cleavage in the presence of 3.75 mM Mg^{2+} by wild-type Ago2, whereas the N domain mutant failed to generate a mature RISC under the same conditions (Fig. 15B), suggesting that 'wedging' is required mostly at the early stage of RISC assembly prior to the cleavage of the passenger-strand. This strong defect of the N domain mutant was partly rescued for the miRNA duplex, although unwinding was still less efficient than for wild-type Ago2 (Fig. 15B). Interestingly, the residual defects were largely rescued at 37°C, indicating that higher temperatures could partially offset the wedging defects (Fig. 15C).

I further investigated the effect of more severe mutations by creating truncated Ago2 proteins that completely lacked the PAZ or N domains (ΔPAZ or ΔN, respectively) (Fig. 14C). Although the ΔN protein was not competent to form RISC complexes (Fig. 14C), the ΔPAZ protein was able to load miRNA duplexes, as previously shown in an *in vivo* study (Gu et al., 2012) (Fig. 15D). For wild-type Ago2, the miRNA duplex was unwound almost instantaneously, whereas the ΔPAZ protein exhibited a severe defect (Fig. 15D and E), indicating that a functional PAZ domain is strictly required for slicer-independent unwinding. When tested with the slicer-resistant siRNA (OMe9), the ΔPAZ protein could not load the siRNA duplex effectively (Fig. 15F). A less severe mutant (F181A) could form the pre-RISC successfully, but exhibited much slower unwinding activity than wild-type Ago2, whereas a PIWI catalytic mutant (D597A) displayed no defects (Fig. 15F). Taken together, I conclude that functional N and PAZ domains are required for slicer-independent unwinding, whereas slicer-activity of Ago2 *per se* is largely dispensable at the physiological temperature of humans.

Figure 15. Slicer-independent unwinding is mediated by the functional domains of the Ago protein

(A) Left panel: A structural representation of the Ago protein during target RNA recognition. The guide strand (red) binds to its target (light blue) from the 5′ seed-portion (nucleation) and extends to form a double helix (propagation) that terminates at position 16, which is blocked by the N domain. During the propagation step, the 3′ end of the guide is released from its anchor site in the PAZ domain with the help of pivotal movement of Ago. Right panel: Slicer-independent unwinding is assumed to be the reverse process of target RNA recognition, with the passenger-strand being a target. The N and PAZ domains might play a role in duplex unwinding because the N domain blocks additional pairing (beyond 16^{th}) at the 3′ end, which could be further disrupted by dynamic 3′ anchoring of the PAZ domain. (B-C) N mutant (F181A) is defective for both slicer-dependent and -independent unwinding. Small RNA duplexes containing radiolabeled guide strands were incubated in lysates expressing tagged wild-type and N mutant (F181A) Ago2 proteins at the indicated temperature and Mg^{2+} concentrations for the indicated times. A higher temperature could partially compensate for the wedging defect. Representative data of at least two independent experiments are shown. (D) PAZ truncation causes a severe defect in slicer-independent unwinding. miRNA duplexes containing radiolabeled guide strands were incubated in lysates expressing tagged wild-type or PAZ-truncated Ago2 proteins at the indicated temperature and Mg^{2+} for the indicated times. Note that the size of the ΔPAZ-RISC complexes shifted downward due to the truncation of the PAZ domain. (E) Quantitation of (D). Data are mean ± SD for two independent experiments. (F) Functional domains of Ago2 are required for unwinding, but Ago2-mediated slicer-activity *per se* is dispensable at the physiological temperature of humans. Slicer-resistant duplex (siRNA-OMe9) containing radiolabeled guide strand was incubated in lysates expressing tagged wild-type, PAZ truncation (ΔPAZ), N mutant (F181A) and PIWI catalytic mutant (D597A) Ago2 proteins at the indicated temperature and Mg^{2+} concentration for the indicated times.

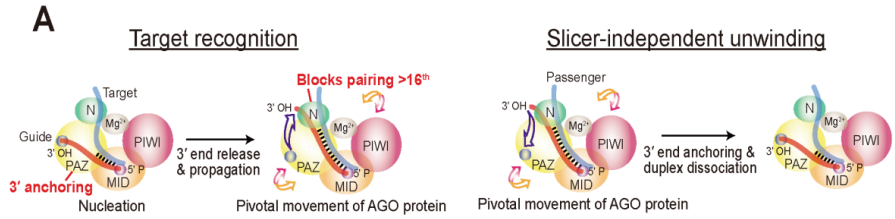
A
Target recognition
Slicer-independent unwinding
Target
Guide
3′ anchoring
Nucleation
3′ end release & propagation
Blocks pairing >16th
Pivotal movement of AGO protein
Passenger
3′ end anchoring & duplex dissociation
Pivotal movement of AGO protein
N
PAZ
PIWI
MID

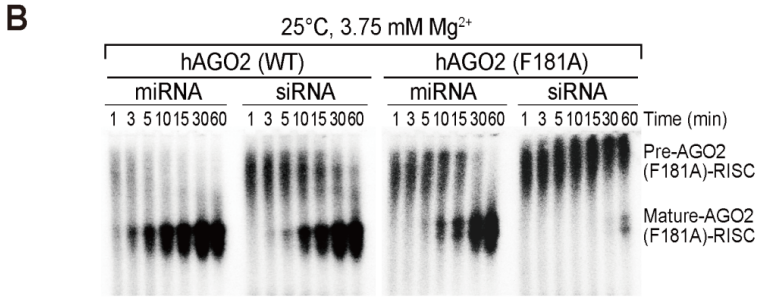
B
25°C, 3.75 mM Mg2+
hAGO2 (WT)
hAGO2 (F181A)
miRNA
siRNA
1 3 5 10 15 30 60 Time (min)
Pre-AGO2 (F181A)-RISC
Mature-AGO2 (F181A)-RISC

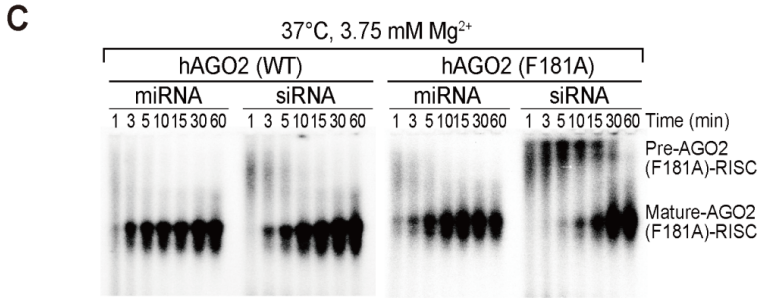
C
37°C, 3.75 mM Mg2+
hAGO2 (WT)
hAGO2 (F181A)
miRNA
siRNA
1 3 5 10 15 30 60 Time (min)
Pre-AGO2 (F181A)-RISC
Mature-AGO2 (F181A)-RISC

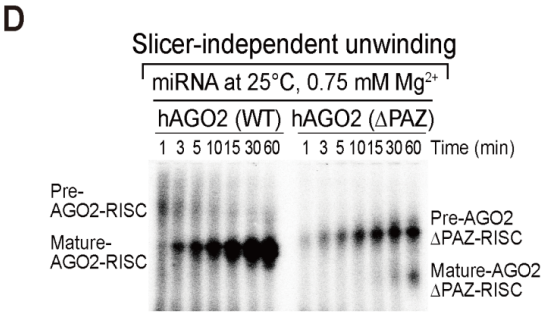
D
Slicer-independent unwinding
miRNA at 25°C, 0.75 mM Mg2+
hAGO2 (WT)
hAGO2 (ΔPAZ)
1 3 5 10 15 30 60 Time (min)
Pre-AGO2-RISC
Mature-AGO2-RISC
Pre-AGO2 ΔPAZ-RISC
Mature-AGO2 ΔPAZ-RISC

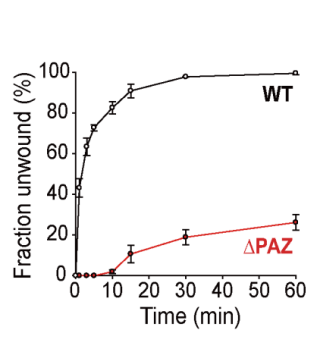
E
Fraction unwound (%)
100
80
60
40
20
0
WT
ΔPAZ
0 10 20 30 40 50 60
Time (min)

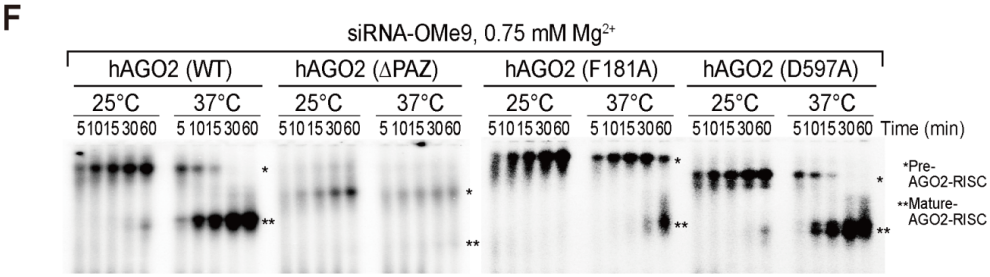
F
siRNA-OMe9, 0.75 mM Mg2+
hAGO2 (WT)
hAGO2 (ΔPAZ)
hAGO2 (F181A)
hAGO2 (D597A)
25°C
37°C
5 10 15 30 60 Time (min)
*Pre-AGO2-RISC
**Mature-AGO2-RISC

Slicer-independent unwinding is a general mechanism for human RISC maturation

My data strongly suggest that slicer-independent unwinding is likely to play a dominant role in human RISC. To substantiate this idea *in vivo*, I designed 'artificial' siRNA duplexes targeting GAPDH mRNA (siGAPDH) (Fig. 16A). The 9th nt from the 5′ end of the passenger-strand was modified by a 2′-*O*-methyl group (siGAPDH-OMe9) that completely blocked passenger-strand cleavage (Fig. 16B). While the knockdown effects were not appreciable at 28°C, the siGAPDH-OMe9 duplex displayed a silencing potency comparable to its conventional counterpart under normal cell culture conditions (Fig. 16C). These results indicate that slicer-independent unwinding plays a dominant role in human RISC maturation, as was also confirmed in other tested duplexes (Fig. 16D and E) and via endogenous Ago2 in HeLa cell lysates (Fig. 16F).

Figure 16. Slicer-independent unwinding is a general mechanism for human RISC maturation

(A) Artificially designed siRNA duplexes targeting an endogenous mRNA. siGAPDH; functionally asymmetric siRNA designed to target GAPDH and siGAPDH-OMe9; 2′-*O*Me modification at the 9th nt to block passenger-strand cleavage. (B) Passenger-strand cleavage in the siGAPDH-OMe9 duplex is abrogated. Small RNA duplexes containing radiolabeled passenger-strands were incubated in lysates expressing tagged Ago2 for the indicated times at 25°C in the presence of 5 mM Mg^{2+} to ensure an efficient passenger-strand cleavage. (C) The siGAPDH-OMe9 duplex can elicit an effective silencing response with similar potency as its conventional counterpart. HeLa S3 cells were transfected with 10 nM of siGFP (mock), siGAPDH and siGAPDH-OMe9. HEK293T cells were co-transfected with 10 nM of the indicated siRNAs and Ago2 plasmids. Cells were then cultured either at 28 or 37°C and harvested at 24 h post-transfection, and analyzed by western blotting. The numbers below the western blot are the relative expression levels, normalized using β-tubulin loading control. (D) let-7a siRNA OMe9; let-7a was perfectly paired to its antisense, except for the 1st position from the 5′ end. 2′-*O*Me modification at the 9th nt from the 5′ end of passenger-strand. Unmodified and 2′-*O*Me-modified nucleotide (denoted by N_m) are shown in black and red, respectively. let-7a siRNA-OMe9 duplex was hardly unwound at 25°C, but effectively unwound at 37°C, as expected. Small RNA duplex containing radiolabeled guide strand was incubated in lysates expressing tagged Ago2 at the indicated temperature for the indicated times. (E) Endogenous miRNAs often have multiple mismatches and G-U wobble base pairs (let-7a as a representative example) that enable highly efficient unwinding. miRNA duplexes containing radiolabeled guide-strands were incubated in lysates expressing tagged Ago2 at 25°C for the indicated times. miRNA duplexes form mature RISCs rapidly and efficiently. (F) Target cleavage assay in an endogenous Ago2 in HeLa cell lysates. Small RNA duplexes were assembled in naive HeLa cell lysates for 15 min at the indicated temperature before the addition of cap-radiolabeled target RNA. These results, largely consistent with the results from HEK293T cells, suggest that slicer-independent unwinding plays a dominant role in human RISC maturation.

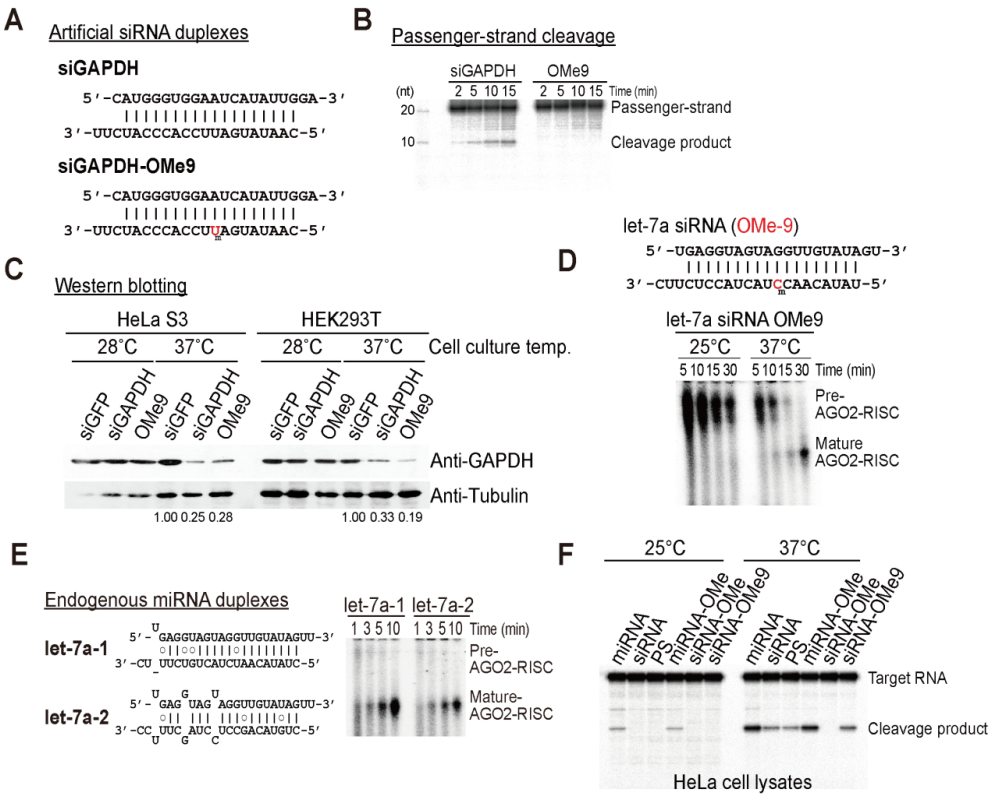
A
Artificial siRNA duplexes
siGAPDH
5′-CAUGGGUGGAAUCAUAUUGGA-3′
3′-UUCUACCCACCUUAGUAUAAC-5′
siGAPDH-OMe9
5′-CAUGGGUGGAAUCAUAUUGGA-3′
3′-UUCUACCCACCUUAGUAUAAC-5′
B
Passenger-strand cleavage
siGAPDH
OMe9
(nt)
2 5 10 15
2 5 10 15
Time (min)
20
10
Passenger-strand
Cleavage product
C
Western blotting
HeLa S3
HEK293T
28°C
37°C
28°C
37°C
Cell culture temp.
siGFP
siGAPDH
OMe9
Anti-GAPDH
Anti-Tubulin
1.00 0.25 0.28
1.00 0.33 0.19
D
let-7a siRNA (OMe-9)
5′-UGAGGUAGUAGGUUGUAUAGU-3′
3′-CUUCUCCAUCAUCCAACAUAU-5′
let-7a siRNA OMe9
25°C
37°C
5 10 15 30
5 10 15 30
Time (min)
Pre-AGO2-RISC
Mature AGO2-RISC
E
Endogenous miRNA duplexes
let-7a-1
let-7a-2
let-7a-1
let-7a-2
1 3 5 10
1 3 5 10
Time (min)
Pre-AGO2-RISC
Mature-AGO2-RISC
F
25°C
37°C
miRNA
siRNA
PS
miRNA-OMe
siRNA-OMe
siRNA-OMe9
Target RNA
Cleavage product
HeLa cell lysates

Slicer-independent unwinding is a conserved mechanism

Small RNAs have been documented in varied organisms, and my results raise an interesting question of how temperature affects the RISC maturation of organisms that maintain a wide range of physiological temperatures. *Drosophila* was the first model organism used to study RNAi *in vitro* (Haley et al., 2003), and its mechanism of action is one of the best characterized. Likewise, slicer-dependent unwinding was mainly demonstrated in *Drosophila* (Matranga et al., 2005; Miyoshi et al., 2005; Rand et al., 2005), which shows a temperature preference for 25°C. Is the mechanism of slicer-independent unwinding also conserved in *Drosophila*? To answer this question, I performed a fly Ago2-mediated target cleavage assay using S2 cell lysates at various ambient temperatures. Only the siRNA exhibited a minimal cleavage activity at 15°C in the presence of 3.75 mM Mg^{2+}, indicating that slicer-independent unwinding was not available at this temperature (Fig. 17A). At the physiological temperature of *Drosophila*, the siRNA produced active RISCs, whereas the OMe9 duplex did much less efficiently (Fig. 17B), suggesting that passenger-strand cleavage greatly accelerates the rate of RISC assembly at 25°C, as shown previously (Matranga et al., 2005; Miyoshi et al., 2005; Rand et al., 2005). In contrast, the contribution of the slicer-dependent pathway became much less important when the temperature was increased to 30°C (Fig. 17C). Finally, the slicer-independent pathway appeared to exert a predominant influence on RISC maturation at 37°C, the physiological temperature of humans (Fig. 17D). An extended incubation (> 30 min) at 37°C severely impaired RISC activity (data not shown), indicating that the *Drosophila* Ago protein does not function optimally (and is even possibly detrimental) at high temperature. Based on these results, I concluded that slicer-independent unwinding

is likely to be a conserved mechanism for RISC maturation, although the extent to which the slicer-dependent pathway contributes to RISC maturation may vary greatly, depending on the respective body temperatures of living organisms.

Figure 17. Slicer-independent unwinding is a conserved mechanism

(A-D) Distinct slicer-dependency at different temperatures in *Drosophila* Ago2. Small RNAs were assembled in S2 cell lysates only for 5 min (to avoid early saturation) at the indicated temperature and Mg^{2+} level. Cap-radiolabeled target RNA was then added and incubated for the indicated times at the indicated temperatures and Mg^{2+} concentrations. Quantitation of the fraction target cleaved (%) is shown below the gel image. Black: siRNA with 3.75 mM Mg^{2+}, Brown: siRNA-OMe9 with 3.75 mM Mg^{2+}, Gray: siRNA with 0.75 mM Mg^{2+}, Red: siRNA-OMe9 with 0.75 mM Mg^{2+}. Data are mean ± SD for at least two independent experiments. (E) A propose model for small RNA maturation in human RISCs. miRNAs are unwound most efficiently in all four human Ago proteins through the aid of internal mismatches. Slicer-deficient Ago proteins (1, 3, and 4) are able to unwind the highly complementary siRNA in a temperature-dependent manner. Ago2 can additionally utilize its slicer-activity for the highly complementary siRNA with slicer-dependency being positively correlated to the Mg^{2+} concentration and negatively correlated to temperature.

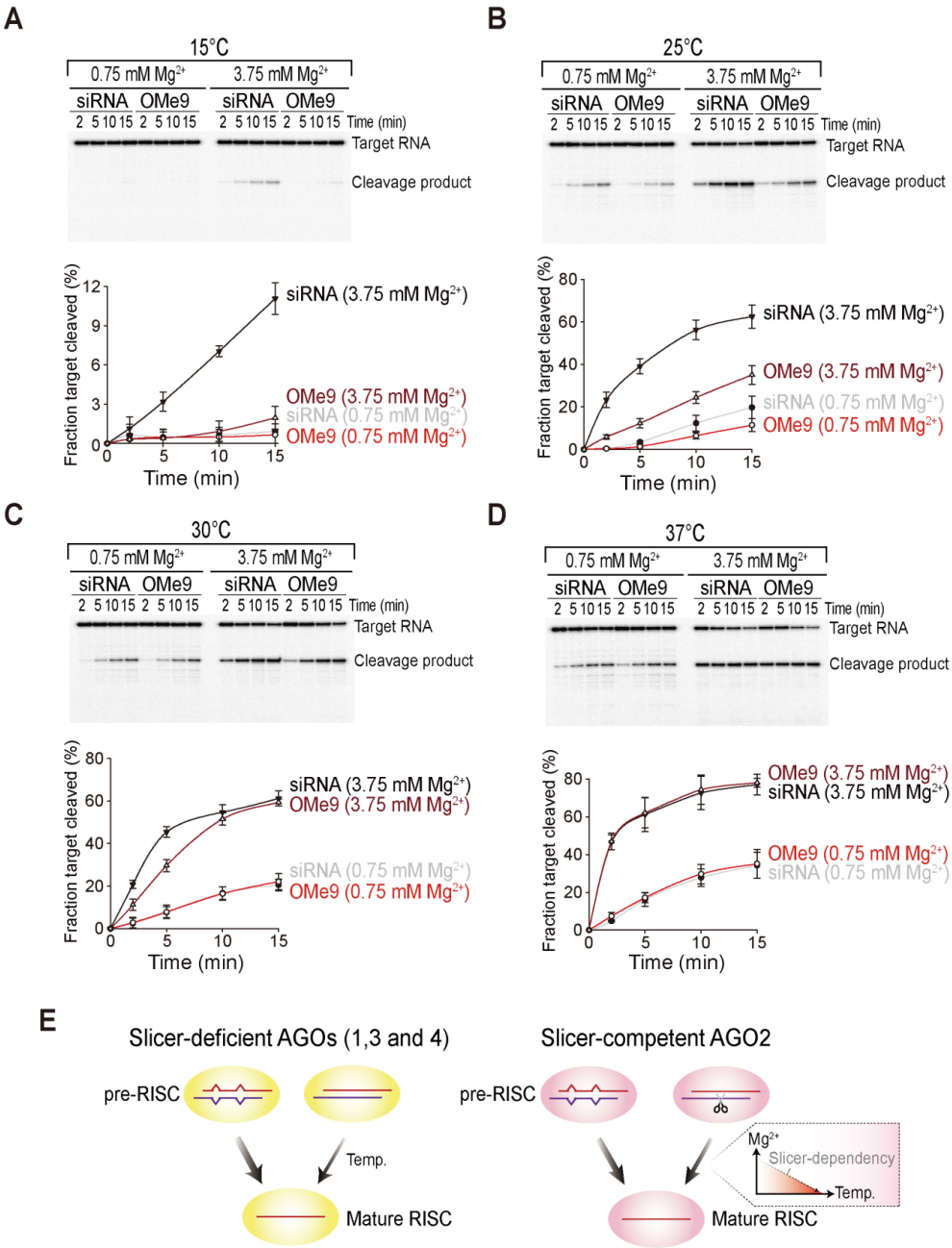
A
15°C
0.75 mM Mg2+
3.75 mM Mg2+
siRNA OMe9 siRNA OMe9
2 5 10 15 2 5 10 15 2 5 10 15 2 5 10 15 Time (min)
Target RNA
Cleavage product
Fraction target cleaved (%)
siRNA (3.75 mM Mg2+)
OMe9 (3.75 mM Mg2+)
siRNA (0.75 mM Mg2+)
OMe9 (0.75 mM Mg2+)
Time (min)
B
25°C
C
30°C
D
37°C
E
Slicer-deficient AGOs (1,3 and 4)
Slicer-competent AGO2
pre-RISC
Temp.
Mature RISC
Mg2+
Slicer-dependency

Discussion

Since the first discovery of the passenger-strand cleavage mechanism a decade ago, it has been widely recognized that slicer-dependent unwinding is a prerequisite for the assembly of highly complementary siRNAs into RISCs (Matranga et al., 2005; Miyoshi et al., 2005; Rand et al., 2005). My collective results indicate that this assumption is typically valid, but not always, particularly for mammals and birds. Earlier biochemical studies relied mainly on target cleavage assays to understand the overall nature of RISC catalysis, which often tended to dismiss important differences during the early stages of RISC assembly. Through a careful reexamination of RISC assembly using a variety of several biochemical analyses, including duplex loading, slicer-dependent and -independent unwinding, and classical target cleavage assays, I established here that slicer-independent unwinding is a more prevalent mechanism for human RISC maturation than previously thought, not only for miRNA duplexes but also for highly complementary siRNAs as well. Aside from the main findings, there are several other findings that are important to discuss in detail.

Small RNA sorting and the Mg^{2+} level in slicer-dependent unwinding

It has been previously recognized that only Ago2 can efficiently unwind siRNA duplexes via passenger-strand cleavage in humans (Yoda et al., 2010), and this is reasonable in the sense that Ago2 is among the most advantageous human Ago proteins that can utilize its slicer-activity (Liu et al., 2004; Meister et al., 2004b) for RISC maturation (Fig. 17E). Nonetheless, I showed that cleavage-deficient Ago proteins (1, 3, and 4) can also be programmed with siRNAs at the physiologically relevant temperature of humans, suggesting that slicer-independent

unwinding is likely a common feature of human Ago proteins. These observations provided a natural explanation for why both miRNAs and siRNAs are found in all four human Ago proteins, irrespective of their sequences (Azuma-Mukai et al., 2008; Su et al., 2009). In contrast with weak small RNA sorting in humans, siRNA duplexes are specifically sorted into fly Ago2 (Forstemann et al., 2007; Tomari et al., 2007), which is essential for antiviral defense (van Rij et al., 2006). The fly Ago2 should therefore acquire an additional strategy for siRNA maturation (i.e., passenger-strand cleavage), otherwise not efficient at their body temperature.

I showed that a certain level of Mg^{2+} is required for slicer-dependent unwinding to occur efficiently (Fig. 6A). While the free cytosolic Mg^{2+} level is less than 1 mM under normal conditions (Gunther, 2006), the total cellular Mg^{2+} concentration can vary from 5 to 20 mM (Maguire and Cowan, 2002; Moomaw and Maguire, 2008), as most Mg^{2+} ions are bound to proteins and negatively charged molecules (Maguire and Cowan, 2002; Moomaw and Maguire, 2008). Therefore, it is difficult to estimate the exact amount of Mg^{2+} bound to Ago2, although previous studies typically used 1.5–5 mM Mg^{2+} for the *in vitro* slicing assays (Liu et al., 2004; Matranga et al., 2005; Meister et al., 2004b; Miyoshi et al., 2005; Miyoshi et al., 2008). In addition, cytosolic Mg^{2+} levels can be altered by ATP, which is capable of chelating Mg^{2+} ions (Grubbs, 2002). In other words, a transient decrease in ATP levels may give rise to a sudden increase in the Mg^{2+} concentration (Grubbs, 2002). During two steps of RISC assembly, duplex loading requires ATP hydrolysis, and subsequent cleavage of the passenger-strand requires a relatively high level of Mg^{2+}. It is tempting to speculate that bursts of metabolic activity during pre-RISC formation may induce a transient decrease in ATP that results in an increase in Mg^{2+} levels that allows for more efficient slicer-activity,

although it is technically difficult to demonstrate such rapid and transient changes.

Slicer-independent unwinding in human RISCs

Although chaperone machinery-mediated duplex loading is relatively well understood (Iki et al., 2010; Iwasaki et al., 2010; Iwasaki et al., 2015; Miyoshi et al., 2010), it is still remain elusive how the loaded duplex unwinds to form the mature RISC. The helicase model was proposed at the beginning of the RNAi field — an ATP-dependent helicase separates the two strands of the duplex before they are loaded into the Ago protein (Nykanen et al., 2001), although such an 'unwindase' has yet to be identified (Kawamata and Tomari, 2010). Another model assumes that duplexes are loaded into the Ago protein, which itself can dissociate the two strands (Gu et al., 2012; Kawamata et al., 2009; Kawamata and Tomari, 2010; Kwak and Tomari, 2012). My findings, combined with those of previous studies, point to the latter model as a more plausible scenario. It has been extensively demonstrated that Ago proteins receive duplexes, rather than single strands, during RISC assembly (Iwasaki et al., 2010; Kawamata et al., 2009; Leuschner et al., 2006; Matranga et al., 2005; Miyoshi et al., 2005; Miyoshi et al., 2010; Rand et al., 2005; Yoda et al., 2010). Once a duplex is deeply buried within the Ago protein, it is difficult to comprehend how the duplex is further transferred from Ago proteins to other regulatory factors in an accessible form. I showed that the unwinding process was significantly influenced by intrinsic factors, such as temperature and Mg^{2+}, both of which were closely related to duplex stability. The functional analyses also indicated that the Ago protein itself is a key factor that is needed for duplex unwinding. Recent structural studies have corroborated the idea that target dissociation is strongly coupled to a profound conformational change in

the Ago proteins, which results in a widening of the N-PAZ channel, thereby leading to a disruption of the base-pairing in the 3′ half of the guide (Jung et al., 2013; Schirle et al., 2014). I postulate that high temperature may favor a conformational change (Bonincontro et al., 2001; Caldwell, 1989) in the Ago protein that accelerates RISC maturation.

miRNAs are the most abundant and common endogenous substrates for human Ago proteins and they often have multiple mismatches and G-U wobble base pairs (or even bulges) that enable highly efficient unwinding (Fig. 16E and 17E). In contrast, a highly complementary siRNA duplex requires either a certain temperature or Ago2-mediated cleavage of passenger-strands, which results in a drastic change in the thermodynamic profile of the duplex. siRNA unwinding by Ago2 depends upon two main factors with opposite effects: temperature and Mg^{2+} (Fig. 17E). At the physiological temperature of humans, siRNAs could also be incorporated into slicer-deficient Ago proteins (1, 3, and 4) to form the mature RISC (Fig. 17E). In mammals, endogenous siRNAs can repress complementary mRNAs and transposons in mouse oocytes (Watanabe et al., 2008) and embryonic stem cells (Babiarz et al., 2008), although little is known about their biological role.

A thermodynamic perspective of RISC maturation

In light of my current findings, as well as those of previous reports, I envision that the overall process of RISC assembly has characteristics closely resembling those of a classical thermodynamic reaction (Fig. 18). Duplex loading requires the energy from ATP hydrolysis (i.e., E_a) to trigger a conformational change in the Ago proteins that is mediated by the Hsc70-Hsp90 chaperone

machinery (Iki et al., 2010; Iwasaki et al., 2010; Iwasaki et al., 2015; Miyoshi et al., 2010). In this regards, the pre-RISC can be considered to be a transition state during RISC assembly (Fig. 18). The mature RISC is thought to be the most stable and energetically favorable state ($\Delta H < 0$) (Fig. 18). This assumption is supported by the fact that Ago proteins mostly co-purify with endogenous guide RNAs and were stable enough to be structurally resolved by crystallography (Elkayam et al., 2012; Faehnle et al., 2013; Schirle and MacRae, 2012; Schirle et al., 2014).

Because duplex unwinding is generally accompanied by an increase in entropy (Gabelica and De Pauw, 2002; Kool, 2001) ($\Delta S > 0$), the spontaneity ($\Delta G = \Delta H - T\Delta S$) of RISC maturation is then largely influenced by the temperature that contributes to the entropy of the system. Although this may seem to be plausible, I cannot warrant further speculation with the present biochemical data alone. Future studies combining structural analyses with biophysical techniques are necessary to reveal the structural basis for duplex unwinding, as well as its thermodynamics.

Homeotherms, such as mammals and birds, have a specific physiological adaptation that enables them to regulate their body temperature from 36 to 42°C (Ruben, 1995). In contrast, poikilotherms, including worms, flies, plants, and fish, lack the means to generate heat (Bennett, 1978). Therefore, the body temperatures of these animals tend to conform to their external environment, and temperature fluctuations may affect numerous aspects of their physiology, including enzyme function, muscle activity, and energy metabolism (Bennett, 1978). My results suggested that the last step of small RNA biogenesis could be largely influenced by such temperature changes, which may provide a means to fine-tune the expression of small RNAs in various living organisms.

Figure 18. An envisioned model for human RISC assembly

An envisioned model is thoroughly described in the discussion section of the subheading ‘A thermodynamic perspective of RISC maturation’. I assume that the mature RISC is among the most stable and energetically favorable form, whereas the free- and pre-RISC are expected to be more dynamic. Slicer-independent unwinding (red) plays a dominant role in small RNA maturation at mammalian body temperatures, whereas slicer-dependent unwinding (blue) may serve as an indispensable strategy for organisms with low body temperatures, and it is enhanced by the presence of high Mg^{2+} levels (light red). The relative stability (green) of the RISC complexes is inversely correlated to the energy states. ΔH, enthalpy; E_a, activation energy.

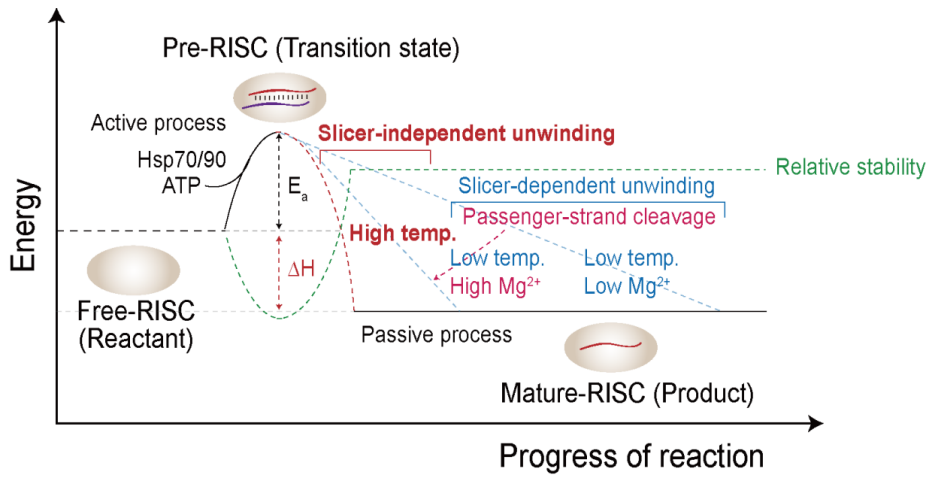
Pre-RISC (Transition state)
Active process
Hsp70/90
ATP
E_a
Slicer-independent unwinding
Relative stability
Slicer-dependent unwinding
Passenger-strand cleavage
High temp.
Low temp.
High Mg^{2+}
Low temp.
Low Mg^{2+}
ΔH
Energy
Free-RISC
(Reactant)
Passive process
Mature-RISC (Product)
Progress of reaction

CHAPTER II

Non-canonical Targets Destabilize MicroRNAs in Human Argonautes

This chapter is to be published as;

Park, J.H., Shin, S.Y., and Shin, C. (2017). Non-canonical targets destabilize microRNAs in human Argonautes. *Nucleic Acids Res.* (*in press*)

** Featured as NAR breakthrough article (Top paper published in the Journal)*

Introduction

MicroRNAs (miRNAs) are ~22-nucleotide (nt), small regulatory RNA molecules that play important roles in a wide range of biological processes. miRNAs are transcribed as primary miRNA (pri-miRNA) transcripts that are processed via two cleavage steps that are mediated by Drosha and Dicer (Kim et al., 2009; Macias et al., 2013). These tandem actions convert pri-miRNAs into precursor miRNAs (pre-miRNAs) and finally results in the production of the ~21–23 nucleotide (nt) miRNA duplexes. The miRNA duplexes, which contain a 5′ phosphate and a 2-nt 3′ overhang on each end, are subsequently loaded into Argonaute proteins with the aid of chaperone machinery (Iwasaki et al., 2010; Miyoshi et al., 2010). The two strands of the duplex are separated within the Argonaute (Ago) proteins. One of the strands is retained as the guide, whereas the other, the passenger strand, is cleaved (Matranga et al., 2005) and/or ejected (Nakanishi, 2016; Park and Shin, 2015). The seed region (nt 2–8) of mature miRNAs directs the RNA-induced silencing complex (RISC) to target mRNAs by binding to complementary sequences (Bartel, 2009), which results in mRNA destabilization and/or translational repression (Iwakawa and Tomari, 2015; Jonas and Izaurralde, 2015).

Precisely controlled expression of miRNAs is important to ensure that their targets are repressed properly. Although much is known about miRNA biogenesis and its regulation, especially at the level of the pre-miRNAs (Ha and Kim, 2014; Heo et al., 2009; Liu et al., 2014), relatively little is known about how functional, mature miRNAs are turned over and degraded. Once loaded into Ago proteins, miRNAs are stabilized (Martinez and Gregory, 2013; Winter and Diederichs, 2011), with half-lives raging from hours to days (Baccarini et al.,

2011). However, mounting evidence suggests that they are also subjected to active regulation under specific cellular contexts, including development, differentiation, viral infection, and in response to stimuli (Hwang et al., 2009; Krol et al., 2010; Olejniczak et al., 2013; Rissland et al., 2011). These observations raise intriguing questions regarding the nature of the general triggers affecting miRNA stability. Because 5′ and 3′ ends of miRNAs are bound to the MID and PAZ domains of Argonaute, respectively (Frank et al., 2010; Ma et al., 2004), they are likely to require dissociation from Argonaute in order to become susceptible to degradation by nucleases (*i.e.*, miRNA destabilization). Recent findings suggest that interactions between miRNAs and their highly complementary targets promote miRNA destabilization and release from Argonautes (De et al., 2013), which is accompanied by the accumulation of 3′ miRNA isoforms (Ameres et al., 2010; de la Mata et al., 2015), although the detailed mechanisms underlying such target RNA-directed miRNA destabilization remain largely unknown.

Here, using an *in vitro* system that consists of a minimal Ago2-RISC in cell lysates, I sought to understand how miRNAs in human Argonautes are destabilized by their targets. During the course of my studies, surprisingly, I found that seedless, non-canonical targets, which are increasingly recognized as being more widespread than initially anticipated (Broughton et al., 2016; Grosswendt et al., 2014; Helwak et al., 2013; Loeb et al., 2012; Moore et al., 2015), destabilize miRNAs in human Argonautes. I also demonstrated that the target-directed mechanism entails not only unloading but also 3′ end destabilization of miRNAs within Argonaute, which is driven by the dynamic nature of the L1-PAZ domain. Furthermore, I analyzed target sequence constraints in detail, and showed that extensive 3′ pairing is primarily responsible for conferring the specificity of non-

canonical interactions. My combined results provide novel mechanistic insights into the dynamic interplay between miRNAs and their targets, which increase our understanding of how miRNAs are regulated in humans.

Materials and methods

Cell culture

HEK293T and HeLa S3 cells were cultured in Dulbecco's modified Eagle's medium that was supplemented with 10% (v/v) fetal bovine serum, 100 U/ml penicillin and 100 μg/ml streptomycin at 37°C in an atmosphere with 5% CO_2. *Drosophila* S2 cells were cultured at 25°C in Schneider's medium supplemented with 10% fetal bovine serum.

Cell lysate preparation

HEK293T cells at 30–50% confluence were transfected with FLAG-tagged Ago expression plasmids (10 μg per 100-mm dish) using the calcium phosphate method, and they were harvested after 48 h. Cytoplasmic lysates from HEK293T cells were prepared essentially as described (Park and Shin, 2015). To obtain the expression plasmids encoding the FLAG-tagged human Ago proteins, the coding region of each cDNA fragment was inserted into pcDNA-based vectors (Invitrogen). The plasmids for hAgo1 and the catalytic (D597A) and hinge (F181A) mutants of hAgo2 were generated previously (Park and Shin, 2015). The PAZ (H271A, R277A, K278A, R280A, Y311A, H316A, Y311A/H316A, H271A/Y311A/H316A, R277A/K278A/R280A, Δ277-280) and L1-PAZ hinge (F181A/Y311A) mutants of hAgo2 were generated by site-directed mutagenesis using the primers listed in Table 2.

In vitro target RNA-directed miRNA destabilization assay

miRNAs were assembled into Ago2-RISC under standard *in vitro* RNAi conditions (Haley et al., 2003) that typically contained 2.5 μl of cell lysate, 1.5 μl of reaction

mix (Haley et al., 2003), and 0.5 μl of 100–200 nM of radiolabeled miRNA duplex (5′-^{32}P-radiolabeled guide strand annealed to an unlabeled phosphorylated passenger strand) at 37°C for 1 h. The final concentration of Mg^{2+} was 1.5 mM. After miRNA assembly, an excess synthetic target RNA or 5′ capped and poly (A) tailed mRNA (10–100 pmol, saturating at ≥ 1 μM) was added and further incubate at 37°C for 1–2 h. The reactions were stopped by adding an equal volume of 2× formamide dye containing 25 mM EDTA and 0.1% SDS, followed by heating at 95°C, and they were resolved by electrophoresis through a 15% urea/polyacrylamide sequencing gel, under highly stringent denaturing conditions (Rocheleau et al., 1992). For the native gel analysis in Fig. 29C, Ficoll was added to 3% (f.c.) after the reactions were terminated, followed by resolution by 15% native PAGE containing 1.5 mM Mg^{2+} in both the gel and running buffer. Phosphorimaging was performed using a BAS-2500 image analyzer (Fujifilm, Tokyo, Japan), and the signal intensities of the full-length miRNAs were quantified for the relative 3′ end stability using MultiGauge (Fujifilm). The target RNA sequences are listed in Table 2.

Target-directed miRNA destabilization in cells

Six-well plates were seeded with 4–6×10^5 cells 16–24 h prior to transfection. HEK293T cells were initially transfected with 10 nM of miRNA duplex, 1 μg of FLAG-Ago2 plasmid (pcDNA3.1), followed by transfection with 100 nM of target RNA or 1 μg of 4x target expressing plasmid (pIS2, Addgene plasmid #12177) at 6 and/or 24 h after the initial transfection. For endogenous miRNA targeting, cells were transfected with 100 nM of target RNA. Lipofectamine 2000 was used for transfections according to the manufacturer's protocol (Invitrogen, Carlsbad, CA,

USA). At 48 h after the initial transfection, cells were washed three times with cold PBS and lysed in buffer containing 20 mM HEPES-KOH, pH 7.4, 150 mM KOAc, 1.5 mM $Mg(OAc)_2$, 0.1% Triton X-100, 5% glycerol and 1x EDTA-free protease Inhibitor Cocktail (Roche, Basel, Switzerland). Cell lysates were incubated for 10 min on ice and cleared by centrifugation at 15,000 rpm for 20 min at 4°C. Total cytoplasmic RNA was extracted using TRI reagent (Ambion, Thermo Fisher Scientific, Waltham, MA, USA). For Ago2 immunoprecipitation, cell lysates were incubated with anti-FLAG M2 affinity gel (Sigma-Aldrich, St. Louis, MO, USA) for 12–16 h with gentle rocking at 4°C, followed by four washes with 10x bead-volumes of IP wash buffer containing 20 mM HEPES-KOH, pH 7.4, 300 mM KOAc, 1.5 mM $Mg(OAc)_2$, 0.01% Triton X-100 and 1x EDTA-free protease Inhibitor Cocktail. RNA was recovered from the beads using TRI reagent for subsequent detection by northern hybridization.

Northern hybridization

RNAs were resolved in a 12.5% denaturing polyacrylamide gel, electrophoretically transferred to Hybond-N+ membrane (GE Healthcare, Little Chalfont, UK), and UV cross-linked at 0.12 J/cm^2. The DNA probe (Table 2) was radiolabeled using T4 polynucleotide kinase (Takara, Shiga, Japan) and [γ-^{32}P] ATP (6000 Ci/mmole, PerkinElmer), and it was hybridized with the membrane using PerfectHyb Plus (Sigma-Aldrich) at 37°C overnight. The hybridize membrane was washed with Buffer I (2x SSC and 0.1% SDS) and Buffer II (0.5X SSC and 0.1% SDS) at 37°C for 25 min each.

Unloading assay

To prepare immunopurified hAgo2, 50 μl of cytoplasmic lysates from HEK293T

cells expressing FLAG-hAgo2 was incubated with 20 µl of anti-FLAG M2 Affinity Gel (Sigma-Aldrich) for 2–4 h with gentle rocking at 4°C, followed by six washes with 10x bead-volumes of wash buffer containing 20 mM HEPES-KOH, pH 7.4, 150 mM KOAc, 1.5 mM $Mg(OAc)_2$, 0.1% Tween-20 and 1x EDTA-free protease Inhibitor Cocktail. The immunopurified hAgo2 was loaded with 20 nM of a single-stranded, 5′-^{32}P-radiolabeled miRNA at 37°C for 1 h, followed by six washes to remove unbound RNAs. Immobilized hAgo2 was eluted from the resin with 300 µg/ml of 3× FLAG peptide (Sigma-Aldrich) for 1 h with gentle rocking at RT. The unloading reactions were performed essentially as described as previously (De et al., 2013). Briefly, miRNA-bound Ago2 was incubated with 5 µM of target RNA at 37°C for 1 h in a 5-µl reaction volume. After the unloading reactions, Ficoll was added to 3% (f.c.), and the samples were directly loaded onto 15% native polyacrylamide gels containing 1.5 mM Mg^{2+} in both the gel and running buffer.

Ago2 cleavage assay

To prepare targets, DNA fragments containing the target site were amplified by the polymerase chain reaction (PCR), *in vitro* transcribed, and radiolabeled at the 5′-cap by guanylyl transferase and [α-^{32}P] GTP (3000 Ci/mmole, PerkinElmer, Waltham, MA, USA) using the mScript mRNA production system (Epicentre, Madison, WI, USA) according to the manufcturer's instructions, followed by denaturing polyacrylamide gel purification. Fifty nM 5′-phosphorylated small RNA duplex was pre-incubated prior to the addition of ~5 nM ^{32}P-cap-radiolabeled target RNA. For the cleavage assay in Fig. 25C and Fig. 31A, the radiolabeled miRNAs were first destabilized by cold targets prior to the addition of cap-radiolabeled perfect targets. The reactions were stopped by adding an equal volume of 2×

formamide dye containing 25 mM EDTA and 0.1% SDS, and then they were resolved in a 15% denaturing polyacrylamide gel.

In vitro RISC assembly assay

In vitro RISC assembly assays were performed essentially as described previously (Kawamata and Tomari, 2011; Park and Shin, 2015). Ten nM of guide strand radiolabeled duplexes (*i.e.*, a 5′-^{32}P-radiolabeled guide strand annealed to an unlabeled phosphorylated passenger-strand) was incubated in the standard reaction mixture with 10 nM of 2′-*O*-methyl antisense oligonucleotide (ASO) as a target for native gel analysis (Fig. 28C and 29B). For an alternative native gel analysis (Fig. 23B), the 2′-*O*-methylated ASO was radiolabeled instead of the guide strand (Table 2). The RISC complexes were resolved by vertical, native 1.4% agarose gel electrophoresis at 300 V in a 4°C cold room.

Antibodies

The primary antibodies included polyclonal rabbit anti-FLAG (1:5,000; Sigma-Aldrich), monoclonal mouse anti-hAgo2 (1:500; Abcam, Cambridge, UK), polyclonal rabbit anti-alpha tubulin (1:15,000; Abcam). The secondary antibodies for chemiluminescent detection were horseradish peroxidase-conjugated goat anti-rabbit (or anti-mouse) IgG antibodies (Jackson ImmunoResearch, West Grove, PA, USA).

Table 2. The sequences of oligonucleotides (5′-3′)

Site-directed mutagenesis

H271A Fwd: GCCTGTGGGCAGATGAAGAGGAAGT
H271A Rev: CGTTATCTCCACCTTTAGACCTTTAAT
R277A Fwd: CTTCGCCTTCATCTGCCCACAGTGCGTTATC
R277A Rev: TACCGCGTCTGCAATGTGACCCGGCGGC
K278A Fwd: CGCCCTCTTCATCTGCCCACAGTGCGTTATC
K278A Rev: TACCGCGTCTGCAATGTGACCCGGCGGC
R280A Fwd: CTTCCTCTTCATCTGCCCACAGTGCGTTATC
R280A Rev: TACGCCGTCTGCAATGTGACCCGGCGGC
Y311A Fwd: GACAGGCACAAGTTGGTTCTGCGCTACC
Y311A Rev: CTTGAAAGCCTGGGCCACCGTGCACTC
H316A Fwd: GACAGGGCCAAGTTGGTTCTGCGCTACC
H316A Rev: CTTGAAATACTGGGCCACCGTGCACTC

Northern hybridization DNA probe

miR-1: TACATACTTCTTTACATTCCA
miR-16: CGCCAATATTTACGTGCTGCTA
miR-20a: CTACCTGCACTATAAGCACTTTA
miR-151: ACTAGACTGTGAGCTCCTCGA
let-7a: AACTATACAACCTACTACCTCA
$tRNA^{lys}$: GAGATTAAGAGTCTCATGCTC
U6 snRNA: TTGCGTGTCATCCTTGCGCAGG

MicroRNA

miR-1 guide: UGGAAUGUAAAGAAGUAUGUA
miR-1 guide 3'U: UGGAAUGUAAAGAAGUAUGUU
miR-1 guide 3'G: UGGAAUGUAAAGAAGUAUGUG
miR-1 guide 3'C: UGGAAUGUAAAGAAGUAUGUC
miR-1 guide 20 nt: UGGAAUGUAAAGAAGUAUGU
miR-1 guide 22 nt: UGGAAUGUAAAGAAGUAUGUAU
miR-1 high GC guide: UGGAAUGUAAAGACGCGCGUA
miR-1 passenger: CAUACUUCUUUAUAUGCCCAUA
miR-1 passenger 21 nt: AUACUUCUUUAUAUGCCCAUA
miR-1 passenger 23 nt: ACAUACUUCUUUAUAUGCCCAUA
miR-1 high GC passenger: CGCGCGUCUUUAUAUGCCCAUA
miR-151 guide: UCGAGGAGCUCACAGUCUAGU
miR-151 passenger: UAGACUGAAGCUCCUUGUGG
miR-196 guide: UAGGUAGUUUCAUGUUGUUGGG
miR-196 passenger: CAACAACAUUAAACCACCCGAU
miR-9 guide: UCUUUGGUUAUCUAGCUGUAUGA
miR-9 passenger: AUAAAGCUAGAUAACCGAAAGUA
let-7a guide: UGAGGUAGUAGGUUGUAUAGUU
let-7a passenger: CUAUACAAUCUACUGUCUUUC
miR-124 guide: UAAGGCACGCGGUGAAUGCCA
miR-124 passenger: GUGUUCACAGCGGACCUUGAU

Target RNA

```
Unrelated: GCAUUCACCGCGUGCCUUAAU
miR-1 seed: AUGUAUGAAGAAAACAUUCCA
miR-1 seed + 3's: AUGUAACUUGAAAACAUUCCA
miR-1 perfect: UACAUACUUCUUUACAUUCCA
miR-1 mm 1-8: UACAUACUUCUUUUGUAAGGU
miR-1 mm 1-4: UACAUACUUCUUUACAUAGGU
miR-1 mm 5-8: UACAUACUUCUUUUGUAUCCA
miR-1 mm 9-12: UACAUACUUGAAAACAUUCCA
miR-1 unrelated(mm 2-4): AUGUAUGAAGAAAACAUAGGA
miR-1 mm 2-3: UACAUACUUCUUUACAUUGGA
miR-1 mm 3-4: UACAUACUUCUUUACAUAGCA
miR-1 mm 4-5: UACAUACUUCUUUACAAACCA
miR-1 mm 5-6: UACAUACUUCUUUACUAUCCA
miR-1 mm 6-7: UACAUACUUCUUUAGUUUCCA
miR-1 mm 7-8: UACAUACUUCUUUUGAUUCCA
miR-1 mm 2-4: UACAUACUUCUUUACAUAGGA
miR-1 mm 2-5: UACAUACUUCUUUACAAAGGA
miR-1 mm 2-6: UACAUACUUCUUUACUAAGGA
miR-1 mm 18-21: AUGUUACUUCUUUACAUUCCA
miR-1 mm 16-21: AUGUAUCUUCUUUACAUUCCA
miR-1 mm 9-12 + mm 21: AACAUACUUGAAAACAUUCCA
miR-1 mm 9-12 + mm 20-21: AUCAUACUUGAAAACAUUCCA
miR-1 mm 9-12 + mm 19-21: AUGAUACUUGAAAACAUUCCA
miR-1 mm 9-12 + mm 17-21: AUGUAACUUGAAAACAUUCCA
miR-1 mm 1-8 + mm 21: AACAUACUUCUUUUGUAAGGU
miR-1 mm 1-8 + mm 20-21: AUCAUACUUCUUUUGUAAGGU
miR-1 mm 1-8 + mm 19-21: AUGAUACUUCUUUUGUAAGGU
miR-1 mm 1-8 + mm 17-21: AUGUAACUUCUUUUGUAAGGU
miR-1 mm 9-10: UACAUACUUCUAAACAUUCCA
miR-1 mm 9-14: UACAUACAAGAAAACAUUCCA
miR-1 mm 9-15: UACAUAGAAGAAAACAUUCCA
miR-1 mm 9-16: UACAUUGAAGAAAACAUUCCA
miR-1 mm 2-4 + mm 9-10: UACAUACUUCUAAACAUAGGA
miR-1 mm 2-4 + mm 9-14: UACAUACAAGAAAACAUAGGA
miR-1 mm 2-4 + mm 9-15: UACAUAGAAGAAAACAUAGGA
miR-1 perfect bulge: UACAUACUUCUCUAUUACAUUCCA
miR-1 mm 2-3 bulge: UACAUACUUCUCUAUUACAUUGGA
miR-1 mm 2-3 + mm 20-21: AUCAUACUUCUCUAUUACAUUGGA
miR-1 mm 2-3 17 nt: UACUUCUUUACAUUGGA
miR-1 mm 2-3 25 nt: UAUACAUACUUCUUUACAUUGGAUA
miR-1 mm 1-10: UACAUACUUCUAAUGUAAGGU
miR-1 mm 1-12: UACAUACUUGAAAUGUAAGGU
miR-1 mm 1-14: UACAUACAAGAAAUGUAAGGU
miR-1 mm 1-15: UACAUAGAAGAAAUGUAAGGU
miR-1 mm 1-16: UACAUUGAAGAAAUGUAAGGU
miR-1 mm 1-8 5'A: AACAUACUUCUUUUGUAAGGU
miR-1 mm 1-8 5'C: CACAUACUUCUUUUGUAAGGU
miR-1 mm 1-8 5'G: GACAUACUUCUUUUGUAAGGU
miR-1 mm 1-8 3' end structure-1: ACAUACUUCUUUUGUAAGGU
miR-1 mm 1-8 3' end structure-2: UACAUACUUCUUUUGUAAGGU
miR-1 mm 1-8 3' end structure-3: AUACAUACUUCUUUUGUAAGGU
```

miR-1 high GC seed: AUGCGCGCAGAAAUGUAAGGU
miR-1 high GC mm 1-8: UACGCGCGUCUUUUGUAAGGU
miR-1 high GC perfect: UACGCGCGUCUUUACAUUCCA
miR-1 high GC mm 2-3: UACGCGCGUCUUUACAUUGGA
miR-151 seed: UGAUCUGACACUCCUCCUCGA
miR-151 perfect: ACUAGACUGUGAGCUCCUCGA
miR-151 mm 2-3: ACUAGACUGUGAGCUCCUGCA
miR-151 mm 1-8: ACUAGACUGUGAGGAGGAGCU
miR-151 mm 1-8 + mm 21: UCUAGACUGUGAGGAGGAGCU
miR-196 seed: GGGUUGUUGUACUUACUACCUA
miR-196 mm 1-8: CCCAACAACAUGAAUGAUGGAU
miR-9 seed: AGUAUGUCGAUCUAUACCAAAGA
miR-9 mm 1-8: UCAUACAGCUAGAUAUGGUUUCU
let-7a seed: UGAUAUGUUGGAUCUACCUCA
let-7a mm 2-3: ACUAUACAACCUACUACCAGA
let-7a mm 1-8: ACUAUACAACCUAGAUGGAGU
let-7a perfect: ACUAUACAACCUACUACCUCA
miR-124 mm 1-8: UGGCAUUCACCGCCACGGAAU
Unrelated 35 nt: UACACAUGCAUUCACCGCGUGCCUUAAUAUCAGAU
miR-1 seed 35 nt: UACACAUAUGUAUGAAGAAAACAUUCCAAUCAGAU
miR-1 mm 2-3 35 nt: UACACAUUACAUACUUCUUUACAUUGGAAUCAGAU
miR-1 perfect 35 nt: UACACAUUACAUACUUCUUUACAUUCCAAUCAGAU
anti-miR-1: UmAmCmAmCmAmUmUmAmCmAmUmAmCmUmUmCmUmUmUmAmCmAmUmUmCmCmAmAmUmCmAmGmAmUm
miR-16 seed: GCGGUUAUAAAUGCUGCUGCUA
miR-16 mm 2-3: CGCCAAUAUUUACGUGCUGGAA
miR-20a seed: GAUGGACGUGAUAUUGCACUUUA
miR-20a mm 2-3: CUACCUGCACUAUAAGCACUAAA

ASO for RISC assembly

Unrelated: UnCmUnUmCnGmCnAmUmUmCmAmCmCnGmCnGmUnGmCnCmUnUmAmAmUmAmCmCnUmUm
Seed: UnCmUnUmCmAmUmGmUmAmUnGmAmAmGmAmAmAmCmAmUmUmCmCmAmAmCmCmUnUm
mm 2-3: UnCmUnUmCmUmAmCmAmUmAmCmUmUmCmUnUmUmAmCmAmUmUmGmGmAmAmCmCmUmUm
Perfect: UmCmUmUmCmUmAmCmAmUmAmCmUmUmCmUmUmAmCmAmUmUmCmCmAmAmCmCmUmUm

4x target mRNA template for *in vitro* transcription and cloning

miR-1 unrelated: CGAGAGCTCGCATTCACCGCGTGCCTTAATGTCGAGGCATTCACCGCGTGCCTTAATGTC-
GAGGCATTCACCGCGTGCCTTAATGTCGAGGCATTCACCGCGTGCCTTAATACTAGTCGA
miR-1 seed: CGAGAGCTCATGTATGAAGAAAACATTCCAGTCGAGATGTATGAAGAAAACATTCCAGTC-
GAGATGTATGAAGAAAACATTCCAGTCGAGATGTATGAAGAAAACATTCCAACTAGTCGA
miR-1 perfect: CGAGAGCTCTACATACTTCTTTACATTCCAGTCGAGTACATACTTCTTTACATTCCAGTC-
GAGTACATACTTCTTTACATTCCAGTCGAGTACATACTTCTTTACATTCCAACTAGTCGA
miR-1 mm 1-4: CGAGAGCTCTACATACTTCTTTACATAGGTGTCGAGTACATACTTCTTTACATAGGTGTC-
GAGTACATACTTCTTTACATAGGTGTCGAGTACATACTTCTTTACATAGGTACTAGTCGA
miR-1 mm 2-3: CGAGAGCTCTACATACTTCTTTACATTGGAGTCGAGTACATACTTCTTTACATTGGAGTC-
GAGTACATACTTCTTTACATTGGAGTCGAGTACATACTTCTTTACATTGGAACTAGTCGA

Results

miRNAs are stable in Argonaute but they are destabilized upon non-canonical target binding

It has been widely considered that Argonautes stabilize mature miRNAs. I hypothesized that if Argonautes are degraded by proteases in cells, miRNAs should be rapidly degraded by nucleases (*i.e.*, miRNA destabilization). To test this idea *in vitro*, I immunopurified Ago2 complexes and subjected them to protease digestion, followed by RNase treatment (Fig. 19A). miRNAs were degraded rapidly by RNases in the protease-treated control, whereas those in Ago2 complexes were largely protected from degradation, suggesting that Argonaute is required for mature miRNA stability (Fig. 19A).

To explore the mechanism of how targets destabilize miRNAs in human Argonautes, I used cell lysates prepared from human embryonic kidney 293T (HEK293T) cells that express epitope-tagged human Ago2 (hAgo2). HEK293T cells are often used for exogenous RISC programming because a naïve HEK293T cell lysate on its own is not competent to reconstitute RNA interference (RNAi) *in vitro* (Park and Shin, 2015; Yoda et al., 2010) (Fig. 20A). I assembled miRNA duplexes in cytoplasmic lysates from naïve HEK293T cells or from those expressing Ago2, and I observed their maturation by native polyacrylamide gel electrophoresis (PAGE) (Fig. 19B). In naïve lysates, single-stranded, mature miRNAs were unstable and presumably degraded by endogenous nucleases, while those of Ago2-expressing lysates remained stable and exhibited greater stability than those of HeLa cell lysates (Fig. 19B).

To examine the fate of miRNAs in Ago2-RISC after binding their targets, I added excess synthetic target RNAs after 1 h of exogenous miRNA programming

(Fig. 21A). These target RNAs included canonical targets (with intact seed matches) and recently reported non-canonical targets (Broughton et al., 2016; Grosswendt et al., 2014; Helwak et al., 2013; Loeb et al., 2012; Moore et al., 2015) that usually contain no, or imperfect, seed matches that are compensated by extensive 3′ pairing (Fig. 21B). The reaction was allowed to proceed for an additional 1 h at 37°C, and then it was quenched directly with formamide dye at 95°C (without ethanol precipitation), which enabled me to detect free RNA species, while ensuring equal loads, during denaturing gel electrophoresis. Surprisingly, the results from my newly developed assay showed that miRNAs were severely destabilized by non-canonical targets in a time- and concentration-dependent manner, irrespective of whether the targets were synthetic or *in vitro*-transcribed mRNAs (Fig. 21C and Fig. 20B–D). These results contrast with those for the canonical targets, which did not have significant, adverse effects on miRNA stability (Fig. 21C). Excess target RNA addition by itself did not affect miRNA stability (unrelated target control) (Fig. 21C). Next, I quantified the level of the full-length miRNAs in multiple replicates, and I concluded that the effects of non-canonical targets were statistically significant ($P < 10^{-3}$) and reproducible (Fig. 21D). Northern hybridization, which was performed with samples as described in Fig. 21A, but which used cold miRNA duplexes, confirmed that the results of my *in vitro* assay quantitatively reflected the levels of miRNAs, and that the *in vitro* assay exhibited higher sensitivity (Fig. 21C and E). Thereafter, I exploited this experimental system to further biochemically dissect how target RNAs destabilize miRNAs in human Ago2-RISC.

Figure 19. miRNAs are stabilized by Argonaute

(A) Top: Schematic of the experiment. Bottom: 5′-^{32}P-radiolabeled miRNAs were subjected to RNase (RNase A and T1) treatment in the presence (Ago2+, immunopurified Ago2) or the absence of Argonaute (Ago2–, deproteinized), and they were analyzed in 15% denaturing-PAGE. (B) Left: miRNA duplexes were assembled in lysates from naïve HEK293T cells, from cells expressing Ago2, or from HeLa S3 cells and they were analyzed by 15% native-PAGE. ds, miRNA duplex; ss, single-stranded miRNA. Right: Western blot analysis using an anti-hAgo2 antibody. Anti-tubulin served as an internal control.

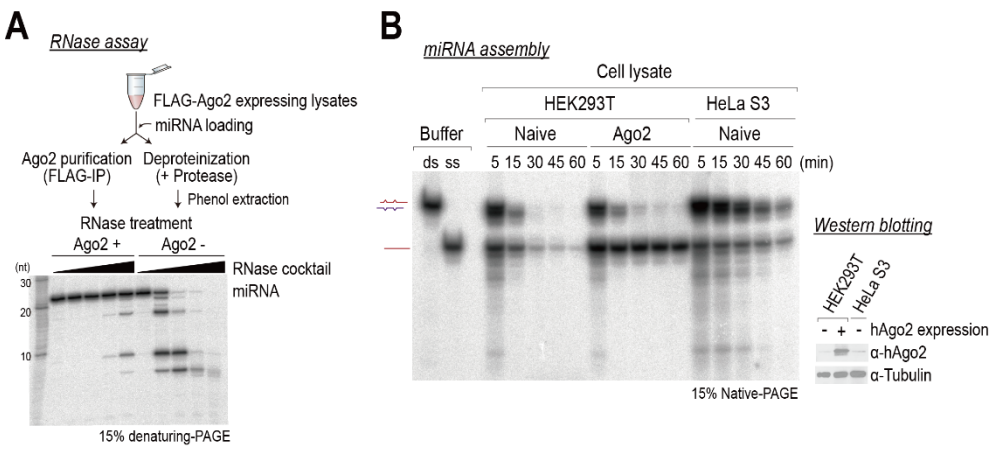
A
RNase assay
FLAG-Ago2 expressing lysates
miRNA loading
Ago2 purification (FLAG-IP)
Deproteinization (+ Protease)
Phenol extraction
RNase treatment
Ago2 +
Ago2 -
(nt)
30
20
10
RNase cocktail
miRNA
15% denaturing-PAGE
B
miRNA assembly
Cell lysate
HEK293T
HeLa S3
Buffer
Naive
Ago2
Naive
ds ss
5 15 30 45 60 5 15 30 45 60 5 15 30 45 60 (min)
15% Native-PAGE
Western blotting
HEK293T
HeLa S3
- + -
hAgo2 expression
α-hAgo2
α-Tubulin

Figure 20. *in vitro* recapitulation of target RNA-directed miRNA destabilization in human Argonaute2

(A) Mammalian cell-free system from HEK293T cells that faithfully recapitulates RNAi *in vitro*. miRNA duplex was assembled in lysates from naive HEK293T cells and from cells expressing hAgo2 for 15 min. Cap-radiolabeled target RNA (78-nt) was then added and further incubated for the indicated times, which yielded a 5′ cleavage product (37-nt), as a diagnostic for hAgo2-mediated catalysis. (B) Left: schematic of the experiment. Right: miRNA-target duplexes are analyzed in 15% native-PAGE following in vitro target-directed miRNA destabilization assay. (C and D) Non-canonical targets destabilize miRNAs in Ago2-RISC in a time- and concentration-dependent manner, irrespective of whether the targets are synthetic or in vitro-transcribed mRNAs. Data are the mean ± SD for two independent experiments.

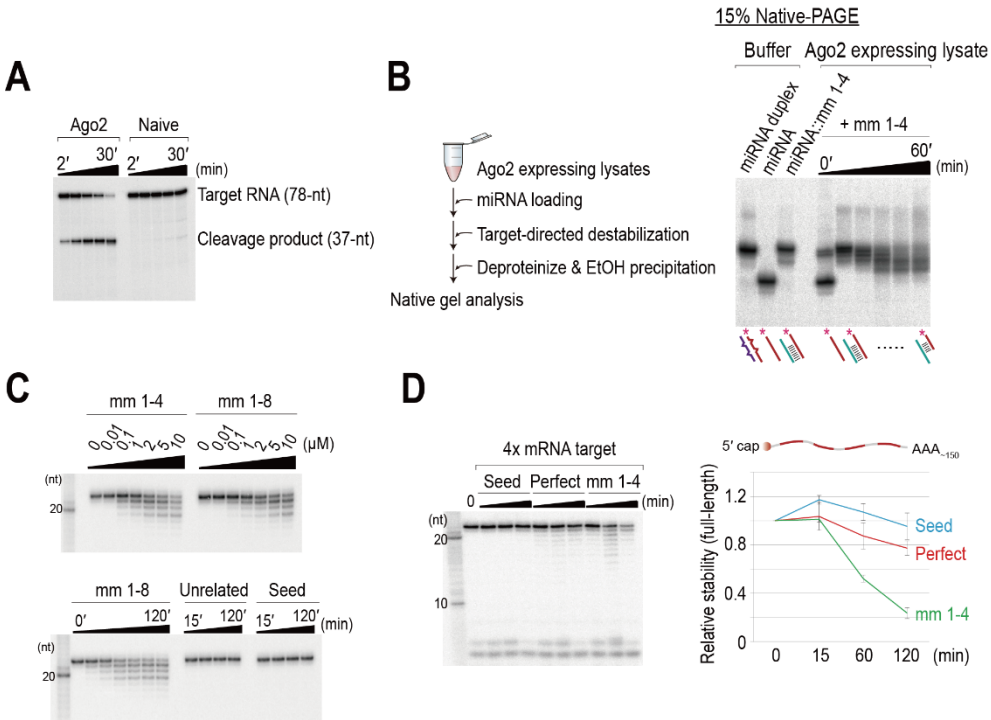
A
Ago2
Naive
2′
30′
2′
30′
(min)
Target RNA (78-nt)
Cleavage product (37-nt)
B
Ago2 expressing lysates
miRNA loading
Target-directed destabilization
Deproteinize & EtOH precipitation
Native gel analysis
15% Native-PAGE
Buffer
Ago2 expressing lysate
miRNA duplex
miRNA
miRNA·:mm 1-4
+ mm 1-4
0′
60′
(min)
C
mm 1-4
mm 1-8
0
0.01
0.1
1
2
5
10
(μM)
(nt)
20
mm 1-8
Unrelated
Seed
0′
120′
15′
120′
15′
120′
(min)
(nt)
20
D
4x mRNA target
Seed
Perfect
mm 1-4
0
(min)
(nt)
20
10
5′ cap
AAA~150
Relative stability (full-length)
1.2
0.8
0.4
0
Seed
Perfect
mm 1-4
0
15
60
120
(min)

Figure 21. *in vitro* recapitulation of target RNA-directed miRNA destabilization in human Argonaute2 - II

(A) *in vitro* recapitulation of target RNA-directed miRNA destabilization in human Argonaute2. Illustrated schematic of the *in vitro* assay for target-directed miRNA destabilization. The asterisk indicates a 5′-^{32}P radiolabel. (B) Schematic of paired miRNAs and complement target RNAs. Targets lacking the canonical perfect seed match are considered to be non-canonical. (C) Non-canonical targets destabilize miRNAs in Ago2-RISC. (D) Quantitation of (C). The means ± standard deviations (SDs) for four independent replicate experiments are shown. The *P*-value was calculated with a Student's *t*-test. (E) Northern hybridization, which was performed with samples as described (A), but used cold miRNA duplexes. The blot was probed for U6 snRNA as a loading control. Ethidium bromide-stained 5S rRNA served as another loading control. The numbers below the blot are the relative expression levels, normalized using the U6 snRNA control.

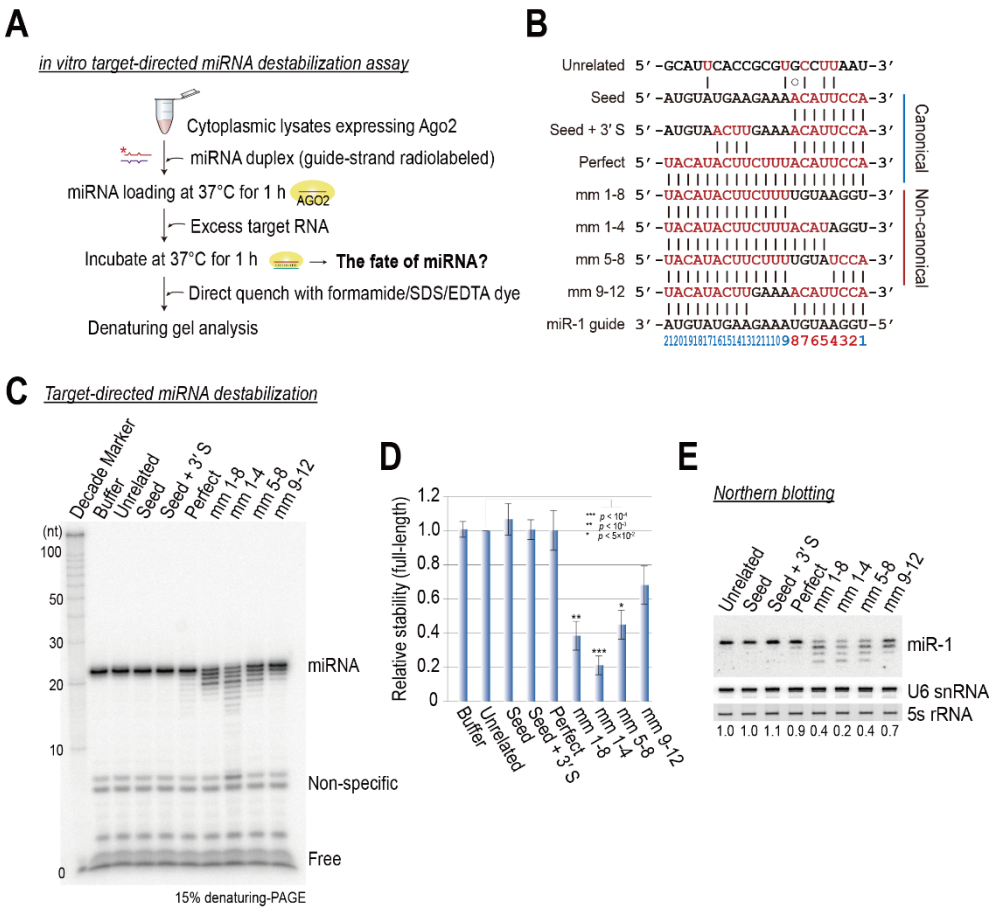
A
in vitro target-directed miRNA destabilization assay
Cytoplasmic lysates expressing Ago2
miRNA duplex (guide-strand radiolabeled)
miRNA loading at 37°C for 1 h
AGO2
Excess target RNA
Incubate at 37°C for 1 h
The fate of miRNA?
Direct quench with formamide/SDS/EDTA dye
Denaturing gel analysis
B
Unrelated 5′-GCAUUCACCGCGUGCCUUAAU-3′
Seed 5′-AUGUAUGAAGAAAACAUUCCA-3′
Seed + 3′ S 5′-AUGUAACUUGAAAACAUUCCA-3′
Perfect 5′-UACAUACUUCUUUACAUUCCA-3′
mm 1-8 5′-UACAUACUUCUUUUGUAAGGU-3′
mm 1-4 5′-UACAUACUUCUUUACAUAGGU-3′
mm 5-8 5′-UACAUACUUCUUUUGUAUCCA-3′
mm 9-12 5′-UACAUACUUGAAAACAUUCCA-3′
miR-1 guide 3′-AUGUAUGAAGAAAUGUAAGGU-5′
Canonical
Non-canonical
C
Target-directed miRNA destabilization
Decade Marker
Buffer
Unrelated
Seed
Seed + 3′ S
Perfect
mm 1-8
mm 1-4
mm 5-8
mm 9-12
(nt)
100
50
30
20
10
0
miRNA
Non-specific
Free
15% denaturing-PAGE
D
Relative stability (full-length)
1.2
1.0
0.8
0.6
0.4
0.2
0
p < 10-4
p < 10-3
p < 5×10-2
Buffer
Unrelated
Seed
Seed + 3′ S
Perfect
mm 1-8
mm 1-4
mm 5-8
mm 9-12
E
Northern blotting
Unrelated
Seed
Seed + 3′ S
Perfect
mm 1-8
mm 1-4
mm 5-8
mm 9-12
miR-1
U6 snRNA
5s rRNA
1.0 1.0 1.1 0.9 0.4 0.2 0.4 0.7

miRNA seed pairing is important for miRNA stability

My initial results indicated that the seed region is not only important for target silencing, but also for miRNA stability. To more precisely examine the effect of seed matches on the stability of miRNAs, I continued my analysis of target RNAs containing dinucleotide mismatches in the seed region (Fig. 22A). A different, unrelated control (seed mismatch without 3′ pairing) showed no effects on miRNA stability, presumably because this type of target rapidly dissociates from Ago2-RISC (Salomon et al., 2015). In contrast, targets with extensive 3′ pairing drastically destabilized miRNAs (Fig. 22B–D), without affecting steady-state levels of Ago2 protein (Fig. 22E). Mismatches in seed nucleotides [guide nt 2–8 (g2–g8)] did not contribute equally to the destabilization, but the loss of interactions involving as little as two to three nucleotides within g2–g4 seemed to be the most critical (Fig. 22D). These results are reminiscent of findings from recent single-molecule studies that showed g2–g4 are important for the initial probing of target sequences (Chandradoss et al., 2015; Salomon et al., 2015). In addition, I heterologously expressed miRNAs and their target RNAs in HEK293T cells, and then I performed a northern hybridization analysis at 48 h post-transfection, which demonstrated that the miRNAs were destabilized by non-canonical targets in cells (Fig. 22F).

Figure 22. miRNAs are destabilized by seedless, non-canonical targets

(A) Schematic of paired miRNAs and complement target RNAs. (B) The effects of dinucleotide mismatches in the seed region on miRNA stability. (C) Time-course analysis of (B); the mm 2-3 target serves as a representative example. (D) Quantitation of (B). The means ± SDs for two independent replicate experiments are shown. (E) Western blot analysis using an anti-FLAG antibody confirmed the expression of the tagged Ago2 protein. Anti-tubulin served as an internal control. (F) HEK293T cells were transfected with 10 nM miRNA duplex, 100 nM target RNA and FLAG-Ago2 expression plasmid. Cell lysates were subjected to FLAG-IP, followed by northern blotting using the miR-1 or miR-151 probe. The numbers below the blot are the relative expression levels, normalized using let7a as a loading control. Ethidium bromide-stained 5s rRNA served as another loading control.

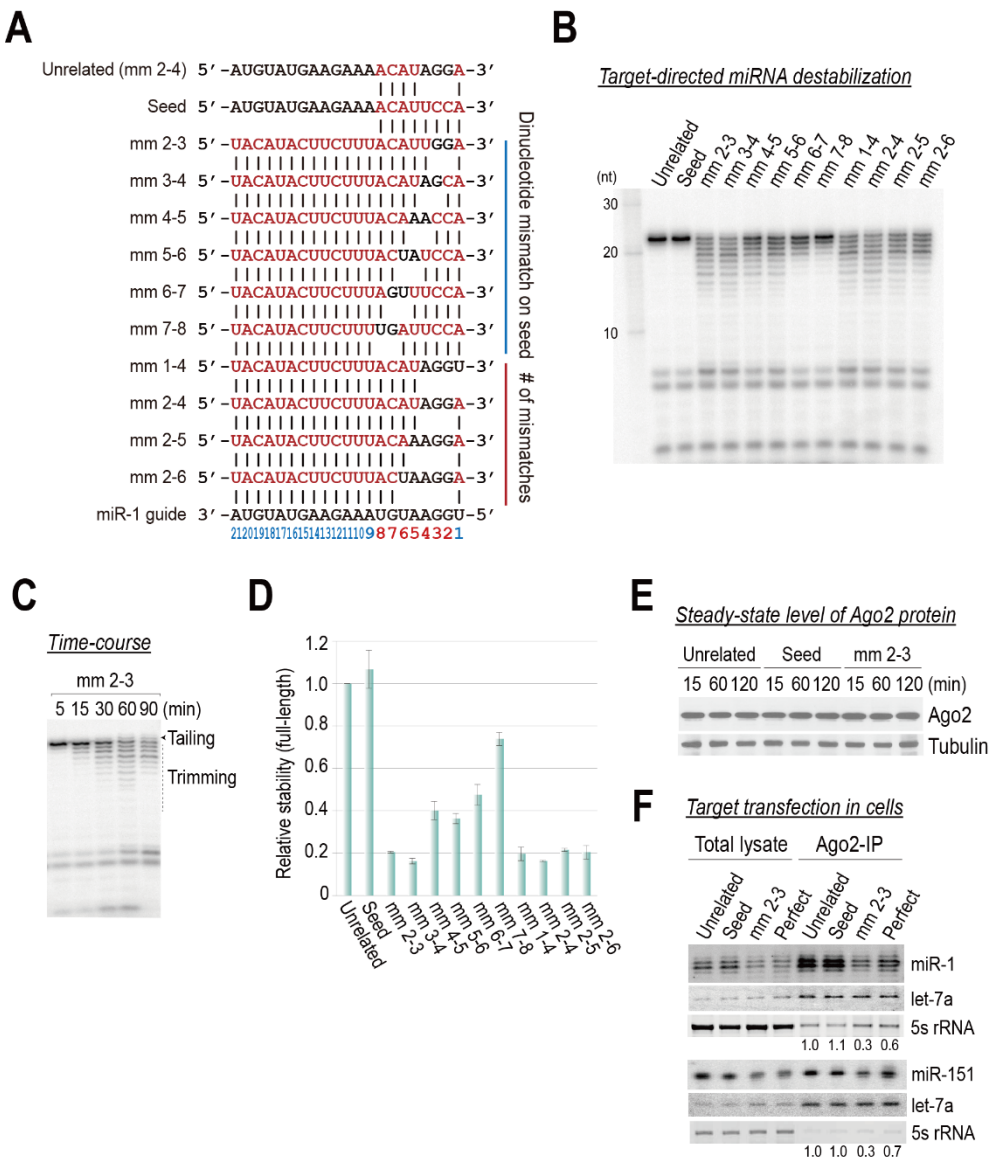
A
Unrelated (mm 2-4) 5′-AUGUAUGAAGAAAACACAUAGGA-3′
Seed 5′-AUGUAUGAAGAAAACACAUUCCA-3′
mm 2-3 5′-UACAUACUUCUUUACACAUUGGA-3′
mm 3-4 5′-UACAUACUUCUUUACACAUAGCA-3′
mm 4-5 5′-UACAUACUUCUUUACAAACCA-3′
mm 5-6 5′-UACAUACUUCUUUACUAUCCA-3′
mm 6-7 5′-UACAUACUUCUUUAGUUUCCA-3′
mm 7-8 5′-UACAUACUUCUUUUGAUUCCA-3′
mm 1-4 5′-UACAUACUUCUUUACACAUAGGU-3′
mm 2-4 5′-UACAUACUUCUUUACACAUAGGA-3′
mm 2-5 5′-UACAUACUUCUUUACAAAGGA-3′
mm 2-6 5′-UACAUACUUCUUUACUAAGGA-3′
miR-1 guide 3′-AUGUAUGAAGAAAUGUAAGGU-5′
212019181716151413121110 9 8 7 6 5 4 3 2 1
Dinucleotide mismatch on seed
# of mismatches
B
Target-directed miRNA destabilization
(nt)
30
20
10
Unrelated
Seed
mm 2-3
mm 3-4
mm 4-5
mm 5-6
mm 6-7
mm 7-8
mm 1-4
mm 2-4
mm 2-5
mm 2-6
C
Time-course
mm 2-3
5 15 30 60 90 (min)
Tailing
Trimming
D
Relative stability (full-length)
1.2
1.0
0.8
0.6
0.4
0.2
0
Unrelated
Seed
mm 2-3
mm 3-4
mm 4-5
mm 5-6
mm 6-7
mm 7-8
mm 1-4
mm 2-4
mm 2-5
mm 2-6
E
Steady-state level of Ago2 protein
Unrelated
Seed
mm 2-3
15 60 120 15 60 120 15 60 120 (min)
Ago2
Tubulin
F
Target transfection in cells
Total lysate
Ago2-IP
Unrelated
Seed
mm 2-3
Perfect
Unrelated
Seed
mm 2-3
Perfect
miR-1
let-7a
5s rRNA
1.0 1.1 0.3 0.6
miR-151
let-7a
5s rRNA
1.0 1.0 0.3 0.7

Non-canonical targets trigger the 3′ end destabilization of miRNAs

To examine whether miRNAs are destabilized from the 5′-3′ or 3′-5′ direction, I first tried labeling the 3′ end of the guide strands via ligation with [5′-^{32}P] cytidine-3', 5'-bis-phosphate (pCp). However, miRNA duplexes with a 3′ pCp on the guide were largely refractory to RISC loading, presumably because the PAZ domain specifically bind to the 3′ OH ends of miRNA duplexes (data not shown). In an alternative strategy, I used miRNA duplexes whose guide strands were 2′-*O*-methylated at their 3′ or 5′ termini (Fig. 23A). I found that 2′-*O*-methylation of the 3′ termini of the miRNAs largely protected them from nuclease degradation (Fig. 23A), whereas 2′-*O*-methylation of the 5′ termini did not. These results suggest that miRNAs are likely to be destabilized at their 3′ ends upon target binding.

I initially used the miRNA miR-1, which is specially expressed in heart and skeletal muscle, as a model of exogenous miRNA assembly in HEK293T cell lysates. To test whether 3′ end destabilization is generally applicable to other miRNA sequences, I examined several other miRNA duplexes (Fig. 24A). The results were broadly consistent across different miRNAs, although each miRNA exhibited a slight different sensitivity (Fig. 24B). Because the different GC contents of miRNAs affects target recognition, I reasoned that the GC content would also play a role in 3′ end destabilization, especially for the 3′ region of miRNAs. To test this idea, I mutated the 3′ region of miR-1 to increase its GC content to 67%, which is higher than that of most miRNAs (Fig. 24C). I found no strong correlation between the GC content and the extent of 3′ end destabilization (Fig. 24C), although the GC content may have had a small effect.

Human Ago2-RISC binds seedless, non-canonical targets with extensive 3′ pairing

My results raised an intriguing question regarding how non-canonical targets induce miRNA destabilization, because it is commonly believed that miRNAs are less likely to bind targets with an imperfect seed. To investigate whether miRNAs indeed bind to such targets, I performed a RISC assembly assay (Kawamata and Tomari, 2011), which was originally intended to exclusively detect the mature RISC. By radiolabeling target RNAs instead of miRNAs, it is possible to monitor RISC complex formation, but this only occurs if the miRNAs are capable of binding targets (Fig. 23B). My analysis indicated that seed pairing alone was usually sufficient for binding, at least for human Ago2 (Fig. 23B). In addition, I demonstrated that the miRNAs were able to bind targets with imperfect seed matches and extensive 3′ pairing, albeit much less efficiently (~12 ± 5%) than the perfect target control (Fig. 23B). My results may partly explain why non-canonical targets are found in the miRNA interactome (Broughton et al., 2016; Grosswendt et al., 2014; Helwak et al., 2013; Loeb et al., 2012; Moore et al., 2015).

Figure 23. Non-canonical targets trigger the 3′ end destabilization of miRNAs and bind with less affinity to human Ago2-RISC

(A) miRNAs are destabilized at their 3′ ends upon target binding. miRNAs that were 2′-*O*-methylated either at their 3′ or 5′ ends were subjected to the target-directed destabilization assay. Un, unrelated control. (B) Left: Schematic of the experiment. Right: miRNAs in Ago2-RISC are able to bind non-canonical targets, albeit less efficiently.

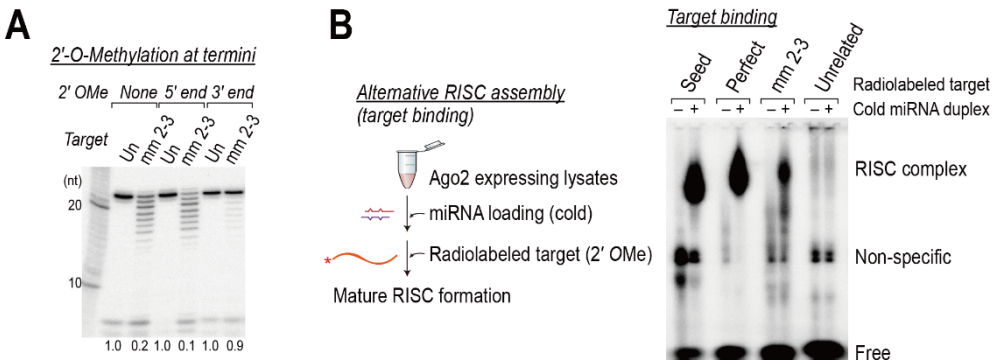
A
2′-O-Methylation at termini
2′ OMe None 5′ end 3′ end
Target
Un mm 2-3 Un mm 2-3 Un mm 2-3
(nt)
20
10
1.0 0.2 1.0 0.1 1.0 0.9
B
Alternative RISC assembly
(target binding)
Ago2 expressing lysates
miRNA loading (cold)
Radiolabeled target (2′ OMe)
Mature RISC formation
Target binding
Seed
Perfect
mm 2-3
Unrelated
– + – + – + – +
Radiolabeled target
Cold miRNA duplex
RISC complex
Non-specific
Free

Figure 24. Non-canonical targets trigger the 3′ end destabilization of many other miRNAs

(A) Various miRNA duplexes used for *in vitro* assay. The GC contents of the seed (g2-8, red) or the 3′ end region (considered as g13-21, blue) are shown. (B) Non-canonical targets destabilize many other miRNAs. (C) The effects of the GC content of the 3′ end region of miRNAs for target-directed destabilization. The 3′ end region of the miR-1 duplex was mutated to have a high GC content (from 22 to 67%).

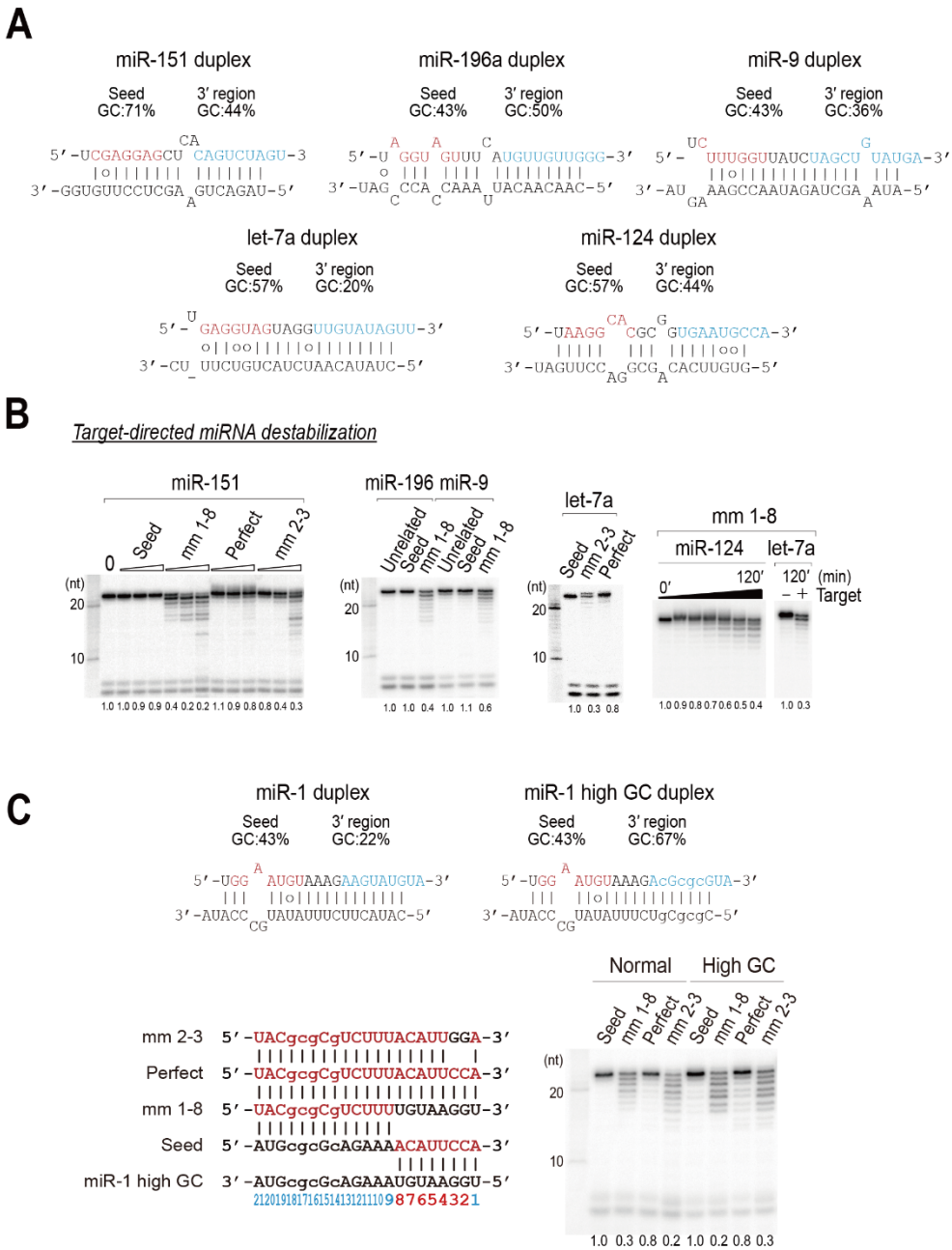
A
miR-151 duplex
Seed GC:71%
3′ region GC:44%
5′-UCGAGGAGCU CAGUCUAGU-3
3′-GGUGUUCCUCGA GUCAGAU-5′
miR-196a duplex
Seed GC:43%
3′ region GC:50%
5′-U GGU GUUU AUGUUGUUGGG-3′
3′-UAG CCA CAAA UACAACAAC-5′
miR-9 duplex
Seed GC:43%
3′ region GC:36%
5′- UUUGGUUAUCUAGCU UAUGA-3′
3′-AU AAGCCAAUAGAUCGA AUA-5′
let-7a duplex
Seed GC:57%
3′ region GC:20%
5′- GAGGUAGUAGGUUGUAUAGUU-3′
3′-CU UUCUGUCAUCUAACAUAUC-5′
miR-124 duplex
Seed GC:57%
3′ region GC:44%
5′-UAAGG CGC GUGAAUGCCA-3′
3′-UAGUUCC GCG CACUUGUG-5′
B
Target-directed miRNA destabilization
miR-151
Seed
mm 1-8
Perfect
mm 2-3
0
(nt)
20
10
1.0 1.0 0.9 0.9 0.4 0.2 0.2 1.1 0.9 0.8 0.8 0.4 0.3
miR-196 miR-9
Unrelated
Seed
mm 1-8
1.0 1.0 0.4 1.0 1.1 0.6
let-7a
Seed
mm 2-3
Perfect
1.0 0.3 0.8
mm 1-8
miR-124
let-7a
0′
120′
120′ (min)
– + Target
1.0 0.9 0.8 0.7 0.6 0.5 0.4
1.0 0.3
C
miR-1 duplex
Seed GC:43%
3′ region GC:22%
5′-UGG AUGUAAAGAAGUAUGUA-3′
3′-AUACC UAUAUUUCUUCAUAC-5′
miR-1 high GC duplex
Seed GC:43%
3′ region GC:67%
5′-UGG AUGUAAAGAcGcgcGUA-3′
3′-AUACC UAUAUUUCUgCgcgC-5′
mm 2-3 5′-UACgcgCgUCUUUACAUUGGA-3′
Perfect 5′-UACgcgCgUCUUUACAUUCCA-3′
mm 1-8 5′-UACgcgCgUCUUUUGUAAGGU-3′
Seed 5′-AUGcgcGcAGAAAACAUUCCA-3′
miR-1 high GC 3′-AUGcgcGcAGAAAUGUAAGGU-5′
21201918171615141312111098765432 1
Normal
High GC
Seed
mm 1-8
Perfect
mm 2-3
(nt)
20
10
1.0 0.3 0.8 0.2 1.0 0.2 0.8 0.3

A large fraction of miRNAs is still in Ago2 following target-directed destabilization

Structural studies revealed that miRNAs are tightly bound to Argonautes and that their 5′ and 3′ ends are anchored in MID and PAZ domains, respectively (Frank et al., 2010; Ma et al., 2004). Therefore, one can expect that miRNAs should be dislodged from Argonautes, to make them accessible to exoribonucleases. This idea was first demonstrated in *Caenorhabditis elegans* Argonaute by Grosshans and his colleagues (Chatterjee and Grosshans, 2009), and more directly by a recent study that used recombinant human Ago2 that was immunopurified from *Spodoptera frugiperda* Sf9 cell lysates (De et al., 2013). The results from my *in vitro* assay likely reflect two different possibilities: 1) miRNAs are completely released from Argonaute and degraded, or 2) while the 5′ end of miRNAs are stably anchored in the MID domain, their 3′ ends are released from the PAZ domain and destabilized (*i.e.*, 3′ end destabilization).

To discriminate between these two possibilities, I first examined the contribution of unloading during the target-directed destabilization process. I performed an unloading assay essentially as described (De et al., 2013), except that I used hAgo2 that was immunopurified from HEK293T cell lysates. In addition, I eluted Ago2 proteins from beads and simultaneously analyzed the fractions of miRNAs that are either bound to or released from Ago2 by native PAGE (Fig. 25A). My analysis showed that ~45 ± 6% of the miRNAs were released from the Ago2 complex by non-canonical targets, whereas most of the miRNAs were stably associated with Ago2 by other targets (Fig. 25A). My *in vitro* assay showed that the 3′ ends of the miRNAs were destabilized to a greater extent (~80%) by non-canonical targets (Fig. 22D). The discrepancy between these two results indicated

that unloading does not fully explain the target-directed destabilization mechanism, and that some parts of the destabilization process occur within the Ago2-complex.

To test this, I performed an *in vitro* assay, after which I fractionated samples via Ago2 immunopurification (Fig. 25B). Consistent with the aforementioned idea, I found that 3′ end destabilizations were observed in Ago2-bound fraction (Fig. 25B). This led me to question whether some parts of 3′ trimmed miRNAs are present in the Ago2-complex, and whether they are functionally active. To answer this question, I performed a target cleavage assay. A conventional cleavage assay includes the assembly of cold miRNA duplexes, followed by the addition of cap-radiolabeled targets. I slightly modified the protocol so that I could monitor the efficiency of target cleavage after 3′ end destabilization (Fig. 25C). Upon canonical target bindings, the cleavage efficiency was minimal, although miRNA stability was not compromised (Fig. 25C). These results indicated that most miRNAs in Ago2-RISC were stably associated with cold canonical targets (*i.e.*, sponge effects). In contrast, miRNAs that were destabilized by non-canonical targets (0.2 ± 0.05) were capable of catalyzing cleavages, whose efficiencies were higher than expected (0.4 ± 0.03) (Fig. 25D). These results support and extend the conclusion that a substantial fraction of 3′ trimmed miRNAs are in functional Ago2-RISCs that can participate in cleavage catalysis. Based on these collective results, I conclude that at least one-half of miRNAs are still associated with Ago2-RISC following target-directed destabilization.

Figure 25. The target-directed mechanism entails a combination of unloading and 3′ end destabilization in Argonaute

(A) Left: Schematic of the experiment. Right: Large fractions of miRNAs were in Ago2-complexes after non-canonical target binding. In the buffer control, single-stranded miRNAs were annealed to each target RNA at 37°C. (B) Left: Schematic of the experiment. Right: 3′ end destabilization occurs in Ago2-bound fraction during non-canonical target binding. (C) Left: Schematic of the experiment. Right: A substantial fraction of 3′ trimmed miRNA species in the Ago2-complex can participate in cleavage catalysis. (D) Top: miRNAs that are destabilized by non-canonical targets (0.2 ± 0.05) are capable of catalyzing cleavages, whose efficiencies are higher than expected (0.4 ± 0.03). Discrepancies between the two results (3′ end stability and target cleavage) indicate that many miRNAs are still in Ago2-RISC following target-directed destabilization. Bottom: Quantitation of the fraction target cleaved is shown. Data are the mean ± SD for two independent experiments.

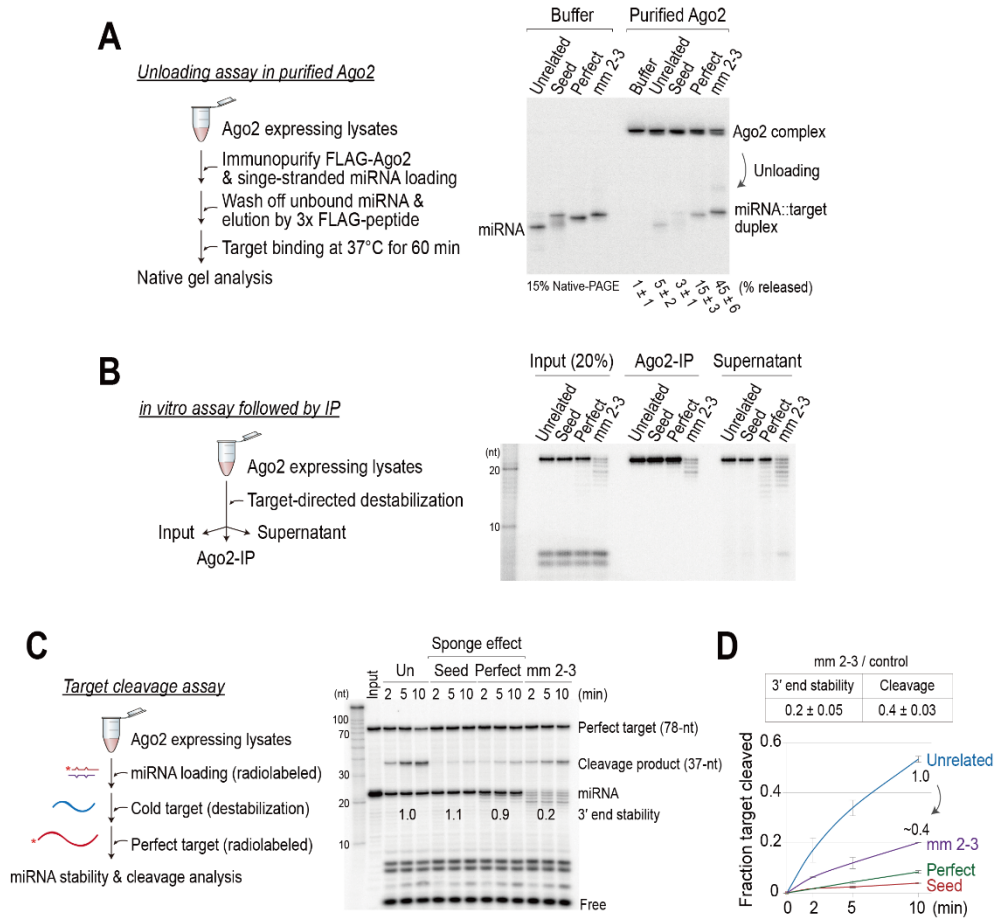
A
Unloading assay in purified Ago2
Ago2 expressing lysates
Immunopurify FLAG-Ago2
& singe-stranded miRNA loading
Wash off unbound miRNA &
elution by 3x FLAG-peptide
Target binding at 37°C for 60 min
Native gel analysis
Buffer
Purified Ago2
Unrelated
Seed
Perfect
mm 2-3
Buffer
Ago2 complex
Unloading
miRNA::target
duplex
miRNA
15% Native-PAGE
(% released)
B
in vitro assay followed by IP
Ago2 expressing lysates
Target-directed destabilization
Input
Supernatant
Ago2-IP
Input (20%)
Ago2-IP
Supernatant
(nt)
20
10
C
Target cleavage assay
Ago2 expressing lysates
miRNA loading (radiolabeled)
Cold target (destabilization)
Perfect target (radiolabeled)
miRNA stability & cleavage analysis
Sponge effect
Input
Un
Seed
Perfect
mm 2-3
2 5 10 2 5 10 2 5 10 2 5 10
(min)
100
70
30
20
10
Perfect target (78-nt)
Cleavage product (37-nt)
miRNA
1.0
1.1
0.9
0.2
3' end stability
Free
D
mm 2-3 / control
3' end stability
Cleavage
0.2 ± 0.05
0.4 ± 0.03
Fraction target cleaved
0.6
0.4
0.2
0
Unrelated
1.0
~0.4
mm 2-3
Perfect
Seed
0
2
5
10 (min)

3′ complementarity confers specificity for target-directed destabilization[1]

I showed that 3′ complementarity is important for miRNA destabilization. To gain additional mechanistic insights into target-directed destabilization, I analyzed target sequence constraints in detail (Fig. 26A and 27A). From this analysis, I arrived at three main conclusions: 1) a mismatch at the last nucleotide inhibits 3′ end destabilization (*e.g.*, mm 1-8 vs. mm 1-8 + mm-21) (Fig. 26B and C); 2) 3′ end destabilization is mostly diminished when miRNAs are seed matched (*e.g.*, mm 9-14 vs. mm 2-4 + mm 9-14) (Fig. 27A); 3) at least 7 nt or more of 3′ end complementarity (from mm 1-8 to mm 1-16) are required for destabilization, which occurs largely independently of the slicer activity of Argonautes (Fig. 27B).

To rigorously validate the first conclusion, I prepared miRNA duplexes whose 3′ end nt varied (A, U, G, or C). These four different miRNA duplexes were programmed in Ago2-RISC and reacted with seedless targets (mm 1-8), which only varied at their 5′ end nt (Fig. 26D). The 3′ ends of the miRNAs were efficiently destabilized only when their 3′ end nts were complementary to their corresponding target (*i.e.*, A:U, U:A, C:G, or G:C) (Fig. 26E), as was also confirmed in the other tested miRNA and via endogenous Ago2 in HeLa cell lysates (Fig. 27C). In addition, I also tested this with miRNAs and their targets that varied in their 3′ end structures (Fig. 26F) or lengths (Fig. 27D), and the results confirmed that the base-complementarity of the 3′ end nt is an important determinant of miRNA stability (Fig. 26G).

A natural miRNA duplex contains a passenger strand that is often mismatched in the 5′ seed region of the guide strand, which leads to the question of

[1]The experiments in this section were carried out in collaboration with **Sang-Yoon Shin**.

whether a passenger strand-like target can trigger the 3′ end destabilization of the guide (Fig. 28A) Interestingly, the passenger strand-like target did not induce any deleterious effects if the guide strand had at least a 1-nt overhang at its 3′ end (Fig. 28B). Consistent with my results regarding the negative impact of the complementarity of the 3′ end nt, these findings suggest that the 3′ end of the guide should be freely available to the PAZ domain, not only for optimal RISC assembly (Fig. 28C), but also for its own stability.

Figure 26. 3′ complementarity confers specificity for target-directed destabilization

(A) Schematic of paired miRNA and complement target RNAs. (B) 3′ complementarity confers a specificity of destabilization. (C) Quantitation of (B). The mean ± SD for at least two independent experiments is shown. (D and E) A single mismatch at the 3′ end nucleotide largely abrogates the destabilization, regardless of the identity of the 3′ end nucleotide of the guides or (F and G) the 3′ end structure of guide-target duplexes.

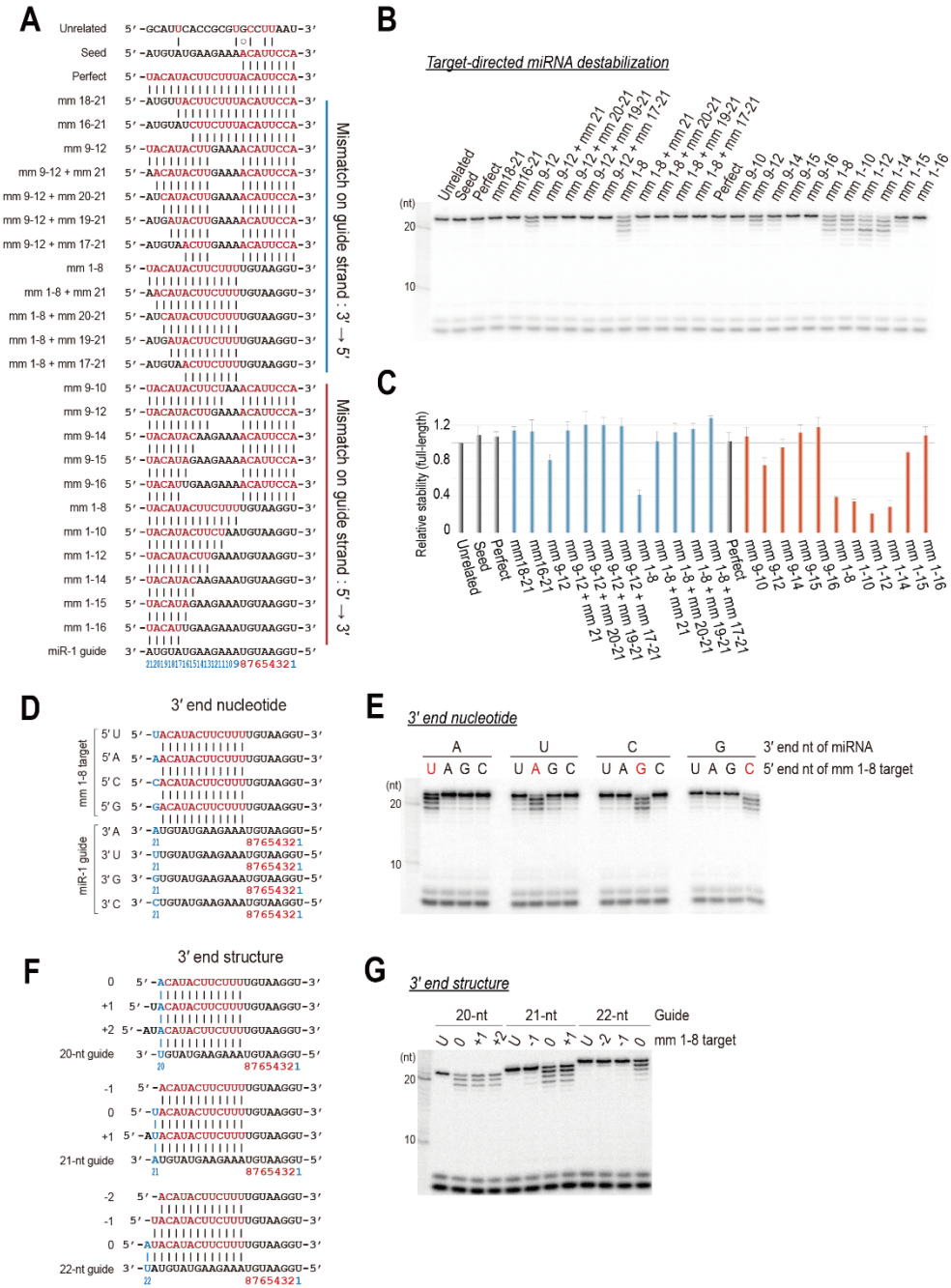
A
Unrelated
Seed
Perfect
mm 18-21
mm 16-21
mm 9-12
mm 9-12 + mm 21
mm 9-12 + mm 20-21
mm 9-12 + mm 19-21
mm 9-12 + mm 17-21
mm 1-8
mm 1-8 + mm 21
mm 1-8 + mm 20-21
mm 1-8 + mm 19-21
mm 1-8 + mm 17-21
mm 9-10
mm 9-14
mm 9-15
mm 9-16
mm 1-10
mm 1-12
mm 1-14
mm 1-15
mm 1-16
miR-1 guide
Mismatch on guide strand : 3′ → 5′
Mismatch on guide strand : 5′ → 3′
B
Target-directed miRNA destabilization
(nt)
20
10
C
Relative stability (full-length)
1.2
0.8
0.4
0
D
3′ end nucleotide
mm 1-8 target
5′ U
5′ A
5′ C
5′ G
miR-1 guide
3′ A
3′ U
3′ G
3′ C
E
3′ end nucleotide
A
U
C
G
3′ end nt of miRNA
5′ end nt of mm 1-8 target
F
3′ end structure
0
+1
+2
20-nt guide
-1
21-nt guide
-2
22-nt guide
G
3′ end structure
20-nt
21-nt
22-nt
Guide
mm 1-8 target

Figure 27. 3′ complementarity confers specificity for target-directed destabilization - II

(A) Schematic of paired miRNAs and complement target RNAs. Left: 3′ end destabilization is mostly diminished when miRNAs are seed matched. Right: 3-nt bulge is tolerable. (B) Human Argonautes are likely to share a similar mechanism for target-directed destabilization, irrespective of their slicer-activity. (C) A mismatch at the 3′ end nucleotide inhibits 3′ end destabilization of miR-151 (left) and miR-1 via endogenous Ago2 in HeLa cell lysates (right). (D) 3′ complementarity is an important determinant of the 3′ end stability, regardless of the lengths of target RNAs.

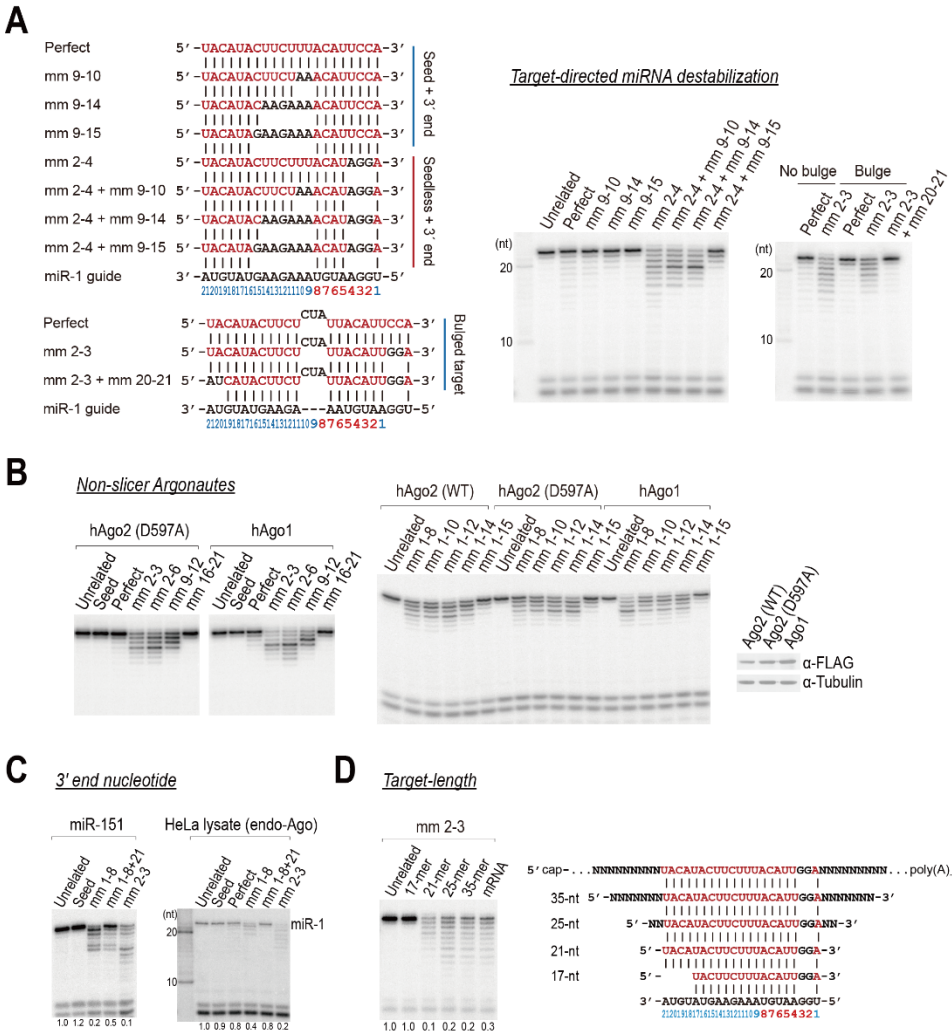
A
Perfect
mm 9-10
mm 9-14
mm 9-15
mm 2-4
mm 2-4 + mm 9-10
mm 2-4 + mm 9-14
mm 2-4 + mm 9-15
miR-1 guide
Seed + 3′ end
Seedless + 3′ end
Perfect
mm 2-3
mm 2-3 + mm 20-21
miR-1 guide
Bulged target
Target-directed miRNA destabilization
Unrelated
Perfect
mm 9-10
mm 9-14
mm 9-15
mm 2-4
mm 2-4 + mm 9-10
mm 2-4 + mm 9-14
mm 2-4 + mm 9-15
No bulge
Bulge
Perfect
mm 2-3
Perfect
mm 2-3
mm 2-3 + mm 20-21
(nt)
20
10
B
Non-slicer Argonautes
hAgo2 (D597A)
hAgo1
Unrelated
Seed
Perfect
mm 2-3
mm 2-6
mm 9-12
mm 16-21
hAgo2 (WT)
hAgo2 (D597A)
hAgo1
Unrelated
mm 1-8
mm 1-10
mm 1-12
mm 1-14
mm 1-15
Ago2 (WT)
Ago2 (D597A)
Ago1
α-FLAG
α-Tubulin
C
3′ end nucleotide
miR-151
HeLa lysate (endo-Ago)
Unrelated
Seed
mm 1-8
mm 1-8+21
mm 2-3
miR-1
(nt)
20
10
1.0 1.2 0.2 0.5 0.1
1.0 0.9 0.8 0.4 0.8 0.2
D
Target-length
mm 2-3
Unrelated
17-mer
21-mer
25-mer
35-mer
mRNA
1.0 1.0 0.1 0.2 0.2 0.3
5′cap-...NNNNNNNNNNUACAUACUUCUUUACAUUGGANNNNNNNNN...poly(A)~150-3′
35-nt 5′-NNNNNNNNUACAUACUUCUUUACAUUGGANNNNNNNN-3′
25-nt 5′-NNUACAUACUUCUUUACAUUGGANN-3′
21-nt 5′-UACAUACUUCUUUACAUUGGA-3′
17-nt 5′- UACUUCUUUACAUUGGA-3′
3′-AUGUAUGAAGAAAUGUAAGGU-5′

Figure 28. Two nucleotide 3′ guide strand overhang is important for miRNA stability and optimal RISC assembly

(A) Schematic of paired miRNAs and passenger strand-like targets. (B) The canonical passenger-strands with 2-nt 3′ overhang do not destabilize miRNAs. (C) miRNA duplexes with 2-nt 3′ overhang are optimal substrate for Ago2-RISC assembly. miRNA duplexes containing radiolabeled guide strands were incubated in lysates expressing tagged Ago2 for the indicated times. The RISC complexes were separated on a vertical agarose native gel at 4°C.

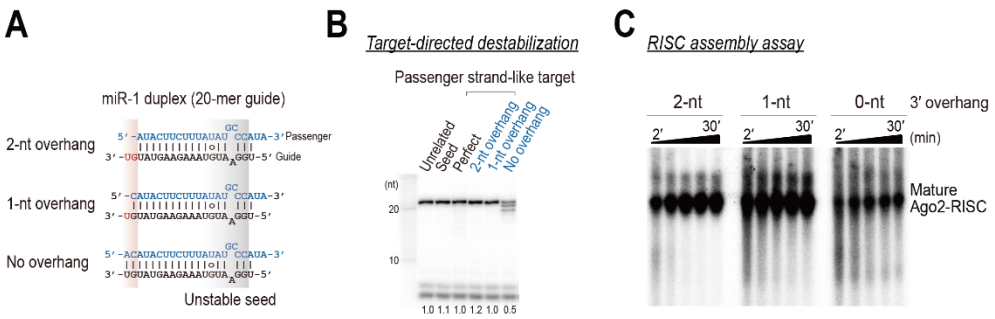
A
miR-1 duplex (20-mer guide)
2-nt overhang
1-nt overhang
No overhang
Passenger
Guide
Unstable seed
B
Target-directed destabilization
Passenger strand-like target
Unrelated
Seed
Perfect
2-nt overhang
1-nt overhang
No overhang
(nt)
20
10
1.0 1.1 1.0 1.2 1.0 0.5
C
RISC assembly assay
2-nt
1-nt
0-nt
3′ overhang
2′
30′
(min)
Mature
Ago2-RISC

Dynamic conformational changes of the PAZ domain drive 3′ end destabilization[2]

How are the 3′ ends of miRNAs destabilized? Ago proteins experience dynamic conformational changes during RISC assembly and catalysis (Meister, 2013; Parker, 2010). A two-state model was originally proposed by Tomari and Zamore (Tomari and Zamore, 2005), based on their biochemical characterization of Argonautes, which was later supported by structural studies (Nakanishi et al., 2012; Wang et al., 2009). This model postulates that the seed region is first organized into an A-form like arrangement that creates a suitable target binding site. The 3′ ends of the miRNAs are initially anchored in the PAZ domain, and it dislodges when the miRNA-target duplex propagates toward the 3′ end of the guide. I hypothesized that 3′ end destabilization could occur during these structural rearrangements that are associated with target binding. To test this idea, I aimed to determine whether functional disruptions of Argonaute alleviate 3′ end destabilization.

First, it has been proposed that the hAgo2 PAZ domain moves like a discrete rigid body along the other domain, and that the 'hinge' for this pivotal conformational change resides in the α7–L1 domain (Schirle et al., 2014). Further supporting this line of thought, a recent study showed that hAgo2 PAZ is largely fixed on the tip of L1 and, therefore, it moves in concert with L1 (Zhu et al., 2016). Moreover, I and others previously showed that F181, which resides in the hinge (L1), is required for efficient small interfering RNA (siRNA) duplex separation during RISC assembly (Kwak and Tomari, 2012; Park and Shin, 2015). Therefore, F181 is a candidate for the hinge of the L1-PAZ domain (Fig. 29A).

[2]The experiments in this section were carried out in collaboration with **Sang-Yoon Shin**.

Second, within the PAZ domain, I focused on residues that are expected to interact with the 3′ end nt of the guide, based on my results (Fig. 26E) and structural modeling (Fig. 30A). To this end, I generated a series of Ago2 mutants (Fig. 29B). The Ago2 mutant proteins that were defective in forming miRNA-guide RISC complex (miRISC) were excluded for further analysis (Fig. 29B). I found that mutation of the F181 hinge drastically compromised 3′ end destabilization (Fig. 30B) and miRNA release from Ago2 (Fig. 29C). Additionally, Y311, which is close to the 3′ end nt of the guide in the PAZ domain, moderately, but reproducibly, reduced the extent of 3′ end destabilization (Fig. 30C).

Then, I analyzed these two mutants using several non-canonical targets (Fig. 29D and 30D). When the seeds were partially matched (mm 2-3), mutation of the hinge largely protected the miRNAs from destabilization, whereas the Y311A mutation mildly increased the level of protection (Fig. 29D). In contrast, when the seeds were completely mismatched (mm 1-8 or mm 1-14), the hinge mutant was less able to protect the miRNAs from destabilization, whereas the Y311A mutant strongly inhibited destabilization (Fig. 29D). These results indicate that even a partial seed match is helpful for positional shifts in the PAZ domain. In support of this hypothesis, a previous molecular dynamic simulation suggested that a partial mutation in the seed region led to a large bending motion of the PAZ domain along the hinge, which facilitated a target interaction in the 3′ half of the guide (Xia et al., 2012). Strikingly, miRNA destabilization was mostly abolished in the F181A/Y311A L1-PAZ double mutant (Fig. 29E and 30E). Taken together, I concluded that residues in the PAZ domain and related conformational changes are likely to be responsible for target-directed miRNA destabilization.

Figure 29. Identification and characterization of human Argonaute2 domains that are required for 3′ end destabilization

(A) A schematic representation of human Ago2 domains. The miRNA is anchored at its ends in the PAZ and MID domains. (B) Top: miRNA duplexes containing radiolabeled guide strands were incubated in lysates expressing tagged wild-type or mutant Ago2 proteins at 37°C for 1 h. The RISC complexes were analyzed in a vertical agarose native gel at 4°C. Middle: miRNAs were analyzed in parallel by 15% denaturing-PAGE. Bottom: Western blot analysis using an anti-FLAG antibody confirmed the expression of the tagged Ago2 mutant proteins. Anti-tubulin served as an internal control. (C) The F181A hinge mutation drastically inhibits miRNA release from the Ago2-complex. The samples were analyzed by 15% native-PAGE following the *in vitro* destabilization reactions in Ago2-expressing lysates or buffers. (D and E) The L1 and PAZ domains of human Ago2 are required for 3′ end destabilization. Data are the mean ± SD for three independent experiments.

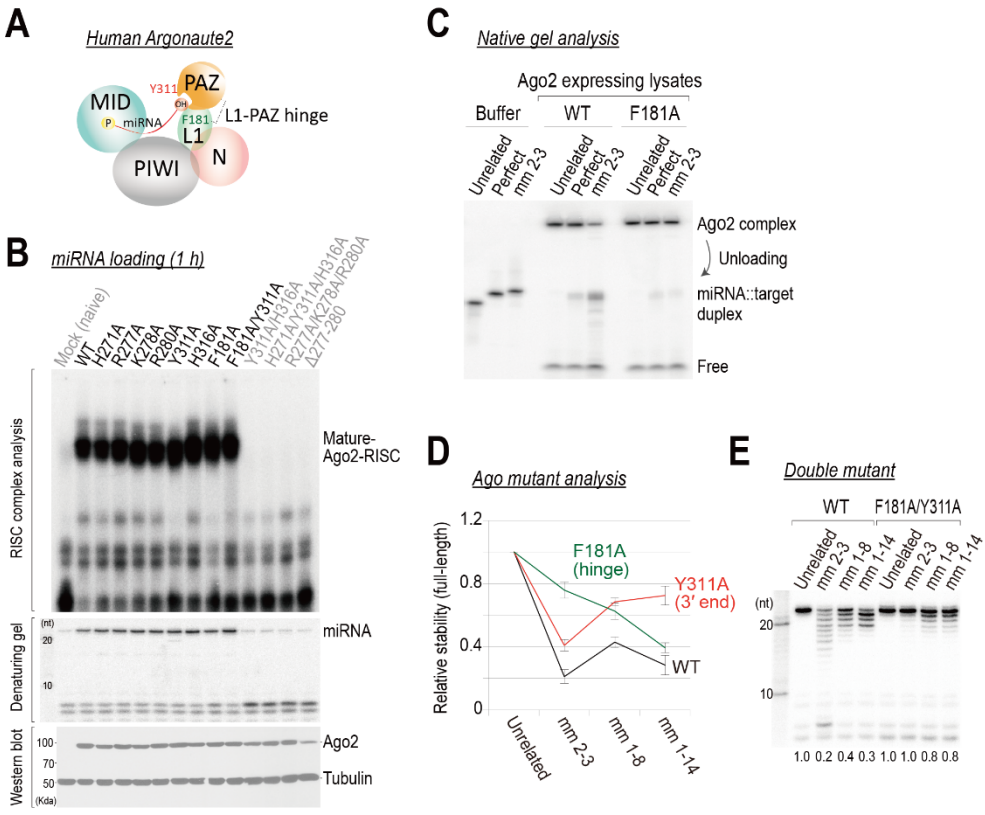
A
Human Argonaute2
PAZ
Y311
MID
OH
P
miRNA
F181
L1
L1-PAZ hinge
PIWI
N
B
miRNA loading (1 h)
Mock (naive)
WT
H271A
R277A
K278A
R280A
Y311A
H316A
F181A
F181A/Y311A
Y311A/H316A
H271A/Y311A/H316A
R277A/K278A/R280A
Δ277-280
RISC complex analysis
Mature-Ago2-RISC
Denaturing gel
(nt)
20
10
miRNA
Western blot
100
70
50
(Kda)
Ago2
Tubulin
C
Native gel analysis
Ago2 expressing lysates
Buffer
WT
F181A
Unrelated
Perfect
mm 2-3
Ago2 complex
Unloading
miRNA::target duplex
Free
D
Ago mutant analysis
Relative stability (full-length)
1.2
0.8
0.4
0
F181A (hinge)
Y311A (3′ end)
WT
Unrelated
mm 2-3
mm 1-8
mm 1-14
E
Double mutant
WT
F181A/Y311A
Unrelated
mm 2-3
mm 1-8
mm 1-14
(nt)
20
10
1.0 0.2 0.4 0.3 1.0 1.0 0.8 0.8

Figure 30. Identification and characterization of human Argonaute2 domains that are required for 3′ end destabilization - II

(A) The residues of the hAgo2 PAZ domain that are expected to interact with the 3′ end nt of the guide (snapshot of the structure 4W5N taken in pymol). (B) The residues, Y311 and F181, are involved in the 3′ end destabilization. (C) The Y311 data (mm 2-3/ctrl) are the mean ± SD for three independent experiments. (D) Representative gel data for Fig. 29D. (E) Repetitive experiment of Fig. 29E.

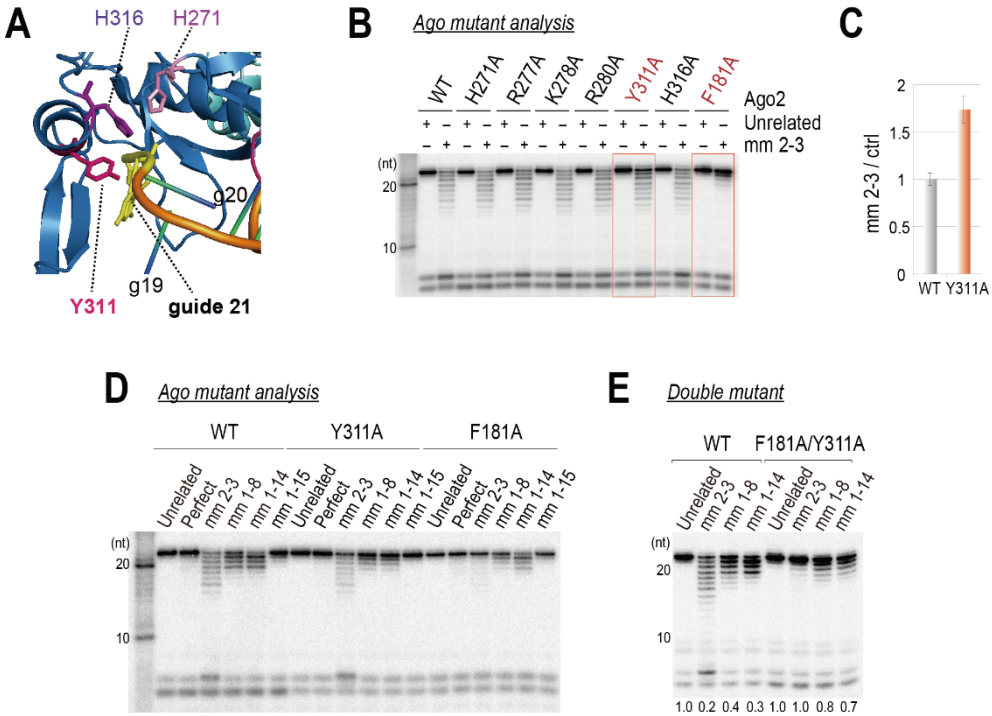
A
H316
H271
g20
g19
Y311
guide 21
B
Ago mutant analysis
WT
H271A
R277A
K278A
R280A
Y311A
H316A
F181A
Ago2
Unrelated
mm 2-3
(nt)
20
10
C
mm 2-3 / ctrl
2
1.5
1
0.5
0
WT Y311A
D
Ago mutant analysis
WT
Y311A
F181A
Unrelated
Perfect
mm 2-3
mm 1-8
mm 1-14
mm 1-15
(nt)
20
10
E
Double mutant
WT
F181A/Y311A
Unrelated
mm 2-3
mm 1-8
mm 1-14
(nt)
20
10
1.0 0.2 0.4 0.3 1.0 1.0 0.8 0.7

Non-canonical target and anti-miR possibly employ distinct mechanisms for miRNA destabilization

Approaches that are based on artificial antisense oligonucleotides have been used to specifically inhibit miRNA function both *in vitro* and *in vivo* (Hutvagner et al., 2004; Meister et al., 2004a). In addition, a recent study employed 2′-*O*-methylated anti-miR to recapitulate target-directed miRNA degradation in cultured cells (Haas et al., 2016). Although the underlying mechanisms are still unclear, it is generally believed that the anti-miR binds with high affinity to the active miRISCs and thereby blocks their binding to endogenous RNA targets, acting as decoy or 'sponges'. Motivated by these, I compared and evaluated miRNA inhibition potencies of non-canonical target and 2′-*O*-methylated anti-miR both *in vitro* and in cultured cells.

I first performed *in vitro* miRNA destabilization assay, followed by cleavage assay, as in Fig. 25C. The addition of 2′-*O*-Me anti-miR completely inhibited cleavage activities (Hutvagner et al., 2004; Meister et al., 2004a) without compromising the stability of miRNAs (Fig. 31A). This is consistent with previous findings that 2′-*O*-Me anti-miR can be used to stably capture Ago protein complexes (Hutvagner et al., 2004; Yoda et al., 2010), indicating that anti-miR do not destabilize miRNAs *in vitro*. In contrast, transfection of 2′-*O*-Me anti-miR in cultured cells resulted in the dramatic reduction in the level of miRNAs in Ago2 (Fig. 31B). The discrepancy between two results (*in vitro* and cultured cells) indicates that non-canonical target and anti-miR possibly employ distinct mechanisms for miRNA destabilization (Fig. 31C).

The results from my *in vitro* system are likely to directly reflect an intrinsic property of Ago proteins; namely, the seedless, non-canonical targets can

potentially induce the rearrangements in Ago structure to cause miRNA destabilization, at least in high concentration (> 1 μM). Because the non-canonical target has approximately 10-fold less affinity to RISC (Fig. 23B), low concentration of the target RNAs in cultured cell-based assay (< 0.1 μM) may not be high enough to overcome the reduced binding affinity of Ago2 for targets that contain mismatches in the seed region. The results from cleavage assay indicate that Ago2 may bind and unbind non-canonical targets multiple times (*i.e.*, unstable, low affinity binding) (Fig. 31C). In contrast, anti-miR appears to be stably associated with Ago proteins (*i.e.*, stable, high affinity binding) (Fig. 31C). Intriguingly, the miRNAs were still found in the input fraction upon transfection of anti-miRs in cultured cells (Fig. 31B). Although the exact mechanism is unclear, I postulate that anti-miR may act either by sequestering the miRNAs without causing significant degradation (Davis et al., 2009) (possibly at early time points), or by slowly promoting the unloading of miRNAs in Ago proteins, thereby inducing their degradation (Krutzfeldt et al., 2007) (Fig. 31C).

Figure 31. Non-canonical target and anti-miR possibly employ distinct mechanisms for miRNA destabilization

(A) The addition of 2′-O-Me anti-miR completely inhibited cleavage activities without compromising the stability of miRNAs. miRNAs were first destabilized by cold targets, prior to the addition of cap-radiolabeled perfect targets (as in Fig. 25C). (B) Transfection of 2′-O-Me anti-miR in cultured cells resulted in the dramatic reduction in the level of miRNAs in Ago2. HEK293T cells were transfected with 10 nM miRNA duplex, 100 nM target RNA and FLAG-Ago2 expression plasmid. Cell lysates were subjected to Ago2-IP, followed by northern blotting using the miR-1 probe. The blot was probed for U6 snRNA as a loading control. The numbers below the blot are the relative expression levels, normalized using the loading control. Ethidium bromide-stained 5s rRNA served as another loading control. (C) An envisioned model of several distinct action mechanisms of target-directed miRNA destabilization.

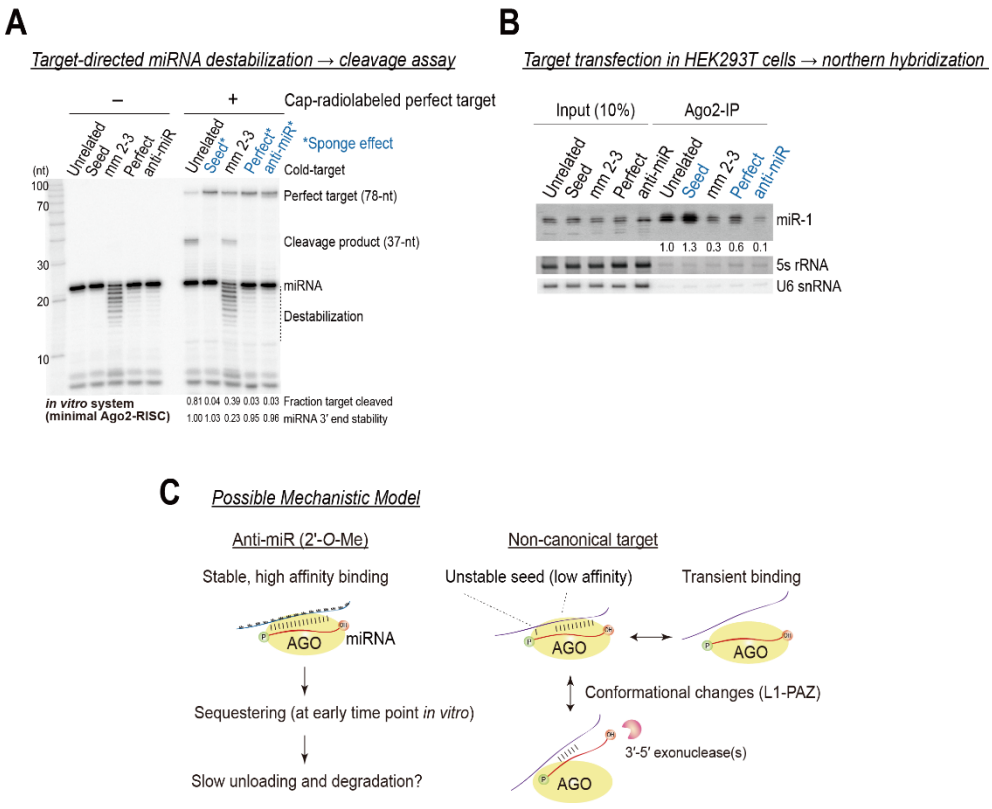
A
Target-directed miRNA destabilization → cleavage assay
–
+
Cap-radiolabeled perfect target
Unrelated
Seed
mm 2-3
Perfect
anti-miR
Unrelated
Seed*
mm 2-3
Perfect*
anti-miR*
*Sponge effect
(nt)
100
70
30
20
10
Cold-target
Perfect target (78-nt)
Cleavage product (37-nt)
miRNA
Destabilization
in vitro system
(minimal Ago2-RISC)
0.81 0.04 0.39 0.03 0.03 Fraction target cleaved
1.00 1.03 0.23 0.95 0.86 miRNA 3′ end stability
B
Target transfection in HEK293T cells → northern hybridization
Input (10%)
Ago2-IP
Unrelated
Seed
mm 2-3
Perfect
anti-miR
Unrelated
Seed
mm 2-3
Perfect
anti-miR
miR-1
1.0 1.3 0.3 0.6 0.1
5s rRNA
U6 snRNA
C
Possible Mechanistic Model
Anti-miR (2′-O-Me)
Stable, high affinity binding
AGO
miRNA
Sequestering (at early time point in vitro)
Slow unloading and degradation?
Non-canonical target
Unstable seed (low affinity)
Transient binding
AGO
AGO
Conformational changes (L1-PAZ)
3′-5′ exonuclease(s)
AGO

Non-canonical target-directed mechanism is likely to operate in living cells

There are two sides to non-canonical targets: 1) non-canonical target has a great potential to destabilize miRNAs; and 2) non-canonical target has reduced binding affinity to RISC because of mismatches in the seed region. This seemingly paradoxical nature of the non-canonical target prompted me to examine what extent my *in vitro* results recapitulate cellular processes. In this regard, I first tested if the addition of non-canonical targets destabilizes endogenous miRNAs that are pre-loaded in Ago proteins both *in vitro* and in cultured cells (Fig. 32A). To this end, I targeted the two most abundantly expressed miRNAs (*i.e.*, miR-20a and miR-16) in HEK293T cells (Jayaprakash et al., 2011). The HEK293T cells were transfected with 100 nM of the corresponding target RNAs of each miRNA and subjected to northern blot analysis. The results showed that non-canonical targets specifically decrease the level of their cognate miRNAs in living cells (Fig. 32A, left), which is largely consistent with the *in vitro* results with saturating target concentrations (1 μM) (Fig. 32A, right).

To efficiently recapitulate miRNA destabilization in cells, I prepared 4x miR-1 target plasmids encoding unrelated, canonical (seed) or non-canonical (mm 2-3) target sites. HEK293T cells were initially co-transfected with miR-1 duplex and Ago2 plasmid for efficient exogenous miRNA assembly. It is of note that Ago protein is the primary rate-limiting factor of both *in vitro* and *in vivo* RNAi efficacy (Borner et al., 2013; Grimm et al., 2010; Lund et al., 2011; Wakiyama et al., 2007). The target plasmids were then sequentially transfected (Fig. 32B). At 48 h post-transfection, RNAs were extracted and subjected to northern blot analysis. The results again showed that the level of miRNAs was significantly and reproducibly reduced by the expression of non-canonical targets, but not by the unrelated or

canonical targets (Fig. 32B). Although the physiological miRNA target concentration may vary greatly, these collective results strongly indicate that miRNAs can be destabilized by the non-canonical targets both *in vitro* and in cells.

Figure 32. Non-canonical targets destabilize miRNAs in human cells

(A) Non-canonical targets specifically decrease the level of the cognate endogenous miRNAs both *in vitro* and in cells. Top: Schematic of the experiment. Bottom: Endogenous miR-16 and miR-20a were detected by northern blotting and each served as a loading control for the other. Blotting for U6 snRNA and $tRNA^{lys}$ also served as loading controls. U: unrelated, C: canonical (seed), N: non-canonical (mm 2-3). (B) miRNAs are destabilized when their non-canonical targets are expressed. Top: Schematic of the experiment. Bottom: Northern blot analysis of miR-1 after transfection with plasmids encoding unrelated, canonical (seed), or non-canonical (mm 2-3) target sites. The blot was re-probed for miR-20a as a loading control. The numbers below the blot are the relative expression levels, normalized using the miR-20a loading control. Blotting for U6 snRNA and $tRNA^{lys}$ also served as loading controls. Three independent experiments are shown. (C) A proposed model for the miRNA destabilization mechanism in human Argonaute. Left: miRNAs preferentially bind to targets containing intact seed matches, which may allow them to exert their regulatory roles. Right: The 3′ end destabilization of miRNAs is enhanced by the interaction with non-canonical targets (an unstable seed compensated by extensive 3′ pairing), and it is driven by the highly dynamic nature of the L1-PAZ domain of human Argonautes. Unloading may occur during some cases, possibly because of the instability of the miRNA seed region.

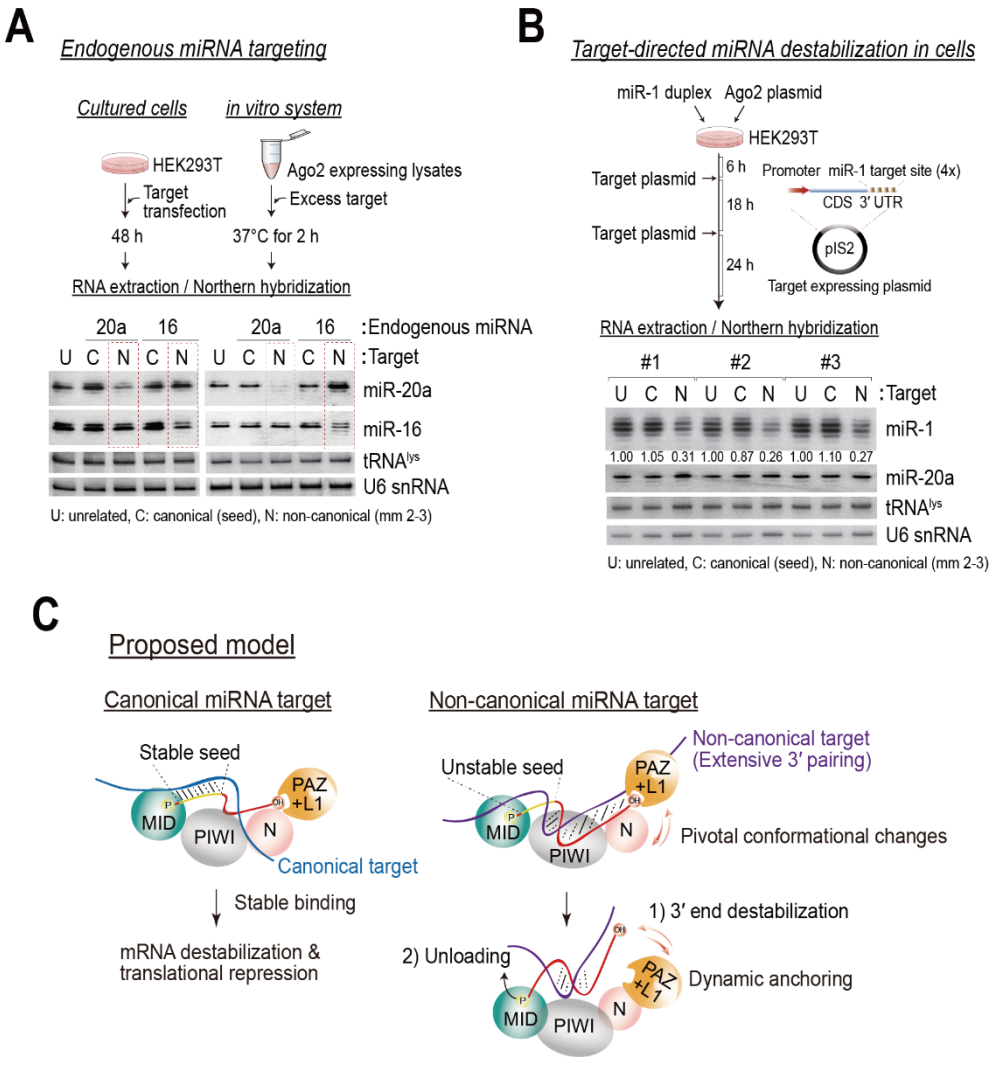
A
Endogenous miRNA targeting
Cultured cells
in vitro system
HEK293T
Target transfection
48 h
Ago2 expressing lysates
Excess target
37°C for 2 h
RNA extraction / Northern hybridization
20a 16 20a 16 :Endogenous miRNA
U C N C N U C N C N :Target
miR-20a
miR-16
tRNAlys
U6 snRNA
U: unrelated, C: canonical (seed), N: non-canonical (mm 2-3)
B
Target-directed miRNA destabilization in cells
miR-1 duplex
Ago2 plasmid
HEK293T
Target plasmid
6 h
18 h
Target plasmid
24 h
Promoter
miR-1 target site (4x)
CDS 3' UTR
pIS2
Target expressing plasmid
RNA extraction / Northern hybridization
#1 #2 #3
U C N U C N U C N :Target
miR-1
1.00 1.05 0.31 1.00 0.87 0.26 1.00 1.10 0.27
miR-20a
tRNAlys
U6 snRNA
U: unrelated, C: canonical (seed), N: non-canonical (mm 2-3)
C
Proposed model
Canonical miRNA target
Stable seed
MID
PIWI
PAZ +L1
N
Canonical target
Stable binding
mRNA destabilization & translational repression
Non-canonical miRNA target
Unstable seed
Non-canonical target (Extensive 3′ pairing)
Pivotal conformational changes
1) 3′ end destabilization
2) Unloading
Dynamic anchoring

Discussion

Steady-state regulation of miRNAs and their targets in cells is a dynamic process that should take into account various factors, including the rates of transcription, processing, and decay (Marzi et al., 2016). Therefore, without a controlled system, it may be difficult to ascertain the contribution of the different proposed mechanisms for miRNA regulation, as one phenomenon can be masked by the other in cells. In the present study, to pinpoint the target RNA-directed mechanism and to study the molecular underpinning of associated regulatory events, I established an *in vitro* experimental system. One advantage of the *in vitro* system is that it enables a detailed examination of target-directed destabilization at early time points, while data from cell-based experiments are obtained after 24–72 h, at which point the process is often saturated. Based on my results, I propose that miRNA destabilization is enhanced by interactions with non-canonical targets.

Non-canonical binding modes — that is, those with mismatches in the miRNA seed region, but which are often accompanied by auxiliary 3′ end pairing — were empirically inferred from high-throughput analyses of an miRNA-target chimera, and they were shown to constitute 15–40% of the captured sites (Broughton et al., 2016; Grosswendt et al., 2014; Hausser and Zavolan, 2014; Helwak et al., 2013; Loeb et al., 2012; Moore et al., 2015). In line with these findings, a molecular simulation study also revealed that mismatches in the seed region are largely allowable without compromising overall Ago-complex stability (Xia et al., 2012). However, despite their prevalence, non-canonical sites are generally less effective in target silencing than canonical sites (Agarwal et al., 2015), which leads to questions regarding their biological roles. My findings

implicate a possible biological role of these non-canonical targets in controlling the stability of miRNAs. I suggest that non-canonical targets are not something to be regulated by miRNAs, but instead, they provide a stability control mechanism in the regulation of miRNAs. I believe that my results may provide a novel insight into the mechanism for stabilizing selection that is expected to maintain a rigid conservation of miRNA seed sequences for the functional and selective targeting.

Currently, no established methods are available to address the genome-wide contribution of a target-directed mechanism (*i.e.*, each target to each miRNA). Destabilization effects were mostly diminished when I incubated miRISC with both canonical and non-canonical targets (data not shown). These results suggest that if canonical targets are abundantly expressed in a given cell type, most miRNAs might preferentially bind to those containing intact seed matches (Fig. 23B), which may allow them to exert their regulatory roles (Fig. 32C). Therefore, a target-directed mechanism may be challenging to generalize, and it should depend on the cell-type specific, spatio-temporally regulated expression of canonical and non-canonical targets. Further studies are needed to determine what extent such mechanisms contribute to the regulation of miRNA function *in vivo.*

An early study hypothesized that miRNAs can be destabilized by targets if their 3′ ends are released from the PAZ pocket (Ameres et al., 2010). Although further structural studies are needed to extensively validate this hypothesis, I first directly demonstrated *in vitro* that residues in the PAZ domain and its hinge are involved in this process. The 3′ end of miRNAs that is free from the PAZ domain may then become susceptible to 3′–5′ exonuclease or nucleotidyltransferases (Haas et al., 2016). I found that miRNAs tend to be 3′ trimmed, rather than tailed, in cytoplasmic lysates from HEK293T or HeLa cells, although the target-directed 3′

tailing of miRNAs has been observed in several other systems, including neuronal cells (de la Mata et al., 2015) and *Drosophila* embryo lysates (Ameres et al., 2010). I believe that the differences are largely attributed to the availability of Argonaute paralogs and distinctive enzymes (*i.e.*, exonucleases or nucleotidyltransferases) within a given system.

Supporting this idea, I was able to observe both 3′ tailing and trimming of miRNAs in *Drosophila* Ago1 by highly complementary targets in S2 cell lysates (Fig. 33). However, this was not the case for those bound to *Drosophila* Ago2 (Fig. 33), because they possesses a 2′-*O*-methyl group at their 3′ end, which is catalyzed by endogenous Hen1 (Ameres et al., 2010). Interestingly, however, miRNAs bound to *Drosophila* Ago1 did not appear to interact with seedless 3′ paired targets (Fig. 33), which is consistent with a previous study (Ameres et al., 2010). Although the distinct mechanisms remain to be elucidated, I postulate that *Drosophila* Ago1 might depart more rapidly from such targets, compared with human Ago2.

My findings suggest that a target-directed mechanism can result in two outcomes: unloading and 3′ end destabilization within Argonautes. My results are generally consistent with the analysis by MacRae and colleagues (De et al., 2013), in which unloading is accelerated by mismatches to the 5′ end and complementarity to the 3′ end of the guide RNA in recombinant hAgo2 expressed in Sf9 cells. In my experimental system, which consists of the minimal hAgo2-RISC and endogenous proteins present in HEK293T cell lysates, I explored the related molecular mechanisms, and I conclude that such features are essentially linked to the seed region of miRNAs. The only exception was that a fully complementary target did not appear to be effective as previously. Perhaps an additional endogenous protein(s) helps stabilize the interaction between the Ago2-complex and miRNAs

containing intact seed matches to the target (Bose and Bhattacharyya, 2016; Chatterjee et al., 2011).

The unloading mechanism is likely to be the most extreme example of miRNA degradation, because Argonaute-free ss-miRNAs are susceptible to both 5′-3′ or 3′-5′ exonuclease(s), and possibly to endonuclease(s). In light of my findings, I propose two consecutive mechanisms of miRNA destabilization (Fig. 32C): 1) 3′ end destabilization is triggered by an extensive 3′ interaction and the large-scale motion of the L1-PAZ domain, while the MID domain still binds to the 5′ phosphate end of miRNAs; and 2) unloading may occur during some cases, possibly because of the instability of the miRNA seed region. The 3′ end destabilization mechanism may explain the 3′ heterogeneity of miRNAs. The 3′ heterogeneity may impact target silencing by influencing the preference for alternative binding sites within target RNAs. Importantly, I showed that 3′ pairing of a miRNA may influence its own stability, which probably correlates with its silencing efficiency and multiple-turnover (Ameres et al., 2007; Brennecke et al., 2005; Broderick et al., 2011; De et al., 2013; Wee et al., 2012). Therefore, the impact and biological consequences of the 3′ end destabilization mechanism can be diverse and dynamic.

In sum, my findings reflect another layer onto the mutual regulatory circuits between miRNAs and their various targets. Rather than transcriptional control of miRNA biosynthesis, regulation of mature miRNA turnover via unloading and 3′ end destabilization in Argonautes serves as a means to refine and diversify miRNAs in cells.

Figure 33. Target-directed tailing and trimming of miRNAs in *Drosophila* S2 cell lysates

The *in vitro* target-directed destabilization assay (as in Fig. 21A) was performed in *Drosophila* S2 cell lysates at 25°C. The different small RNA duplexes were used to favor the assembly of miRNA duplexes into dAgo1-RISC or siRNA duplexes into dAgo2-RISC (Tomari et al., 2007).

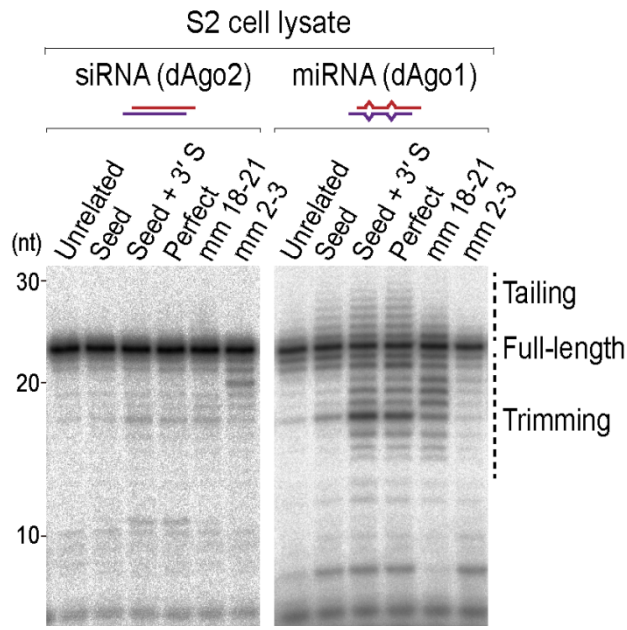
S2 cell lysate
siRNA (dAgo2)
miRNA (dAgo1)
Unrelated
Seed
Seed + 3′ S
Perfect
mm 18-21
mm 2-3
Unrelated
Seed
Seed + 3′ S
Perfect
mm 18-21
mm 2-3
(nt)
30
20
10
Tailing
Full-length
Trimming

CONCLUSION AND PROSPECT

The process of separating the small RNA duplex and discarding the one of strands (*i.e.*, passenger-strand) has been historically referred to as ‘unwinding’. Although this term is often used throughout this dissertation, the ‘unwinding’ has been used to refer to the process by which helicases catalyze the separation of double-stranded DNA/RNA hybrids by disrupting hydrogen bonds in an ATP-dependent manner, with the energy from ATP hydrolysis. My findings, combined with those of previous studies, suggest that the strand separation of the small RNA duplexes occurs without the need for ATP hydrolysis. Therefore, the recent literatures are indeed reluctant to use the term ‘unwinding’, in order not to give a false impression, but rather to use the term ‘passenger-strand ejection’ (Nakanishi, 2016).

Proteins generally follow energetically favorable pathways to form stable and orderly structures. They can perform their catalytic functions only when they are properly folded into the native structure. I envision that the RISC maturation process can be viewed as a protein-folding pathway, whereby an Ago protein undergoes structural changes to reach its native structure (*i.e.*, mature RISC). I postulate that free-Ago proteins (apo; no substrate) are flexible and intrinsically unstable and require chaperone machinery to take the conformation competent for the small RNA duplex loading. Upon loading, the 5′ phosphate group of a guide strand helps to anchor the nucleotide to the binding pocket of the MID domain, while the N and L1/2 domains are protruded outward (Fig. 34). This, in turn, creates an inward pressure that forces an unanchored passenger strand to be ultimately ejected (Fig. 34). The larger thermal dynamics of the L1-PAZ domain at

37°C are likely to robustly shake the 3′ end of the guide strand, and thereby help pry the duplex apart (Fig. 34) (Nakanishi, 2016). The resultant mature RISC presumably takes the most energetically favorable conformation, which is now ready for subsequent enzymatic catalysis (*i.e.*, target repression).

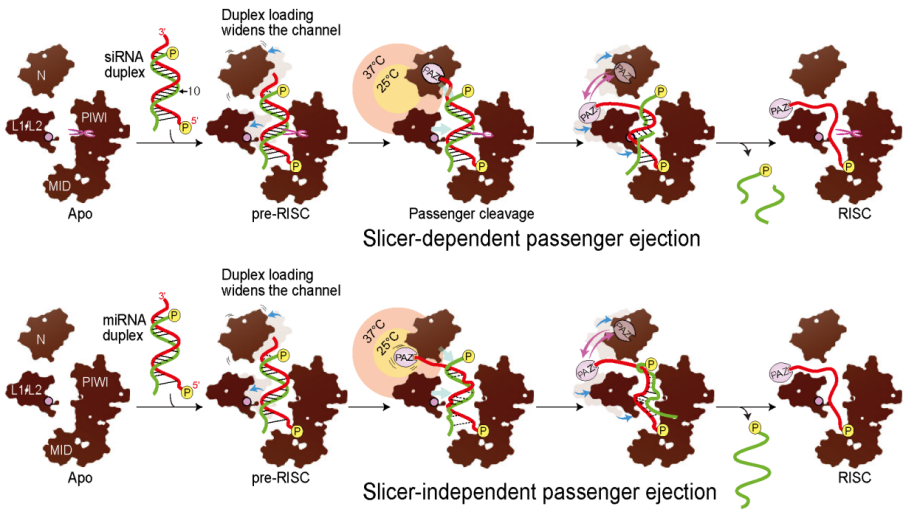

Figure 34. Two model mechanisms of passenger ejection [Nakanishi, K. (2016). Anatomy of RISC: how do small RNAs and chaperones activate Argonaute proteins? *Wiley Interdiscip. Rev. RNA* 7, 637-660.]

The mature RISCs use the miRNAs as a guide to identify complementary target RNAs for their regulation. By contrast, it is also suggested that target binding may have the opposite effect that leads to the negative regulation of miRNAs (*i.e.*, miRNA destabilization). By developing a highly sensitive method, I further discovered that target-directed mechanism entails not only unloading from Ago (De et al., 2013), but also 3′ end destabilization occurred within Ago, which is driven by the dynamic nature of the L1-PAZ domain. Importantly, I showed that a complete seed pairing dramatically inhibits these processes, and thus, the most effective sites for stimulating destabilization have not only perfect pairing to the 3' region of the miRNAs, but also mismatches in the seed region (*i.e.*, non-canonical

miRNA targets). Non-canonical miRNA binding sites are thought to comprise more than 20% of miRNA interactome (Broughton et al., 2016; Grosswendt et al., 2014; Helwak et al., 2013; Loeb et al., 2012; Moore et al., 2015); however, their biological roles are subject to considerable debate because they are generally not effective in target silencing (Agarwal et al., 2015). Although further *in vivo* studies, including high-throughput analysis, are required to extensively validate this hypothesis, the current findings represent a 'paradigm shift' in how we perceive the non-canonical targets. I suggest that non-canonical targets are not something to be regulated by miRNAs, but instead, they provide a stability control mechanism in the regulation of miRNAs. I believe that these results may provide a novel insight into the mechanism for stabilizing selection that is expected to maintain a rigid conservation of miRNA seed sequences for the functional and selective targeting.

Research in the RNAi field has profited greatly from recent developments in high-throughput sequencing technologies that allow an unprecedented level of small RNA profiling, which seems to have reached a plateau in our capacity to functionally or mechanistically characterize these molecules. Our understanding of miRNA biology is still very limited by our poor appreciation of their cell-type specific and spatio-temporal regulation. Many miRNAs exhibit discrete expression patterns and their mutual regulations (*i.e.*, miRNA ↔ target) may depend largely on the availability of particular Ago proteins and distinct target RNAs (*i.e.*, canonical or non-canonical) within a given cell type. Although many exhaustive studies have identified more than a million small RNAs, the biological function of only a few have been identified. The combinatorial analysis of small RNA sequencing and accurate expression data for target mRNA/proteins and various miRNA processing enzymes, could ultimately provide us with a better

understanding of these complex networks. In addition, more detailed *in vitro* kinetic studies, along with the structural analysis of Ago proteins (especially in their apo form or pre-RISC, which has not been determined yet), may illustrate an elegant interplay of Ago proteins, small RNAs and their targets.

REFERENCES

Addo-Quaye, C., Eshoo, T.W., Bartel, D.P., and Axtell, M.J. (2008). Endogenous siRNA and miRNA targets identified by sequencing of the Arabidopsis degradome. *Curr. Biol.* 18, 758-762.

Agarwal, V., Bell, G.W., Nam, J.W., and Bartel, D.P. (2015). Predicting effective microRNA target sites in mammalian mRNAs. *eLife* 4.

Ameres, S.L., Horwich, M.D., Hung, J.H., Xu, J., Ghildiyal, M., Weng, Z., and Zamore, P.D. (2010). Target RNA-directed trimming and tailing of small silencing RNAs. *Science* 328, 1534-1539.

Ameres, S.L., Martinez, J., and Schroeder, R. (2007). Molecular basis for target RNA recognition and cleavage by human RISC. *Cell* 130, 101-112.

Azuma-Mukai, A., Oguri, H., Mituyama, T., Qian, Z.R., Asai, K., Siomi, H., and Siomi, M.C. (2008). Characterization of endogenous human Argonautes and their miRNA partners in RNA silencing. *Proc. Natl. Acad. Sci. USA* 105, 7964-7969.

Babiarz, J.E., Ruby, J.G., Wang, Y., Bartel, D.P., and Blelloch, R. (2008). Mouse ES cells express endogenous shRNAs, siRNAs, and other Microprocessor-independent, Dicer-dependent small RNAs. *Genes Dev.* 22, 2773-2785.

Baccarini, A., Chauhan, H., Gardner, T.J., Jayaprakash, A.D., Sachidanandam, R., and Brown, B.D. (2011). Kinetic analysis reveals the fate of a microRNA following target regulation in mammalian cells. *Curr. Biol.* 21, 369-376.

Bartel, D.P. (2004). MicroRNAs: genomics, biogenesis, mechanism, and function. *Cell* 116, 281-297.

Bartel, D.P. (2009). MicroRNAs: target recognition and regulatory functions. *Cell* 136, 215-233.

Bazzini, A.A., Lee, M.T., and Giraldez, A.J. (2012). Ribosome Profiling Shows That miR-430 Reduces Translation Before Causing mRNA Decay in Zebrafish. *Science* 336, 233-237.

Bennett, A.F. (1978). Activity metabolism of the lower vertebrates. *Annu. Rev. Physiol.* 40, 447-469.

Bernstein, E., Caudy, A.A., Hammond, S.M., and Hannon, G.J. (2001). Role for a bidentate ribonuclease in the initiation step of RNA interference. *Nature* 409, 363-366.

Betancur, J.G., and Tomari, Y. (2012). Dicer is dispensable for asymmetric RISC loading in mammals. *RNA* 18, 24-30.

Bohmert, K., Camus, I., Bellini, C., Bouchez, D., Caboche, M., and Benning, C. (1998). AGO1 defines a novel locus of Arabidopsis controlling leaf development. *EMBO J* 17, 170-180.

Boland, A., Huntzinger, E., Schmidt, S., Izaurralde, E., and Weichenrieder, O. (2011). Crystal structure of the MID-PIWI lobe of a eukaryotic Argonaute protein. *Proc. Natl. Acad. Sci. USA* 108, 10466-10471.

Bonincontro, A., Bultrini, E., Calandrini, V., and Onori, G. (2001). Conformational changes of proteins in aqueous solution induced by temperature in the pre-melting region. *Phys. Chem. Chem. Phys.* 3, 3811-3813.

Borner, K., Niopek, D., Cotugno, G., Kaldenbach, M., Pankert, T., Willemsen, J., Zhang, X., Schurmann, N., Mockenhaupt, S., Serva, A., et al. (2013). Robust RNAi enhancement via human Argonaute-2 overexpression from plasmids, viral vectors and cell lines. *Nucleic Acids Res.* 41, e199.

Bose, M., and Bhattacharyya, S.N. (2016). Target-dependent biogenesis of cognate microRNAs in human cells. *Nat. Commun.* 7, 12200.

Bouasker, S., and Simard, M.J. (2012). The slicing activity of miRNA-specific Argonautes is essential for the miRNA pathway in C. elegans. *Nucleic Acids Res.* 40, 10452-10462.

Brennecke, J., Stark, A., Russell, R.B., and Cohen, S.M. (2005). Principles of microRNA-target recognition. *PLoS Biol.* 3, e85.

Broderick, J.A., Salomon, W.E., Ryder, S.P., Aronin, N., and Zamore, P.D. (2011). Argonaute protein identity and pairing geometry determine cooperativity in mammalian RNA silencing. *RNA* 17, 1858-1869.

Broughton, J.P., Lovci, M.T., Huang, J.L., Yeo, G.W., and Pasquinelli, A.E. (2016). Pairing beyond the Seed Supports MicroRNA Targeting Specificity. *Mol. Cell* 64, 320-333.

Caldwell, C.R. (1989). Temperature-Induced Protein Conformational Changes in Barley Root Plasma Membrane-Enriched Microsomes: III. Effect of Temperature and Cations on Protein Sulfhydryl Reactivity. *Plant Physiol.* 91, 1339-1344.

Carmel, I., Shomron, N., and Heifetz, Y. (2012). Does base-pairing strength play a role in microRNA repression? *RNA* 18, 1947-1956.

Cerutti, L., Mian, N., and Bateman, A. (2000). Domains in gene silencing and cell differentiation proteins: the novel PAZ domain and redefinition of the Piwi domain. *Trends Biochem. Sci.* 25, 481-482.

Chandradoss, S.D., Schirle, N.T., Szczepaniak, M., MacRae, I.J., and Joo, C. (2015). A Dynamic Search Process Underlies MicroRNA Targeting. *Cell* 162, 96-107.

Chatterjee, S., Fasler, M., Bussing, I., and Grosshans, H. (2011). Target-mediated protection of endogenous microRNAs in C. elegans. *Dev. Cell* 20, 388-396.

Chatterjee, S., and Grosshans, H. (2009). Active turnover modulates mature microRNA activity in Caenorhabditis elegans. *Nature* 461, 546-549.

Davis, S., Propp, S., Freier, S.M., Jones, L.E., Serra, M.J., Kinberger, G., Bhat, B., Swayze, E.E., Bennett, C.F., and Esau, C. (2009). Potent inhibition of microRNA in vivo without degradation. *Nucleic Acids Res.* 37, 70-77.

de la Mata, M., Gaidatzis, D., Vitanescu, M., Stadler, M.B., Wentzel, C., Scheiffele, P., Filipowicz, W., and Grosshans, H. (2015). Potent degradation of neuronal miRNAs induced by highly complementary targets. *EMBO Rep.* 16, 500-511.

De, N., Young, L., Lau, P.W., Meisner, N.C., Morrissey, D.V., and MacRae, I.J. (2013). Highly complementary target RNAs promote release of guide RNAs from human Argonaute2. *Mol. Cell* 50, 344-355.

Elkayam, E., Kuhn, C.D., Tocilj, A., Haase, A.D., Greene, E.M., Hannon, G.J., and Joshua-Tor, L. (2012). The structure of human argonaute-2 in complex with miR-20a. *Cell* 150, 100-110.

Ender, C., and Meister, G. (2010). Argonaute proteins at a glance. *J. Cell Sci.* 123, 1819-1823.

Faehnle, C.R., Elkayam, E., Haase, A.D., Hannon, G.J., and Joshua-Tor, L. (2013). The making of a slicer: activation of human Argonaute-1. *Cell Rep.* 3, 1901-1909.

Forstemann, K., Horwich, M.D., Wee, L., Tomari, Y., and Zamore, P.D. (2007). Drosophila microRNAs are sorted into functionally distinct argonaute complexes after production by Dicer-1. *Cell* 130, 287-297.

Frank, F., Sonenberg, N., and Nagar, B. (2010). Structural basis for 5'-nucleotide base-specific recognition of guide RNA by human AGO2. *Nature* 465, 818-822.

Friedman, R.C., Farh, K.K., Burge, C.B., and Bartel, D.P. (2009). Most mammalian mRNAs are conserved targets of microRNAs. *Genome Res.* 19, 92-105.

Gabelica, V., and De Pauw, E. (2002). Comparison of the collision-induced dissociation of duplex DNA at different collision regimes: Evidence for a multistep dissociation mechanism. *J. Am. Soc. Mass. Spectr.* 13, 91-98.

Garcia, D.M., Baek, D., Shin, C., Bell, G.W., Grimson, A., and Bartel, D.P. (2011). Weak seed-pairing stability and high target-site abundance decrease the proficiency of lsy-6 and other microRNAs. *Nat. Struct. Mol. Biol.* 18, 1139-1146.

German, M.A., Pillay, M., Jeong, D.H., Hetawal, A., Luo, S., Janardhanan, P., Kannan, V., Rymarquis, L.A., Nobuta, K., German, R., et al. (2008). Global identification of microRNA-target RNA pairs by parallel analysis of RNA ends.

Nat. Biotechnol. 26, 941-946.

Gregory, B.D., O'Malley, R.C., Lister, R., Urich, M.A., Tonti-Filippini, J., Chen, H., Millar, A.H., and Ecker, J.R. (2008). A link between RNA metabolism and silencing affecting Arabidopsis development. *Dev. Cell* 14, 854-866.

Grimm, D., Wang, L., Lee, J.S., Schurmann, N., Gu, S., Borner, K., Storm, T.A., and Kay, M.A. (2010). Argonaute proteins are key determinants of RNAi efficacy, toxicity, and persistence in the adult mouse liver. *J. Clin. Invest.* 120, 3106-3119.

Grosswendt, S., Filipchyk, A., Manzano, M., Klironomos, F., Schilling, M., Herzog, M., Gottwein, E., and Rajewsky, N. (2014). Unambiguous identification of miRNA:target site interactions by different types of ligation reactions. *Mol. Cell* 54, 1042-1054.

Grubbs, R.D. (2002). Intracellular magnesium and magnesium buffering. *Biometals* 15, 251-259.

Gu, S., Jin, L., Huang, Y., Zhang, F., and Kay, M.A. (2012). Slicing-independent RISC activation requires the argonaute PAZ domain. *Curr. Biol.* 22, 1536-1542.

Gu, S., Jin, L., Zhang, F., Huang, Y., Grimm, D., Rossi, J.J., and Kay, M.A. (2011). Thermodynamic stability of small hairpin RNAs highly influences the loading process of different mammalian Argonautes. *Proc. Natl. Acad. Sci. USA* 108, 9208-9213.

Gunther, T. (2006). Concentration, compartmentation and metabolic function of intracellular free Mg^{2+}. *Magnes. Res.* 19, 225-236.

Ha, M., and Kim, V.N. (2014). Regulation of microRNA biogenesis. Nature reviews. *Nat. Rev. Mol. Cell Biol.* 15, 509-524.

Haas, G., Cetin, S., Messmer, M., Chane-Woon-Ming, B., Terenzi, O., Chicher, J., Kuhn, L., Hammann, P., and Pfeffer, S. (2016). Identification of factors involved in target RNA-directed microRNA degradation. *Nucleic Acids Res.* 44, 2873-2887.

Haley, B., Tang, G., and Zamore, P.D. (2003). In vitro analysis of RNA interference in Drosophila melanogaster. *Methods* 30, 330-336.

Hauptmann, J., Dueck, A., Harlander, S., Pfaff, J., Merkl, R., and Meister, G. (2013). Turning catalytically inactive human Argonaute proteins into active slicer enzymes. *Nat. Struct. Mol. Biol.* 20, 814-817.

Hausser, J., and Zavolan, M. (2014). Identification and consequences of miRNA-target interactions--beyond repression of gene expression. *Nat. Rev. Genet.* 15, 599-612.

Helwak, A., Kudla, G., Dudnakova, T., and Tollervey, D. (2013). Mapping the human miRNA interactome by CLASH reveals frequent noncanonical binding.

Cell 153, 654-665.

Heo, I., Joo, C., Kim, Y.K., Ha, M., Yoon, M.J., Cho, J., Yeom, K.H., Han, J., and Kim, V.N. (2009). TUT4 in concert with Lin28 suppresses microRNA biogenesis through pre-microRNA uridylation. *Cell* 138, 696-708.

Hibio, N., Hino, K., Shimizu, E., Nagata, Y., and Ui-Tei, K. (2012). Stability of miRNA 5'terminal and seed regions is correlated with experimentally observed miRNA-mediated silencing efficacy. *Sci. Rep.* 2, 996.

Huntzinger, E., and Izaurralde, E. (2011). Gene silencing by microRNAs: contributions of translational repression and mRNA decay. *Nat. Rev. Genet.* 12, 99-110.

Hutvagner, G., and Simard, M.J. (2008). Argonaute proteins: key players in RNA silencing. *Nat. Rev. Mol. Cell Biol.* 9, 22-32.

Hutvagner, G., Simard, M.J., Mello, C.C., and Zamore, P.D. (2004). Sequence-specific inhibition of small RNA function. *PLoS Biol.* 2, E98.

Hwang, H.W., Wentzel, E.A., and Mendell, J.T. (2009). Cell-cell contact globally activates microRNA biogenesis. *Proc. Natl. Acad. Sci. USA* 106, 7016-7021.

Iki, T., Yoshikawa, M., Nishikiori, M., Jaudal, M.C., Matsumoto-Yokoyama, E., Mitsuhara, I., Meshi, T., and Ishikawa, M. (2010). In vitro assembly of plant RNA-induced silencing complexes facilitated by molecular chaperone HSP90. *Mol. Cell* 39, 282-291.

Iwakawa, H.O., and Tomari, Y. (2015). The Functions of MicroRNAs: mRNA Decay and Translational Repression. *Trends Cell Biol.* 25, 651-665.

Iwasaki, S., Kobayashi, M., Yoda, M., Sakaguchi, Y., Katsuma, S., Suzuki, T., and Tomari, Y. (2010). Hsc70/Hsp90 chaperone machinery mediates ATP-dependent RISC loading of small RNA duplexes. *Mol. Cell* 39, 292-299.

Iwasaki, S., Sasaki, H.M., Sakaguchi, Y., Suzuki, T., Tadakuma, H., and Tomari, Y. (2015). Defining fundamental steps in the assembly of the Drosophila RNAi enzyme complex. *Nature* 521, 533-536.

Jayaprakash, A.D., Jabado, O., Brown, B.D., and Sachidanandam, R. (2011). Identification and remediation of biases in the activity of RNA ligases in small-RNA deep sequencing. *Nucleic Acids Res.* 39, e141.

Jinek, M., and Doudna, J.A. (2009). A three-dimensional view of the molecular machinery of RNA interference. *Nature* 457, 405-412.

Jonas, S., and Izaurralde, E. (2015). Towards a molecular understanding of microRNA-mediated gene silencing. *Nat. Rev. Genet.* 16, 421-433.

Jones-Rhoades, M.W., Bartel, D.P., and Bartel, B. (2006). MicroRNAs and their regulatory roles in plants. *Annu. Rev. Plant Biol.* 57, 19-53.

Jung, S.R., Kim, E., Hwang, W., Shin, S., Song, J.J., and Hohng, S. (2013). Dynamic anchoring of the 3'-end of the guide strand controls the target dissociation of Argonaute-guide complex. *J. Am. Chem. Soc.* 135, 16865-16871.

Katayanagi, K., Miyagawa, M., Matsushima, M., Ishikawa, M., Kanaya, S., Ikehara, M., Matsuzaki, T., and Morikawa, K. (1990). Three-dimensional structure of ribonuclease H from E. coli. *Nature* 347, 306-309.

Kawamata, T., Seitz, H., and Tomari, Y. (2009). Structural determinants of miRNAs for RISC loading and slicer-independent unwinding. *Nat. Struct. Mol. Biol.* 16, 953-960.

Kawamata, T., and Tomari, Y. (2010). Making RISC. *Trends Biochem. Sci.* 35, 368-376.

Kawamata, T., and Tomari, Y. (2011). Native gel analysis for RISC assembly. *Methods Mol. Biol.* 725, 91-105.

Khvorova, A., Reynolds, A., and Jayasena, S.D. (2003). Functional siRNAs and miRNAs exhibit strand bias. *Cell* 115, 209-216.

Kim, V.N., Han, J., and Siomi, M.C. (2009). Biogenesis of small RNAs in animals. Nature reviews. *Nat. Rev. Mol. Cell Biol.* 10, 126-139.

Knight, S.W., and Bass, B.L. (2001). A role for the RNase III enzyme DCR-1 in RNA interference and germ line development in Caenorhabditis elegans. *Science* 293, 2269-2271.

Kool, E.T. (2001). Hydrogen bonding, base stacking, and steric effects in DNA replication. *Annu. Rev. Biophys. Biomol. Struct.* 30, 1-22.

Krol, J., Busskamp, V., Markiewicz, I., Stadler, M.B., Ribi, S., Richter, J., Duebel, J., Bicker, S., Fehling, H.J., Schubeler, D., et al. (2010). Characterizing light-regulated retinal microRNAs reveals rapid turnover as a common property of neuronal microRNAs. *Cell* 141, 618-631.

Krutzfeldt, J., Kuwajima, S., Braich, R., Rajeev, K.G., Pena, J., Tuschl, T., Manoharan, M., and Stoffel, M. (2007). Specificity, duplex degradation and subcellular localization of antagomirs. *Nucleic Acids Res.* 35, 2885-2892.

Kwak, P.B., and Tomari, Y. (2012). The N domain of Argonaute drives duplex unwinding during RISC assembly. *Nat. Struct. Mol. Biol.* 19, 145-151.

Lee, R.C., Feinbaum, R.L., and Ambros, V. (1993). The C. elegans heterochronic gene lin-4 encodes small RNAs with antisense complementarity to lin-14. *Cell* 75, 843-854.

Lee, Y., Ahn, C., Han, J., Choi, H., Kim, J., Yim, J., Lee, J., Provost, P., Radmark, O., Kim, S., et al. (2003). The nuclear RNase III Drosha initiates microRNA processing. *Nature* 425, 415-419.

Lee, Y., Kim, M., Han, J., Yeom, K.H., Lee, S., Baek, S.H., and Kim, V.N. (2004). MicroRNA genes are transcribed by RNA polymerase II. *EMBO J* 23, 4051-4060.

Leuschner, P.J., Ameres, S.L., Kueng, S., and Martinez, J. (2006). Cleavage of the siRNA passenger strand during RISC assembly in human cells. *EMBO Rep.* 7, 314-320.

Lim, L.P., Lau, N.C., Garrett-Engele, P., Grimson, A., Schelter, J.M., Castle, J., Bartel, D.P., Linsley, P.S., and Johnson, J.M. (2005). Microarray analysis shows that some microRNAs downregulate large numbers of target mRNAs. *Nature* 433, 769-773.

Lingel, A., Simon, B., Izaurralde, E., and Sattler, M. (2003). Structure and nucleic-acid binding of the Drosophila Argonaute 2 PAZ domain. *Nature* 426, 465-469.

Liu, J.D., Carmell, M.A., Rivas, F.V., Marsden, C.G., Thomson, J.M., Song, J.J., Hammond, S.M., Joshua-Tor, L., and Hannon, G.J. (2004). Argonaute2 is the catalytic engine of mammalian RNAi. *Science* 305, 1437-1441.

Liu, X., Jin, D.Y., McManus, M.T., and Mourelatos, Z. (2012). Precursor microRNA-programmed silencing complex assembly pathways in mammals. *Mol. Cell* 46, 507-517.

Liu, X., Zheng, Q., Vrettos, N., Maragkakis, M., Alexiou, P., Gregory, B.D., and Mourelatos, Z. (2014). A MicroRNA precursor surveillance system in quality control of MicroRNA synthesis. *Mol. Cell* 55, 868-879.

Llave, C., Xie, Z., Kasschau, K.D., and Carrington, J.C. (2002). Cleavage of Scarecrow-like mRNA targets directed by a class of Arabidopsis miRNA. *Science* 297, 2053-2056.

Loeb, G.B., Khan, A.A., Canner, D., Hiatt, J.B., Shendure, J., Darnell, R.B., Leslie, C.S., and Rudensky, A.Y. (2012). Transcriptome-wide miR-155 binding map reveals widespread noncanonical microRNA targeting. *Mol. Cell* 48, 760-770.

Lund, E., Sheets, M.D., Imboden, S.B., and Dahlberg, J.E. (2011). Limiting Ago protein restricts RNAi and microRNA biogenesis during early development in Xenopus laevis. *Genes Dev.* 25, 1121-1131.

Ma, J.B., Ye, K., and Patel, D.J. (2004). Structural basis for overhang-specific small interfering RNA recognition by the PAZ domain. *Nature* 429, 318-322.

Macias, S., Cordiner, R.A., and Caceres, J.F. (2013). Cellular functions of the microprocessor. *Biochem. Soc. Trans.* 41, 838-843.

Maguire, M.E., and Cowan, J.A. (2002). Magnesium chemistry and biochemistry. *Biometals* 15, 203-210.

Majlessi, M., Nelson, N.C., and Becker, M.M. (1998). Advantages of 2'-O-methyl oligoribonucleotide probes for detecting RNA targets. *Nucleic Acids Res.* 26, 2224-2229.

Martinez, N.J., and Gregory, R.I. (2013). Argonaute2 expression is post-transcriptionally coupled to microRNA abundance. *RNA* 19, 605-612.

Marzi, M.J., Ghini, F., Cerruti, B., de Pretis, S., Bonetti, P., Giacomelli, C., Gorski, M.M., Kress, T., Pelizzola, M., Muller, H., et al. (2016). Degradation dynamics of microRNAs revealed by a novel pulse-chase approach. *Genome Res.* 26, 554-565.

Matranga, C., Tomari, Y., Shin, C., Bartel, D.P., and Zamore, P.D. (2005). Passenger-strand cleavage facilitates assembly of siRNA into Ago2-containing RNAi enzyme complexes. *Cell* 123, 607-620.

Meister, G. (2013). Argonaute proteins: functional insights and emerging roles. *Nat. Rev. Genet.* 14, 447-459.

Meister, G., Landthaler, M., Dorsett, Y., and Tuschl, T. (2004a). Sequence-specific inhibition of microRNA- and siRNA-induced RNA silencing. *RNA* 10, 544-550.

Meister, G., Landthaler, M., Patkaniowska, A., Dorsett, Y., Teng, G., and Tuschl, T. (2004b). Human Argonaute2 mediates RNA cleavage targeted by miRNAs and siRNAs. *Mol. Cell* 15, 185-197.

Miyoshi, K., Tsukumo, H., Nagami, T., Siomi, H., and Siomi, M.C. (2005). Slicer function of Drosophila Argonautes and its involvement in RISC formation. *Genes Dev.* 19, 2837-2848.

Miyoshi, K., Uejima, H., Nagami-Okada, T., Siomi, H., and Siomi, M.C. (2008). In vitro RNA cleavage assay for Argonaute-family proteins. *Methods Mol. Biol.* 442, 29-43.

Miyoshi, T., Takeuchi, A., Siomi, H., and Siomi, M.C. (2010). A direct role for Hsp90 in pre-RISC formation in Drosophila. *Nat. Struct. Mol. Biol.* 17, 1024-1026.

Moomaw, A.S., and Maguire, M.E. (2008). The unique nature of Mg^{2+} channels. *Physiology* 23, 275-285.

Moore, M.J., Scheel, T.K., Luna, J.M., Park, C.Y., Fak, J.J., Nishiuchi, E., Rice, C.M., and Darnell, R.B. (2015). miRNA-target chimeras reveal miRNA 3'-end pairing as a major determinant of Argonaute target specificity. *Nat. Commun.* 6, 8864.

Nakanishi, K. (2016). Anatomy of RISC: how do small RNAs and chaperones activate Argonaute proteins? Wiley interdisciplinary reviews. *RNA* 7, 637-660.

Nakanishi, K., Weinberg, D.E., Bartel, D.P., and Patel, D.J. (2012). Structure of yeast Argonaute with guide RNA. *Nature* 486, 368-374.

Nakano, S., Fujimoto, M., Hara, H., and Sugimoto, N. (1999). Nucleic acid duplex stability: influence of base composition on cation effects. *Nucleic Acids Res.* 27, 2957-2965.

Nowotny, M., Gaidamakov, S.A., Crouch, R.J., and Yang, W. (2005). Crystal structures of RNase H bound to an RNA/DNA hybrid: substrate specificity and metal-dependent catalysis. *Cell* 121, 1005-1016.

Nykanen, A., Haley, B., and Zamore, P.D. (2001). ATP requirements and small interfering RNA structure in the RNA interference pathway. *Cell* 107, 309-321.

Olejniczak, S.H., La Rocca, G., Gruber, J.J., and Thompson, C.B. (2013). Long-lived microRNA-Argonaute complexes in quiescent cells can be activated to regulate mitogenic responses. *Proc. Natl. Acad. Sci. USA* 110, 157-162.

Park, J.H., and Shin, C. (2014). MicroRNA-directed cleavage of targets: mechanism and experimental approaches. *BMB Rep.* 47, 417-423.

Park, J.H., and Shin, C. (2015). Slicer-independent mechanism drives small-RNA strand separation during human RISC assembly. *Nucleic Acids Res.* 43, 9418-9433.

Parker, J.S. (2010). How to slice: snapshots of Argonaute in action. *Silence* 1, 3.

Rand, T.A., Petersen, S., Du, F., and Wang, X. (2005). Argonaute2 cleaves the anti-guide strand of siRNA during RISC activation. *Cell* 123, 621-629.

Rhoades, M.W., Reinhart, B.J., Lim, L.P., Burge, C.B., Bartel, B., and Bartel, D.P. (2002). Prediction of plant microRNA targets. *Cell* 110, 513-520.

Rissland, O.S., Hong, S.J., and Bartel, D.P. (2011). MicroRNA destabilization enables dynamic regulation of the miR-16 family in response to cell-cycle changes. *Mol. Cell* 43, 993-1004.

Rivas, F.V., Tolia, N.H., Song, J.J., Aragon, J.P., Liu, J., Hannon, G.J., and Joshua-Tor, L. (2005). Purified Argonaute2 and an siRNA form recombinant human RISC. *Nat. Struct. Mol. Biol.* 12, 340-349.

Rocheleau, M.J., Grey, R.J., Chen, D.Y., Harke, H.R., and Dovichi, N.J. (1992). Formamide modified polyacrylamide gels for DNA sequencing by capillary gel electrophoresis. *Electrophoresis* 13, 484-486.

Ruben, J. (1995). The evolution of endothermy in mammals and birds: from physiology to fossils. *Annu. Rev. Physiol.* 57, 69-95.

Salomon, W.E., Jolly, S.M., Moore, M.J., Zamore, P.D., and Serebrov, V. (2015). Single-Molecule Imaging Reveals that Argonaute Reshapes the Binding Properties

of Its Nucleic Acid Guides. *Cell* 162, 84-95.

Schirle, N.T., and MacRae, I.J. (2012). The crystal structure of human Argonaute2. *Science* 336, 1037-1040.

Schirle, N.T., Sheu-Gruttadauria, J., and MacRae, I.J. (2014). Structural basis for microRNA targeting. *Science* 346, 608-613.

Schurmann, N., Trabuco, L.G., Bender, C., Russell, R.B., and Grimm, D. (2013). Molecular dissection of human Argonaute proteins by DNA shuffling. *Nat. Struct. Mol. Biol.* 20, 818-826.

Schwab, R., Palatnik, J.F., Riester, M., Schommer, C., Schmid, M., and Weigel, D. (2005). Specific effects of MicroRNAs on the plant transcriptome. *Dev. Cell* 8, 517-527.

Schwarz, D.S., Hutvagner, G., Du, T., Xu, Z., Aronin, N., and Zamore, P.D. (2003). Asymmetry in the assembly of the RNAi enzyme complex. *Cell* 115, 199-208.

Schwarz, D.S., Tomari, Y., and Zamore, P.D. (2004). The RNA-induced silencing complex is a Mg^{2+}-dependent endonuclease. *Curr. Biol.* 14, 787-791.

Serra, M.J., Baird, J.D., Dale, T., Fey, B.L., Retatagos, K., and Westhof, E. (2002). Effects of magnesium ions on the stabilization of RNA oligomers of defined structures. *RNA* 8, 307-323.

Song, J.J., Liu, J., Tolia, N.H., Schneiderman, J., Smith, S.K., Martienssen, R.A., Hannon, G.J., and Joshua-Tor, L. (2003). The crystal structure of the Argonaute2 PAZ domain reveals an RNA binding motif in RNAi effector complexes. *Nat. Struct. Mol. Biol.* 10, 1026-1032.

Song, J.J., Smith, S.K., Hannon, G.J., and Joshua-Tor, L. (2004). Crystal structure of Argonaute and its implications for RISC slicer activity. *Science* 305, 1434-1437.

Su, H., Trombly, M.I., Chen, J., and Wang, X. (2009). Essential and overlapping functions for mammalian Argonautes in microRNA silencing. *Genes Dev.* 23, 304-317.

Subtelny, A.O., Eichhorn, S.W., Chen, G.R., Sive, H., and Bartel, D.P. (2014). Poly(A)-tail profiling reveals an embryonic switch in translational control. *Nature* 508, 66-71.

Suzuki, H.I., Katsura, A., Yasuda, T., Ueno, T., Mano, H., Sugimoto, K., and Miyazono, K. (2015). Small-RNA asymmetry is directly driven by mammalian Argonautes. *Nat. Struct. Mol. Biol.* 22, 512-521.

Tomari, Y., Du, T., and Zamore, P.D. (2007). Sorting of Drosophila small silencing RNAs. *Cell* 130, 299-308.

Tomari, Y., and Zamore, P.D. (2005). Perspective: machines for RNAi. *Genes Dev.* 19, 517-529.

Tuschl, T., Zamore, P.D., Lehmann, R., Bartel, D.P., and Sharp, P.A. (1999). Targeted mRNA degradation by double-stranded RNA in vitro. *Genes Dev.* 13, 3191-3197.

van Rij, R.P., Saleh, M.C., Berry, B., Foo, C., Houk, A., Antoniewski, C., and Andino, R. (2006). The RNA silencing endonuclease Argonaute 2 mediates specific antiviral immunity in Drosophila melanogaster. *Genes Dev.* 20, 2985-2995.

Wakiyama, M., Takimoto, K., Ohara, O., and Yokoyama, S. (2007). Let-7 microRNA-mediated mRNA deadenylation and translational repression in a mammalian cell-free system. *Genes Dev.* 21, 1857-1862.

Wang, Y., Juranek, S., Li, H., Sheng, G., Tuschl, T., and Patel, D.J. (2008a). Structure of an argonaute silencing complex with a seed-containing guide DNA and target RNA duplex. *Nature* 456, 921-926.

Wang, Y., Juranek, S., Li, H., Sheng, G., Wardle, G.S., Tuschl, T., and Patel, D.J. (2009). Nucleation, propagation and cleavage of target RNAs in Ago silencing complexes. *Nature* 461, 754-761.

Wang, Y., Sheng, G., Juranek, S., Tuschl, T., and Patel, D.J. (2008b). Structure of the guide-strand-containing argonaute silencing complex. *Nature* 456, 209-213.

Watanabe, T., Totoki, Y., Toyoda, A., Kaneda, M., Kuramochi-Miyagawa, S., Obata, Y., Chiba, H., Kohara, Y., Kono, T., Nakano, T., et al. (2008). Endogenous siRNAs from naturally formed dsRNAs regulate transcripts in mouse oocytes. *Nature* 453, 539-543.

Wee, L.M., Flores-Jasso, C.F., Salomon, W.E., and Zamore, P.D. (2012). Argonaute divides its RNA guide into domains with distinct functions and RNA-binding properties. *Cell* 151, 1055-1067.

Winter, J., and Diederichs, S. (2011). Argonaute proteins regulate microRNA stability: Increased microRNA abundance by Argonaute proteins is due to microRNA stabilization. *RNA Biol.* 8, 1149-1157.

Xia, Z., Clark, P., Huynh, T., Loher, P., Zhao, Y., Chen, H.W., Ren, P., Rigoutsos, I., and Zhou, R. (2012). Molecular dynamics simulations of Ago silencing complexes reveal a large repertoire of admissible 'seed-less' targets. *Sci. Rep.* 2, 569.

Yan, K.S., Yan, S., Farooq, A., Han, A., Zeng, L., and Zhou, M.M. (2003). Structure and conserved RNA binding of the PAZ domain. *Nature* 426, 468-474.

Yoda, M., Kawamata, T., Paroo, Z., Ye, X., Iwasaki, S., Liu, Q., and Tomari, Y. (2010). ATP-dependent human RISC assembly pathways. *Nat. Struct. Mol. Biol.* 17, 17-23.

Zhu, L., Jiang, H., Sheong, F.K., Cui, X., Gao, X., Wang, Y., and Huang, X. (2016). A Flexible Domain-Domain Hinge Promotes an Induced-fit Dominant Mechanism for the Loading of Guide-DNA into Argonaute Protein in Thermus thermophilus. *J. Phys. Chem. B.* 120, 2709-2720.

ABSTRACT IN KOREAN

마이크로RNA (miRNA), 짧은 간섭RNA (siRNA)를 비롯한 스몰RNA (small RNA)는 세포 내에서 유전자 발현을 억제하여 조절하는 기능을 수행하며, 이를 일컬어 RNA간섭이라 부른다. 이는 small RNA가 RNA-induced silencing complex (RISC)와 결합함을 통해 실질적으로 기능하며, 이 RISC 복합체의 중추적인 역할을 담당하는 단백질이 Argonaute (Ago)이다. RISC 생성의 마지막 과정은 두 가닥으로 이루어진 small RNA duplex가 최종적으로 가이드 (guide)의 역할을 수행하는 가닥만 Ago단백질에 남고, 동반자 (passenger) 가닥은 제거되는 과정을 수반한다. 이러한 과정에서 절단 활성을 지닌 human Ago2 단백질의 경우 passenger 가닥을 절단함을 통해 이러한 과정을 촉진한다고 알려져 있으며, 이 절단 메커니즘 (passenger-strand cleavage)은 두 가닥의 상보성이 완전할 경우 일어나기에 siRNA duplex에 특이적이다. 하지만 불완전한 상보성을 지니는 miRNA duplex, 또는 절단 활성이 없는 다른 human Ago 단백질 (Ago 1, 3, 4)은 이 과정에서 slicer-independent mechanism에 전적으로 의존할 수 밖에 없다. 나는 본 연구에서 이를 생화학적 방법을 통해 구체적으로 분석한 결과, human cell의 경우 높은 생리학적 온도와 Ago 단백질의 domain들이 직접적으로 기능하여, 외부 helicase나 절단 메커니즘의 도움 없이 small RNA 두 가닥이 분리되어 최종 성숙됨을 확인하였다. 이러한 결과는 무엇보다 절단 활성이 없는 human Ago 단백질들이 어떻게 siRNA을 보유하고 있는지에 대한 궁금증을 해결한 생물학적 의의를 지닌다.

miRNA는 타겟 RNA를 조절하는 역할을 수행하기에, 반대로 miRNA 자체 조절 역시 생물학적으로 중요할 것으로 여겨진다. 하지만 최종 성숙된 miRNA가 어떻게 불안정화 및 분해가 되는지는 아직까지 잘 알려지지 않았다. miRNA는 Ago 단백질에 결합하면 핵산가수분해 효소의 작용으로부터 보호되고, 따라서 반감기가 세포 내에서 수 일 (days)에 달한다고 알려져 있다. 하지만 최근 연구에 따르면 miRNA의 타겟 RNA가 반대로 miRNA를 Ago protein 밖으로 방출 (unloading)시켜 miRNA의 분해를 촉

진하는 것으로 보고되었으나, 아직까지 위 과정에 대한 구체적인 메커니즘은 잘 밝혀지지 않은 상태이다. 나는 이를 구체적으로 분석하기 위해 위 현상을 *in vitro*에서 재현하는 실험 방법 (assay)를 개발하였고, 이를 통해 miRNA가 상보적인 타겟 RNA를 통해 어떻게 불안정화 되는지 분자 수준에서 알고자 하였다. 이를 통해 놀랍게도, miRNA seed 부분이 불완전한, 비정규적인 (non-canonical) 타겟 RNA가 이러한 불안정화 메커니즘에 매우 크게 기여함을 밝혀내었다. 더 나아가 이러한 현상이 unloading에만 의존하는 것이 아닌, Ago 단백질 내에서 3′ 말단 부분이 불안정화 되는, 서로 다른 두 가지의 메커니즘으로 작동함을 밝혀내었다. 돌연변이 Ago 단백질을 이용한 기능 분석을 수행한 결과, Ago 단백질의 L1과 PAZ domain 부분이 이러한 3′ 말단 불안정화에 직접적으로 기여함을 밝혀내었다. 이러한 결과들을 종합하였을 때 small RNA의 두 가닥이 분리되어 성숙한 RISC를 형성하는 과정, 그리고 이 small RNA가 타겟 RNA와 결합하여 불안정화되는 두 과정 모두 Ago 단백질의 본질적인 특성인, 입체구조의 역동성 (dynamic conformational changes)에 상당 부분 기인한다는 사실을 확인할 수 있었다. 나는 본 연구를 통해, Ago 단백질이 small RNA와 효율적으로 결합하여 기질복합체 (RISC)를 형성하고, 이 복합체의 small RNA가 또 다른 기질인 타겟 RNA를 만나서 불안정화 되는 일련의 연속적 과정이 small RNA를 양적으로 미세 조절하고, 3′ 말단 서열을 다양화 시키는 메커니즘에 기여함을 알 수 있었다.

주요어: 스몰 RNA, 마이크로 RNA, 짧은 간섭 RNA, 동반자 (passenger) 가닥 절단, 절단 비 의존성 메커니즘, Argonaute 단백질, 타겟 RNA 에 의한 miRNA 불안정화

학번: 2012-30322

PUBLICATIONS

Park, J.H., Shin, S.Y., Shin, C. (2017) Non-canonical targets destabilize microRNAs in human Argonautes. *Nucleic Acids Res.* (*in press*). (IF=9.202)
**** Featured as NAR breakthrough article (Top paper published in the Journal)***

Park, J.H., Shin, C. (2015) Slicer-independent mechanism drives small-RNA strand separation during human RISC assembly. *Nucleic Acids Res.* 43(19):9418-9433. (IF=9.202)

Park J.H., Shin C. (2015) The role of plant small RNAs in NB-LRR regulation. *Brief Funct. Genomics* 14(4):268-274. (IF=3.124)

Lee, H.J., Park, Y.J., Kwak, K.J., Kim, D.H., **Park, J.H.**, Lim, J.Y., Shin, C., Yang, K.Y., Kang, H. (2015) MicroRNA844-guided Downregulation of Cytidinephosphate Diacylglycerol Synthase3 (CDS3) mRNA Affects the Response of Arabidopsis thaliana to Bacteria and Fungi. *Mol. Plant Microbe Interact.* 28(8):892-900. (IF=4.145)

Park, J.H.*, Hong, S.W.*, Yun, S., Lee, D.K., Shin, C. (2014) Effect of siRNA with an asymmetric RNA/dTdT overhang on RNA interference activity. *Nucleic Acid Ther.* 24, 364-371. **(*co-first authors)** (IF=2.813)

Park, J.H., Shin, C. (2014) MicroRNA-directed cleavage of targets: mechanism and experimental approaches. *BMB Rep.* 47, 417-423. (IF=2.782)

Hong, S.W.*, **Park, J.H.***, Yun, S., Lee, C.H., Shin, C., Lee, D.K. (2014) Effect of the guide strand 3'-end structure on the gene-silencing potency of asymmetric siRNA. *Biochem. J.* 461, 427-434. **(*co-first authors)** (IF=3.562)

Kim, S. Park, M. Yeom, S. Kim, Y. Lee, J. Lee, H. Seo1, E. Choi, J. Cheong, K. Kim, K. Jung, K. Lee, G. Oh, K. Bae, D. Kim, S. Lee, H. Kim, S. Kim, M. Kang, B. Jo, Y. Yang, H. Jeong, H. Kang, W. Kwon, J. Shin, C. Lim, **Park, J. H.**, et. al., Lee, Y-H & Doil Choi*. (2014) Genome sequence of the hot pepper provides insights into the evolution of pungency in Capsicum species. *Nat. Genet.* 46, 270-278. (IF=31.616)

Park, J. H., Ahn, S., Kim, S., Lee, J., Nam, J. W., and Shin, C. (2013) Degradome sequencing reveals an endogenous microRNA target in C. elegans. *FEBS Lett.* 587, 964-969. (IF=3.519)

Hwang, D. G.*, **Park, J. H.***, Lim, J. Y.*, Kim, D., Choi, Y., Kim, S., Reeves, G., Yeom, S. I., Lee, J. S., Park, M., Kim, S., Choi, I. Y., Choi, D., and Shin, C. (2013) The hot pepper (Capsicum annuum) microRNA transcriptome reveals novel and conserved targets: a foundation for understanding MicroRNA functional roles in hot pepper. *PLoS One*, 8, e64238. **(*co-first authors)** (IF=3.057)

Lee, J.*, Kim, D. I.*, **Park, J. H.***, Choi, I. Y., and Shin, C. (2013) MiRAuto: an automated user-friendly microRNA prediction tool utilizing plant small RNA sequencing data. *Mol. Cells* 35, 342-347. **(*co-first authors)** (IF=2.670)

Kim, J.*, **Park, J. H.***, Lim, C. J., Lim, J. Y., Ryu, J. Y., Lee, B. W., Choi, J. P., Kim, W. B., Lee, H. Y., Choi, Y., Kim, D., Hur, C. G., Kim, S., Noh, Y. S., Shin, C., Kwon, S. Y. (2012) Small RNA and transcriptome deep sequencing proffers insight into floral gene regulation in Rosa cultivars. *BMC Genomics* 13, 657. **(*co-first authors)** (IF=3.867)